Applications of the C^*-algebraic reformulation of Quantum Statistical Mechanics to the description of experimentally investigated spin systems

Dissertation
zur Erlangung des Doktorgrades
des Fachbereichs Physik
der Universität Hamburg

vorgelegt von
Kolja Them
aus
Reinbek

Hamburg
2014

Gutachter der Dissertation:
Prof. Dr. R. Wiesendanger
Prof. Dr. K. Fredenhagen

Gutachter der Disputation:
Prof. Dr. R. Wiesendanger
Prof. Dr. R. Lichtenstein

Datum der Disputation:
10.11.2014

Vorsitzender des Prüfungsausschusses:
Prof. Dr. D. Pfannkuche

Vorsitzender des Promotionsausschusses:
Prof. Dr. D. Pfannkuche

Dekan der MIN-Fakultät:
Prof. Dr. H. Graener

Zusammenfassung

In der vorliegenden Arbeit werden exakte, perturbative und mean-field artig approximative, numerische und algebraische Methoden angewendet, um die Realzeit-Dynamik und die Magnetisierungsstruktur von nanoskaligen Spin-Systemen zu analysieren. Die Magnetisierungsdynamik von einzelnen Cobaltatomen auf der Oberfläche von Platin und der Relaxationsprozess des Spins von einem Eisenatom auf der Oberfläche von Indium-Antimonid und anderen Substraten werden simuliert, wobei der Einfluss eines spin-polarisierten Rastertunnelmikroskopes berücksichtigt wird. Dies ermöglicht eine einsichtigere Interpretation und Vorhersage der experimentellen Daten. Der magnetische Informationstransport in Spinketten aus Eisenatomen auf Iridium und anderen Substraten wird untersucht und Lieb-Robinson bounds werden als obere Schranke für die Maximierung der Signalgeschwindigkeit eingeführt. Eine exakte obere Schranke für den Fehler von Erwartungswerten, verursacht durch physikalische Approximationen der Umgebung eines lokalen Spin-Untersystems, wird untersucht und beispielhaft auf ein spinbasiertes Logik-Bauelement angewendet. Approximierte KMS-Zustände werden für eine numerische Behandlung von vielfachen thermodynamischen Gleichgewichtszuständen von Spin-Systemen eingeführt und kritisch diskutiert.

Abstract

The present work is devoted to the application of exact, perturbative, and mean-field type approximate, numerical and algebraic methods, for the investigation of the real-time dynamics and magnetization structures of nanoscale spin systems. The magnetization dynamics of single cobalt atoms on the surface of platinum, and the spin relaxation process of iron atoms on the surface of indium-antimonide and other substrates are simulated. The influence of a spin-polarized scanning tunneling microscope is included in the calculations. This enables a clear interpretation and prediction of the experimental data. The magnetic information transfer in spin chains consisting of iron atoms on iridium and other substrates is investigated and Lieb-Robinson bounds are used to obtain upper limits on the enhancement of the signal speed. An exact upper bound on expectation value errors of quantum subsystems is investigated, when the environment is physically approximated, and exemplarily applied to an all-spin based atomic-scale logic device. Approximated KMS states are developed for a numerical handling of multiple thermodynamic equilibrium states of spin systems and critically discussed in this work.

Contents

1 Introduction

In February 1922, the experimental investigations of Otto Stern and Walther Gerlach revealed a discontinuous distribution of silver atoms, when an external magnetic field was applied. Wolfgang Pauli proposed a quantum mechanical concept of spin and worked out a corresponding mathematical theory in 1927. An agreement between Pauli's concept of spin and the Stern-Gerlach experiment was found, which provided the foundations for upcoming spin structure determinations and applications. The nuclear spin was found to be helpful for structural investigations of chemical and biological systems by using nuclear magnetic resonance spectroscopy, and properties arising from unpaired electron spins in magnetic atoms was useful in developing hard disks for computer systems.

The development of future spintronic devices [1–5] begins from the scale of single magnetic atoms and is a bottom-up approach for the ongoing miniaturization of hard disks and other computer chips. The improvement of these devices requires the consideration of certain magnetic properties, such as, the stability and conservation of spin structures for a sufficient length of time, the ability to locally manipulate a spin structure by an external influence, and lastly a faster transport of magnetic information. Theoretical investigations towards the prediction and interpretation of experimental findings assist in the quest for suitable magnetic structures that provide the required properties adequately. As such, spin-sensitive studies of individual magnetic adatoms and atomic ensembles on surfaces by spin-polarized scanning tunneling microscopy (SP-STM) [1, 6–11] have given rise to the necessity of a quantum mechanical description of the atomic and molecular spin structures and spin dynamics [12, 13].

A variety of numerical methods were developed to estimate expectation values of quantum systems [14–24]. Depending on the physical situation, different approximations are used in these methods [25–37]. Density functional theory (DFT) was applied as an ab-initio method to obtain the ground state and the corresponding electronic structure, which provided fruitful progress at the intersection of theory and experimentation; e.g., the theoretical description of the experimental findings of magnetic skyrmions in a monolayer of iron on iridium [38]. Extremely cold systems or properties that are not very temperature sensitive are interesting for ground state approximations obtained by DFT. The expansion of DFT to finite temperatures has also made progress [39]. Numerical ab-initio methods were also developed to obtain parameters that enter effective Hamiltonians of Quantum Spin Systems (QSS), which can then be further used in other numerical methods, such as

"exact diagonalization" (ED) or Quantum Monte Carlo methods (QMC). As the name suggests, ED enables an exact handling of QSS and is applicable to system sizes up to $\approx$ twenty spin 1/2 particles, depending on the numerical code and memory capacity of the used computer system. QMC principally uses the MC methods to handle the multi-dimensional integrals that arise from many-body quantum systems, and has applications to impurity models at finite temperatures [40]. Continuous-Time (CT)-QMC provides a dynamical description of these systems [41]. The mean-field theory approximates the effect of a large number of particles on single particles as an averaged field effect [42].

A numerical simulation of a system at inverse temperature β and Hamiltonian H, which is initially in thermodynamic equilibrium, is commonly performed using the density matrix $\rho = e^{-\beta H}$ (or also $\rho = e^{-\beta H - \nu N}$) as initial state. For finite-dimensional QSS $\rho = e^{-\beta H}$ is the unique density matrix which minimizes the free energy (and satisfies the maximum entropy principle). But if the thermodynamic limit is a suitable approximation for the considered system, there might exist other equilibrium states which can be captured by the system. Suitable examples in spin-based nanotechnology are the experimentally investigated nanoislands [43] which possess two different relatively stable magnetization directions. It is evident that the density matrix $\rho = e^{-\beta H}$ cannot describe both states. Thus, it is interesting to ask which density matrix might be used instead of $\rho = e^{-\beta H}$ to describe the other thermodynamic equilibrium states. We will investigate this question based on the results of the Kubo-Martin-Schwinger (KMS) states in [44] and a mean-field type approximation. The obtained approximated KMS states are interesting candidates to describe thermodynamically stable spin structures of finite size which are desired in high-density data storage.

In general, the environment (often called the bath) influences the equilibrium properties of a local subsystem and is a fundamental problem for simulations; only a few model systems exist that can be solved exactly [45]. Therefore, one commonly uses simplified and idealized interactions for the description of the environment (bath), e.g., itinerant electrons are assumed to be absolutely free, or several interacting quantum spin particles are assumed to form a "macro spin". The exact error produced by these physical approximations is often difficult to estimate and remains unclear. Thus, the quality of the obtained expectation values is often unknown, and the deviation to the values one would obtain by using more realistic interactions is uncertain. These questions will be investigated quantitatively by introducing an exact bound ϵ on these errors, and a particular example will be discussed in which the bound ϵ provides useful results for weakly interacting systems, depending on the temperature. The bound also provides the maximum error

for certain numerical approximations, due to the neglect of higher orders in perturbation theory.

A further difficulty arises if a certain physical property, such as the signal velocity, has to be maximized by varying several experimental parameters, e.g., the temperature, the external magnetic field, anisotropy energies or differently prepared initial states. While the signal speed is crucial for the efficiency of future spintronic devices, finding the maximum velocity can be a considerable numerical challenge and is often impossible for large and realistic quantum systems. Even for small systems, a large number of calculations are required until an accurate maximum value is found, which costs valuable research time. Hence, a general upper limit on the desired physical property that is independent of these parameters is ideal. This will be examined in detail using particular examples of information transfer in spin chains and using Lieb-Robinson bounds as limits on the signal speed.

Several other interesting and unanswered questions are related to the length scale where nanotechnology operates, which is in transition between quantum and classical physics. Classical spin systems have the advantage that simulations can be performed with relatively large particle numbers compared to most quantum spin models. But if quantum effects are important, simulations using classical spin systems might lead to inaccurate predictions and complexities in the interpretation of experimental data. We will investigate this important question by applying ensemble- and time-averaged magnetization curves of Cobalt atoms on Platinum for the interpretation of experimental data. A key leading to the interface between experimental research activities and the algebraic framework of mathematical physics is also found and will be discussed.

All of our investigations are based on the C^*-algebraic [46–58] reformulation of Quantum Statistical Mechanics [44, 59–61]. It is a mathematical reformulation of the original mathematical structure of Quantum Mechanics from the early 1930s and provides additional analytical techniques to the above mentioned numerical methods. The general analysis of equilibrium states in the mid 1960s revealed that the algebraic framework facilitates useful techniques for their characterization by the KMS condition. A deep connection between the Tomita-Takesaki modular theory and the KMS condition was found which led to powerful computational techniques. This enabled investigations of basic physical questions, such as the problem of "return to equilibrium" and the "stability of equilibrium states under local perturbations", in a more wholesome analytical fashion, which numerical methods alone could not capture. It was also found that ground states have the tendency to be less stable than states that satisfy the KMS condition (KMS states) at finite temperatures [44]. In 1967 Robinson introduced an

algebraic approach to the statistical mechanics of QSS [62–64]. Since that invention, there has been ongoing development [65–73]. It was found that KMS states also satisfying the condition of "local thermodynamic stability" [44]. Thus, these states provide the most stable magnetization structures. A citation from a two pages long conclusion ensuing the 1052 page long disquisition on the utility of operator algebras in quantum statistical mechanics [44, 60] serves as an introductive overview:

"*...all the basic examples such as the Heisenberg and Ising models, can be described by C^*-dynamical systems $(\mathfrak{A}, \tau)$ and states of these systems correspond to the physical states described by the model. A global viewpoint of this type is essential if one desires understanding of such basic questions as the nature of thermodynamic phases, mixture properties of the phases, etc., and this is perhaps the greatest single advantage of the algebraic methods. Traditionally, equilibrium states had been described by a variety of methods, e.g., implicit or explicit thermodynamic limits of the Gibbs ensembles, the principle of maximum entropy, etc., but in all these methods the affine properties of the states were unclear. Phase transitions were partially understood in terms of nondifferentiability of the thermodynamic functions, or through lack of clustering of the states, but no framework really existed for the definition and characterization of pure phases and mixed phases. The realization that the equilibrium states could in fact be identified as states over the appropriate C^*-dynamical systems immediately provided this framework. The equilibrium states at each fixed temperature were seen to form a convex set with the extremal points corresponding to pure phases and the mixed states to mixtures of phases. This immediately motivated much of the analysis of decomposition theory, invariant states, periodic states, almost periodic states, etc., described in Chapter 4. ... The second striking feature in the algebraic description of equilibrium phenomena is the role played by the KMS condition. Starting from the Gibbs ensemble it is evident that this condition is satisfied but it is completely unclear that this condition alone should characterize equilibrium. Nevertheless, this is the case for a large class of quantum spin systems, and also for the ideal Fermi gas. This rather surprising result is both of practical and conceptual utility. ... On the other hand, we have seen in Chapter 5 that the KMS condition has a variety of characterizations which emphasize different physical features such as stability under perturbations and ergodicity in the form of asymptotic abelanness. This clarifies to a large extent the nature of the equilibrium states even if it does not provide any profound explanation for their definition.*"

Another area of fruitful progress was founded by the derivation of physically meaningful inequalities, i.e., values which represent the upper or lower lim-

its of a quantitative physical property. The following achievements of the algebraic approach to QSM are of interest to some of our purposes:

1. A well-defined and correct handling of quantum systems in the thermodynamic limit [44],

2. The analysis of multiple equilibrium states ω^β and the association with thermodynamic phases [44],

3. General bounds on specific physical quantities, e.g., Lieb-Robinson bounds on the signal velocity or bounds on the approximation of ground states [74] and finite temperature equilibrium states, and

4. A framework to investigate the stability properties of equilibrium states ω^β under local perturbations P [44].

It is interesting to question how far these algebraic methods would be suitable for the assistance of experimental research activities and in supplementing numerical methods in modern condensed matter theory. It is worthy to mention that an explicit form of the KMS condition is often used in modern numerical quantum many-body methods as a boundary condition, however, personal conversations indicated that the algebraic characterization of equilibrium states as KMS states and the corresponding analytical techniques are unfamiliar in condensed matter theory. A structural application of the algebraic methods to experimentally investigated spin systems will be provided by the general principle $(\mathfrak{A}, \tau) \rightleftarrows (\mathfrak{A}, \tau^P)$. Some cases in which the algebraic methods supplement the commonly used numerical methods are discussed. The connections are illustrated in specific examples which are now briefly introduced and elaborated further in chapters 3,4,5 and 6.

Two different magnetization directions, e.g., "up" and "down", of a magnetic particle serve as a storage unit, which is called a bit. Self-evidently, the size of the magnetic particle should be as small as possible, so that a maximum density of stored data can be achieved. In 2007, SP-STM studies showed that a magnetic STM tip could be used to switch between two non-zero magnetization orientations of nanoislands consisting of approximately 100 iron atoms (a surface area of ≈ 7 nm^2) placed on the surface of tungsten (110) [43]. Interestingly, the nanoislands which were less than 100 atoms in [75] were seemingly large enough, such that these islands could be investigated theoretically in the thermodynamic limit. Besides the current-induced magnetization switching, there was a thermally activated magnetization switching. The two different magnetization directions were separated by an energy barrier and the finite temperature was responsible for a fluctuation of the

energy of the nanoisland. If the temperature is relatively high, the magnetization switches relatively often from one direction "over the energy barrier" to the opposite direction. It was found experimentally, that the temperature dependence of the switching rate for Fe/W(110) nanoislands was in good agreement with the so-called Néel-Brown law [43, 75]. Thus, a high energy barrier in combination with a low enough temperature should provide (at least) two stable magnetization orientations of a magnetic particle, i.e., an appropriately low switching frequency between "up" and "down" so that the magnetic particle can be used as a data storage unit. Single cobalt atoms on the surface of platinum (111) possess a very high anisotropy energy barrier of $K = 9$ meV. If a classical spin model is used for the description of the Co/Pt(111) system and the temperature is sufficiently low (≈ 0.3 K), one obtains two stable magnetization directions "up" and "down" and the Néel-Brown law predicts a life-time of a few million years for these orientations. From this point of view, this system seems to be an exciting candidate for the investigation of a high density data storage device. However, the experimental SP-STM results at a temperature of $T = 0.3$ K and $T = 4.2$ K [12] showed that there is only a single stable magnetization direction and a switching rate of less than a few milliseconds. This discrepancy will be clarified quantitatively in chapter 4.2 based on our results in [13], in which quantum effects are identified for the observed discrepancy. The classical spin description provides an agreement between the classical ensemble average and the experimentally time averaged expectation value of a single adatom. However, the classical descriptions are unable to capture the correct dynamics of the adatom within the resolution time of the SP-STM setup. The quantum description provides agreement for both, the ensemble- and the time-averaged magnetization curves. There is also an interesting qualitative algebraic explanation, because a small system (the single cobalt adatom), which is coupled to an ideal gas of fermions (the substrate electrons of the platinum) holds a single and, therefore, unique KMS state. This can be checked by an application of Theorem 5.2.24. together with Corollary 5.4.5. in [44].

As mentioned in the beginning, apart from the storage of bits, the transport of magnetic information is a further crucial process for spintronic devices. The all spin-based atomic-scale logic device [2] uses spin chains consisting of 5 iron atoms on copper(111) to transport the magnetization information of the input islands to the output atom. In 2012 it was found that spin chains consisting of approximately 100 iron atoms on the surface of an iridium(001) crystal [76] are promising systems for the transport of magnetic information. The enhancement of the magnetic signal speed is of primary interest for spintronic applications and there are several experimental pa-

rameters which may influence this, such as, exchange energies, anisotropy energies, external magnetic fields, the applied bias voltage and the initial state. In principle, there is an infinite number of possibilities for an adjustment of these parameters. We give an upper bound on the enhancement of the signal velocity, which is independent of most of these parameters [77].

The third basic spintronic operation includes magnetization switching by the SP-STM tip. The conversion of one stable magnetic structure into another stable magnetic structure is a central goal in spin-based nanotechnology. From the algebraic point of view, the action of the magnetic tip corresponds to a small perturbation of the investigated sample, e.g., the norm of the modified Tersoff-Hamann model is finite (in the C^*-algebra, and not in the Banach space of interactions). This fact validates the application of said algebraic techniques for the investigation of the stability of KMS states under local perturbations, as explained in [44, 60]. Interesting connections to experimental research activities are provided by the creation and deletion of magnetic skyrmions [78]. Approximated KMS states are constructed for a numerical investigation of problems concerning "stability of equilibrium states under local perturbations" and we critically discuss problems as well as potential future work.

Organization of the thesis

The "Mathematical basis" in chapter 2 serves as an introduction into the algebraic language and starts with the elementary properties of C^*-algebras, states, representations, derivations and *-automorphisms. These properties are of general nature, i.e., they are valid for all physical quantum theories which can be described using the algebraic approach. In this chapter and the next, we also refer to parts that are shifted to the appendix, which contains further mathematical structures for future developments.

Chapter 3 then focuses on QSS and describes the mathematical structure of systems with a finite number of particles as well as systems in the thermodynamic limit (systems with an infinite number of particles). We discuss properties of KMS states, introduce mean-field approximated KMS states and derive simplified formulas for the latest, most general Lieb-Robinson bound.

In chapter 4 we describe the functionality of SP-STM by a general principle, a C^*-dynamical system $(\mathfrak{A}, \tau)$ and a related perturbed C^*-dynamical system $(\mathfrak{A}, \tau^P)$. This is the foundation of the thesis and provides the interface between the algebraic reformulation of QSM and the experimental research activities on magnetic quantum systems. The time-averaged measurements are explained theoretically and then calculated to clarify and support the experimentally found magnetization curves of single cobalt atoms on plat-

inum(111). We also numerically investigate the relaxation process of a single magnetic adatom and corroborate the findings with the experimental results for Fe/InSb, thereby validating its structural application. We then discuss how the general principle could be used to include even more fundamental physical theories in addition to QSS, e.g., QFT, for a more realistic modeling of the tunneling current and substrate electrons.

Chapter 5 discusses information transport in magnetic spin chains. The exact signal propagation is investigated and a Lieb-Robinson bound is used to examine the maximum enhancement of the signal speed when several experimental parameters are changed.

In chapter 6 a further bound is derived which provides an exact limit on errors that are encountered during certain physical approximations. The bound is applied to examine quantitatively how an atomic-scale logic device should be designed to work also at higher temperatures.

The appendix contains a brief summary of well-known results [44, 60], which are important for some of the calculations in this work, and might be relevant for future work. This thesis is then concluded with a summary of achievements and an outlook towards potential future work.

2 Mathematical basis

In this section we will introduce the elementary mathematical objects, which are essential for the description of a quantum theory in the algebraic framework [60, 79–84]. The central object is a C^*-algebra $\mathfrak{A}$, which constitutes the intrinsic mathematical description of the theory. The algebraic framework has special advantages for infinite-dimensional systems, which appear in quantum field theoretical models as well as in QSS, if the thermodynamic limit is considered. The ladder case is of notably interest for condensed matter systems.

A mathematical framework for the physical description of nature consists essentially of two basic concepts: A kinematical structure describing the states and observables at a fixed time, e.g., $t = 0$, and a dynamical rule describing the change of these states and observables with time. The algorithms of this section are of general nature, i.e., valid for several physical quantum theories as QSS, fermionic lattice systems (including the Hubbard and Anderson model) as well as for QFT. This generality establish the opportunity to change to physically more fundamental models without changing the abstract mathematical framework. Therefore, several techniques based on the general framework (see the appendix) are applicable to investigate the change of physical properties when the level of the physical approximation is up- or degraded. In general, there are two approaches to the algebraic structure associated with a quantum theory [44, 60]. One could start with the Hilbert space $\mathfrak{H}$ of vector states of the particles and subsequently introduces algebras of bounded operators corresponding to observables of the particles. Alternatively, one can choose a more abstract approach, starting with structural features of a C^*-algebra $\mathfrak{A}$, and recover the other approach by passing through a particular representation $(\mathfrak{H}, \pi)$. π maps an abstract operator $A \in \mathfrak{A}$ to a representative $\pi(A) \in \mathfrak{B}(\mathfrak{H})$ in a set $\mathfrak{B}(\mathfrak{H})$ of bounded operators on the Hilbert space $\mathfrak{H}$. Before we start with introducing C^*-algebras, we will first summarize structural differences of the original formulation of quantum physics and the algebraic reformulation:

Quantum mechanics by the early 1930s [60]:

1. an *observable* is a selfadjoint operator A on a Hilbert space $\mathfrak{H}$;
2. a (pure) *state* is given by a vector $\psi \in \mathfrak{H}$;
3. the *expectation value* of A in the state ψ is given by $(\psi, A\psi)$;
4. the *time evolution* of the system is determined by the selfadjoint Hamil-

tonian operator H through either of the algorithms

$$A \mapsto A(t) = e^{itH} A e^{-itH}, \quad \text{or} \quad \psi \mapsto \psi(t) = e^{-itH}\psi. \tag{1}$$

Algebraic reformulation:

1. a bounded *observable* A is a selfadjoint element of a C^*-algebra $\mathfrak{A}$;
2. a *state* ω is a positive, normalized, and linear functional on $\mathfrak{A}$, i.e., $\omega \in \mathfrak{A}^*$, where $\mathfrak{A}^*$ is the dual of $\mathfrak{A}$;
3. an *expectation value* is given by $\omega(A) = (\psi_\omega, \pi_\omega(A)\psi_\omega)$, where $\pi_\omega : \mathfrak{A} \to \mathfrak{B}(\mathfrak{H})$ and $\psi_\omega \in \mathfrak{H}_\omega$, where the index ω denotes the association of the representation $(\mathcal{H}_\omega, \pi_\omega)$ with the state ω;
4. the *time evolution* of the system is given by a one-parametric (semi-) group of *-automorphisms τ_t, which is generated by a derivation δ. Thus, the derivation δ contains the information of the Hamiltonian. A rough estimate provides

$$A \mapsto \tau_t(A) = e^{\frac{t}{\hbar}\delta}(A). \tag{2}$$

For finite-dimensional systems we have

$$\tau_t(A) = e^{\frac{itH}{\hbar}} A e^{-\frac{itH}{\hbar}}. \tag{3}$$

However, in the thermodynamic limit this is in general not the case, because the Hamilton operator may becomes unbounded. In this case, the derivation δ provides the correct description. The action of δ is described in section 2.3.

2.1 C^*-algebras

A complex vector space $\mathfrak{A}$ which is equipped with a multiplication law $\mathfrak{A} \times \mathfrak{A} \longrightarrow \mathfrak{A}$, $(A, B) \mapsto AB$, is called an algebra. The product satisfies

1. $A(BC) = (AB)C$,
2. $A(B + C) = AB + AC$,
3. $\alpha\beta(AB) = (\alpha A)(\beta B)$

for $A, B, C \in \mathfrak{A}$, $\alpha, \beta \in \mathbb{C}$. A *-algebra is an algebra equipped with an involution $\mathfrak{A} \ni A \mapsto A^* \in \mathfrak{A}$ with the following properties:

1. $A^{**} = A$,

2. $(AB)^* = B^*A^*$,

3. $(\alpha A + \beta B)^* = \overline{\alpha}A^* + \overline{\beta}B^*$,

where $\overline{\alpha}$ denotes the complex conjugate of α. The * operation corresponds to the adjoint operation † in the common fashion of quantum physics. A subset $\mathfrak{B}$ of $\mathfrak{A}$ is called selfadjoint if $A \in \mathfrak{B}$ implies $A^* \in \mathfrak{B}$. A normed algebra $\mathfrak{A}$ is obtained if to each element $A \in \mathfrak{A}$ there is associated a real number $\| A \|$, called the norm of A, satisfying the requirements

1. $\| A \| \geq 0$ and $\| A \| = 0$ if, and only if, $A = 0$,

2. $\| \alpha A \| = |\alpha| \, \| A \|$,

3. $\| A + B \| \leq \| A \| + \| B \|$,

4. $\| AB \| \leq \| A \| \| B \|$.

The norm induces a metric topology on $\mathfrak{A}$, called the uniform topology. Neighborhoods in this topology are given by

$$\mathfrak{U}(A;\epsilon) = \{B; B \in \mathfrak{A}, \| B - A \| < \epsilon\}, \tag{4}$$

where $\epsilon > 0$. If $C \in \mathfrak{U}(A;\epsilon)$, then C is said to be an ϵ-neighbor of A. A normed and complete algebra with involution, satisfying $\| A \| = \| A^* \|$, is called a Banach *-algebra. A C^*-algebra is then defined by

Definition 2.1. *([60], 2.1.1.): A C^*-algebra is a Banach *-algebra $\mathfrak{A}$ with the property*

$$\| A^*A \| = \| A \|^2 \tag{5}$$

for all $A \in \mathfrak{A}$.

A connection from this abstract description to the Hilbert space of a quantum theory is provided by

Theorem 2.2. *([60], 2.1.10.): Let $\mathfrak{A}$ be a C^*-algebra. It follows that $\mathfrak{A}$ is isomorphic to a norm-closed selfadjoint algebra $\mathfrak{B}(\mathfrak{H})$ of bounded operators on a Hilbert space $\mathfrak{H}$.*

In our applications the operator norm of an element $A \in \mathfrak{B}(\mathfrak{H})$ is given by

$$\| A \| = \sup\{\| A\Psi \|; \Psi \in \mathfrak{H}, \| \Psi \| = 1\}. \tag{6}$$

Thus, our chosen operator norm is related to the norm $\| \Psi \| = (\Psi, \Psi)$ of a vector state in a Hilbert space. It is evident that the expectation value of A in an arbitrary normed vector state Φ is smaller or equal than the norm of A, i.e., $(\Phi, A\Phi) \leq \| A \|$.

2.2 Representations and states

States and representations are closely related. If one starts from an abstract C^*-algebra and wants to calculate an expectation value one has to pass through a representation. As the name illustrates, a representation "represents" an abstract observable as an explicit operator, e.g., the z-component of a spin-1/2 operator can be represented by a diagonal 2×2-matrix. In 1931 a uniqueness theorem for the representations of finite dimensional quantum systems was obtained, called the Stone von Neumann uniqueness theorem. However, if the thermodynamic limit is performed the system gets infinite-dimensional and the uniqueness theorem is no longer valid, which is also the case for a QFT. This lack of uniqueness was not generally recognized until the 1950s when Segal, Friedrichs, and others gave examples of inequivalent regular representations. A theorem which essentially showed that two pure ground states are either equal or generate unitarily inequivalent representations was proved by Haag in 1955. Later it was found that unitarily inequivalent representations are also present by the non-uniqueness of KMS states (thermodynamic equilibrium states). Thus, the Schrödinger representation suffices for the description of a finite number of particles, but other representations of operators on Hilbert spaces are essential, if a system is investigated in the thermodynamic limit [44, 60].

Representations

A *-morphism between two *-algebras $\mathfrak{C}$ and $\mathfrak{B}$ is defined as a mapping $\pi : A \in \mathfrak{C} \longrightarrow \pi(A) \in \mathfrak{B}$ for all $A \in \mathfrak{C}$ and such that

1. $\pi(\alpha A + \gamma C) = \alpha\pi(A) + \gamma\pi(C)$,
2. $\pi(AC) = \pi(A)\pi(C)$,
3. $\pi(A^*) = \pi(A)^*$

for all $A, C \in \mathfrak{C}$ and $\alpha, \gamma \in \mathbb{C}$. The kernel of a *-morphism is given by the set

$$ker(\pi) = \{A \in \mathfrak{A}; \pi(A) = 0\}. \tag{7}$$

The definition of a representation can now be introduced.

Definition 2.3. *([60], 2.3.2.): A representation of a C^*-algebra $\mathfrak{A}$ is defined to be a pair $(\mathfrak{H}, \pi)$, where $\mathfrak{H}$ is a complex Hilbert space and π is a *-morphism of $\mathfrak{A}$ into $\mathfrak{B}(\mathfrak{H})$. The representation is said to be faithful if, and only if, π is a *-isomorphism between $\mathfrak{A}$ and $\pi(\mathfrak{A})$, i.e., if, and only if, $ker(\pi) = \{0\}$.*

The space $\mathfrak{H}$ is called the representation space and the operator examples $\pi(A)$ are called the representatives of $\mathfrak{A}$. A faithful representation π also satisfies $\| \pi(A) \| = \| A \|$, for all $A \in \mathfrak{A}$. This is certainly an important fact for the calculation of bounds, which include the operator norm, e.g., Lieb-Robinson bounds or our bound ϵ on physical approximations. A *-isomorphism of a C^*-algebra $\mathfrak{A}$ into itself is called a *-automorphism τ. An important result for the norm of an observable during the dynamical evolution of a physical system is given by

Theorem 2.4. *([60], 2.3.4.): Each *-automorphism τ_t of a C^*-algebra $\mathfrak{A}$ is norm preserving, i.e., $\| \tau_t(A) \| = \| A \|$ for all $A \in \mathfrak{A}$.*

This theorem is of special interest for the derivation of dynamical bounds (e.g. Lieb-Robinson bounds).

States

The dual of a C^*-algebra $\mathfrak{A}$ is denoted by $\mathfrak{A}^*$ and consists of continuous, linear functionals over $\mathfrak{A}$. The norm of any functional f over $\mathfrak{A}$ is defined by

$$\| f \| \doteq \sup\{|f(A)|; \| A \| = 1\}. \tag{8}$$

The physical states form a convex subset of this dual and they are introduced by

Definition 2.5. *([60], 2.3.9.): A linear functional ω over the C^*-algebra $\mathfrak{A}$ is defined to be positive if*

$$\omega(A^*A) \geq 0 \tag{9}$$

for all $A \in \mathfrak{A}$. A positive linear functional ω over a C^*-algebra $\mathfrak{A}$ with $\| \omega \| = 1$ is called a state.

Starting from a state ω, we can construct a representation $(\mathfrak{H}_\omega, \pi_\omega)$ of $\mathfrak{A}$ and a vector $\Omega_\omega \in \mathfrak{H}_\omega$ such that ω is identified as the vector state ω_{Ω_ω}, i.e., such that

$$\omega(A) = (\Omega_\omega, \pi_\omega(A)\Omega_\omega) \tag{10}$$

for all $A \in \mathfrak{A}$. Existence and uniqueness of this representation is checked by

Theorem 2.6. *([60], 2.3.16): Let ω be a state over the C^*-algebra $\mathfrak{A}$. It follows that there exists a cyclic representation $(\mathfrak{H}_\omega, \pi_\omega, \Omega_\omega)$ of $\mathfrak{A}$ such that*

$$\omega(A) = (\Omega_\omega, \pi_\omega(A)\Omega_\omega) \tag{11}$$

for all $A \in \mathfrak{A}$ and, consequently, $\| \Omega_\omega \|^2 = \| \omega \| = 1$. Moreover, the representation is unique up to unitary equivalence.

The set of all states is denoted by $E_{\mathfrak{A}}$ and the set of pure states by $P_{\mathfrak{A}}$. Because the sets $E_{\mathfrak{A}}$ and $P_{\mathfrak{A}}$ are subsets of the dual $\mathfrak{A}^*$, they can be topologized through restriction of any of the topologies of $\mathfrak{A}$. The uniform topology is determined by specifying the neighborhoods of ω to be

$$\mathfrak{U}(\omega;\epsilon) = \{\omega';\omega' \in \mathfrak{A}^*, \parallel \omega - \omega' \parallel < \epsilon\}, \tag{12}$$

where $\epsilon > 0$. We will derive a radius ϵ for an application to maximum errors caused by physical approximations and apply the bound exemplarily to the all-spin based atomic-scale logic device. In view of physical equivalence between different states as well as for the analysis of different convergence properties, the weak* topology is also of interest. This topology is defined by neighborhoods of ω, which are indexed by finite sets of elements $A_1, A_2, ..., A_n \in \mathfrak{A}$, and $\epsilon > 0$. The neighborhoods are given by

$$\mathfrak{U}(\omega; A_1, ..., A_n; \epsilon) = \{\omega';\omega' \in \mathfrak{A}^*, |\omega(A_i) - \omega'(A_i)| < \epsilon, \quad i = 1, 2, ..., n\}. \tag{13}$$

However, we will not work with this topology in this thesis. But we mentioned it as an interesting point for future work.

2.3 Derivations and C^*-dynamical systems

For systems consisting of a finite number of particles, where each particle has a finite number of degrees of freedoms, the states are given by rays in a Hilbert space $\mathfrak{H}$. The observables act as operators on $\mathfrak{H}$. However, if the thermodynamic limit is considered, the system becomes infinite-dimensional. In this case, the algebraic reformulation of quantum physics identifies the states with linear functionals over the appropriate algebra $\mathfrak{A}$ of observables. For a finite-dimensional system, as well as for an infinite-dimensional system the dynamics is given by a flow in a Banach space. For the finite-dimensional quantum system it is generated by a group of unitary operators U_t on the Hilbert space, and for the infinite-dimensional system (when the thermodynamic limit was performed) it is generated by a one-parameter group of *-automorphisms τ of the algebra $\mathfrak{A}$ of observables. The natural description of the dynamics is in terms of the infinitesimal change of the system. For a finite-dimensional quantum system, this infinitesimal change is given by a Hamilton operator H, and for an infinite-dimensional system it is given by a derivation δ of the associated algebra $\mathfrak{A}$.

Definition 2.7. *([60] Definition 3.2.21.): A symmetric derivation δ of a C^*-algebra $\mathfrak{A}$ is a linear operator from a *-subalgebra $D(\delta)$, the domain of δ, into $\mathfrak{A}$ with the properties that*

1. $\delta(A)^* = \delta(A^*)$, $A \in D(D(\delta))$,

2. $\delta(AB) = \delta(A)B + A\delta(B)$, $A, B \in D(\delta)$.

The two defining properties originate by differentiation, in the topology dictated by the continuity of τ, of the relations

$$\tau_t(A)^* = \tau_t(A^*), \qquad \tau_t(AB) = \tau_t(A)\tau_t(B). \tag{14}$$

For finite-dimensional systems the Hamiltonian H and the derivation δ are related via the action on a bounded operator A:

$$\delta(A) = [iH, A]. \tag{15}$$

For infinite-dimensional systems one usually considers derivations δ_n, $\delta_n(A) = [iH_n, A]$, of finite-dimensional subsystems $\mathfrak{A}_{\Lambda_n}$ and then uses the norm closure $\bar{\delta}$ for the infinite case. However, this requires more detailed techniques, see the appendix and Theorem 3.2.25. [60] for UHF algebras (Example 2.6.12. [60]).

The flow in the Banach space, which gives the dynamics, is obtained by the integration of the infinitesimal prescriptions and a differential equation of the form

$$\frac{dA_t}{dt} = SA_t \tag{16}$$

has to be investigated under several circumstances and assumptions. In every case the symbol A corresponds to an observable, or a state, of the physical system and will be represented by an element of some suitable space X. The map $t \in \mathbb{R} \mapsto A_t \in X$ describes the dynamics of A and S is an operator on X, which generates the infinitesimal change of A. Existence, uniqueness and stability under small perturbations are of fundamental interest for solutions of this equation. Formally, the solution is given by $A_t = U_t A$, where $U_t = e^{tS}$. However, there are several different types of continuity of $t \mapsto U_t$, which leads to a structural hierarchy. However, these continuity properties require more detailed mathematical knowledge and we advise the mathematically interested physicist to read [44, 60] for more details. Therefore, we will just mention some different types of continuity and the one which is of importance for our purpose, such that we can apply and use the required Theorems of [44] and derive our simplified Lieb-Robinson bound. Uniform, strong, and weak* continuity are of basic interest. A group $\{U_t\}_{t\in\mathbb{R}}$ of bounded operators on the Banach space X is uniformly continuous if, and only if, its generator S is bounded. However, these groups are of limited use for thermodynamic systems, because they imply that the associated Hamilton

operators are necessarily bounded. The systems we are interested in are C^*-dynamical systems $(\mathfrak{A}, \tau)$, where τ is a strongly continuous one-parameter group such that most of the results in [44] are applicable. For QSS, strong continuity can be checked by Theorem 6.2.4. [44], our favorite ones. Thus, we keep in mind that our time-evolution group τ is strongly continuous.

2.4 Remarks on mathematical reformulations of physical theories

Empirically, most phenomena of the dead matter can be described by a physical theory. The description of a phenomenon by a physical theory consists of three fundamental concepts:

- A physical notion of the matter, space, and time,
- a mathematical formulation of the physical notion with a (set of) basic, physical equation(s), and
- its application to the desired problem.

The first concept visualizes the matter, e.g., as a point particle, a continuous matter distribution, a matter wave or some other physical notion, while space is chosen to be discrete or continuous. In the mathematical formulation we associate with each real, existing physical object a mathematical object, e.g., the position of the point particle is associated with an element x, in position space $\mathbb{R}^3$, or the matter wave is associated with a wave function ψ in a Hilbert space $\mathfrak{H}$. Each physical theory possesses a single, or a set of basic equations (equations of motion), which provides the dynamic behavior of the dead matter from an initial configuration. The specific application usually requires the solution of the equations of motion, e.g., Newton's equations, the Maxwell equations, the Schrödinger equation or Einstein's field equations. For the application to a specific problem, a variety of numerical methods are developed to solve these differential equations.

Over the years, most of the valid physical theories where reformulated in a newer, more general and more abstract mathematical language. This mathematical reformulation enables, basically:

- The introduction of new and additional analytical techniques and methods,
- a more abstract and more general understanding of physical processes,
- the absolute exclusion of possibilities, which could destroy the derived results, and

- the elimination of mathematical impreciseness and errors.

Special Relativity in Minkowski space is an instructive example for a sustainable mathematical reformulation of a physical theory. We will briefly exemplify it's development to evaluate some of the purposes of this doctoral thesis. Special Relativity was formulated in 1905 by Albert Einstein and describes the movement of matter through space and time for different observers in uniform motion. While the physical consequences for fast moving bodies are drastically different from Newton's theory, the original mathematical structure of Special Relativity is surprisingly easy. In 1907, Hermann Minkowski reformulated the physical laws of Special Relativity as a geometrical theory in a 4-dimensional space-time, nowadays called the Minkowski space.

Hermann Minkowski, "Das Relativtätsprinzip", Annalen der Physik 352 (15): 927-938:

"Von der elektromagnetischen Lichttheorie ausgehend, scheint sich in der jüngsten Zeit eine vollkommene Wandlung unserer Vorstellungen von Raum und Zeit vollziehen zu wollen, die kennen zu lernen für den Mathematiker jedenfalls von ganz besonderem Interesse sein muss. Auch ist er besonders gut prädisponiert, die neuen Anschauungen aufzunehmen, weil es sich dabei um eine Akklimatisierung an Begriffsbildungen handelt, die dem Mathematiker längst äußerst geläufig sind, während die Physiker jetzt diese Begriffe zum Teil neu erfinden und sich durch einen Urwald von Unklarheiten mühevoll einen Pfad durchholzen müssen, indessen ganz in der Nähe die längst vortrefflich angelegte Straße der Mathematiker bequem vorwärts führt."

While Einstein was first disaffected to Minkowskis reformulation, he realized a few years later that his formulation of General Relativity in 1916 can further be simplified by the concept of the Minkowski space. This was the case, because Einstein could use the "excellently developed mathematical road" of differential geometry, from that Minkowski was talking about. In the weak field limit of the gravitational field (the absence of massive matter and gravitation) and for extremely local events, the Minkowski space is the correct approximation for space-time regions of very low curvature. Today, Einsteins original formulation of Special Relativity is mainly of historical interest and the Minkowski space has become a standard tool in modern relativistic physics, and is also commonly being used for computer simulations in elementary particle physics. While the physical content of Relativity is still the same, the mathematical reformulation facilitated the development of new techniques, e.g., the covariant formulation of wave equations, as well as several new theoretically visualizing concepts, e.g, such as space-time diagrams with light cones. Finally, the mathematical road further lead to the

navigation of satellites. The usefulness of Minkowski's reformulation to other parts of physics can only become evident looking backwards on its connection to other problems, because it was not a solution of a physical problem.

The development of the mathematical reformulation of quantum physical models [79], in terms of C^*- and W^*-algebras, took significantly more time and is still actual of research interest. The theory of algebras of operators on Hilbert space is an excellently developed mathematical road for Quantum Field Theory and Quantum Spin Systems. The foundations were laid in the 1930s by von Neumann and Murray. In between the late 1924 and the early 1925, Heisenberg and Schrödinger independently proposed explanations for the empirical quantization rule for the experimentally observed discontinuous energy levels for electrons in an atom. At first, these two approaches seemed to be disparate, and nowadays this difference is reflected in the distinction between the Heisenberg picture, where the operator A is time dependent, i.e., $A(t)$, and the Schrödinger picture, where the wave function ψ is time dependent, i.e., $\psi(t)$. The complementarity between the dynamical laws can be expressed as follows:

$$(\psi, A(t)\psi) = (\psi(t), A\psi(t)). \tag{17}$$

In the late 1920s and early 1930s Stone and von Neumann used algebraic methods to clarify the connection between the above formalisms. They provided a mathematically coherent description of quantum mechanics, and proved that the theory was essentially unique [44]. A fruitful interplay between experimental physics, theoretical physics, and mathematical physics was achieved which is, in some kind, contained in the above equation concerning discreteness of energy levels, derived from two seemingly different quantum mechanical descriptions and uniqueness. Despite these important and significant results, the relevance of the theory of operator algebras to quantum physics was not fully appreciated for more than twenty years. It was not until 1957, when Haag emphasized the importance of the quasi-local structure of operator algebras in quantum field theory. It was a groundbreaking work in elementary particle physics and its synthesis with the theory of relativity. Subsequently, a large field of applications were developed in cosmology.

In the 1960s it was found that the quasi-local structure of operator algebras is also of importance for Quantum Statistical Mechanics (QSM), i.e., the statistical properties of many-body quantum systems. It turned out that several problems for infinite systems can be corrected and solved by the algebraic point of view, e.g., there is no distinguished Hilbert space. The abstract application of operator algebras to QSS by Bratteli, Robinson and

co-workers thereby demonstrated novel and powerful techniques for investigations of magnetic quantum systems on atomic length scales (see chapter 6 [44]). However, its connection to the description of experimentally investigated spin systems was still missing...

3 Quantum spin systems

A C^*-algebra $\mathfrak{A}$ of a QSS is a specific kind of a C^*-algebra, which possesses a so-called quasi-local structure. Thus, the general calculation rules of the previous chapter are still valid. First we will explain the structure of a QSS and introduce realistic magnetic interactions. Then, we briefly discuss KMS states as equilibrium states and its association with thermodynamic phases. The occurrence of unique as well as the occurrence of multiple KMS states is of central interest. The multiplicity (non-uniqueness) of KMS states is our motivation for the derivation of approximated KMS states for a numerical handling. The well-known equilibrium state $e^{-\beta H}$ is commonly used for equilibrium situations in condensed matter systems, but not always the best suited one. Our approximated KMS states are an extension to handle also other states satisfying thermodynamic stability conditions. A related problem leads us to the derivation of a bound ϵ on physical approximations. In the last subsection we derive a simplified formula [85, 86] for the latest most general Lieb-Robinson bound on signal velocities. The mathematical structure described in this section is taken from [44]

3.1 The quantum spin algebra

Magnetic atoms placed on a substrate form a spin system on a lattice $L = \mathbb{Z}^d$. The position of the magnetic atoms are described by points $x \in \mathbb{Z}^d$ in the lattice $L = \mathbb{Z}^d$. We associate with each point $x \in \mathbb{Z}^d$ a Hilbert space $\mathcal{H}_x$ of dimension $2s(x) + 1$. The lattice can be equipped with a metric $d(\cdot, \cdot)$. The typical distance $d(x, y) = |x - y|$ between two neighboring points $x, y \in \mathbb{Z}^d$ in a realistic magnetic quantum system, as investigated in SP-STM, is typically in the subnanometer regime. With a finite subset $\Lambda \subset \mathbb{Z}^d$ we associate the tensor product space $\mathcal{H}_\Lambda = \bigotimes_{x\in\Lambda} \mathcal{H}_x$. The local physical observables are contained in the algebra of all bounded operators $\mathfrak{B}(\mathcal{H}_\Lambda)$ acting on $\mathcal{H}_\Lambda$. This is the C^*-algebra $\mathfrak{A}_\Lambda \cong \bigotimes_{x\in\Lambda} M_{2s(x)+1}$ in which M_n denote the algebra of $n \times n$ complex matrices. Physically, this can be interpreted as follows: at each lattice site x there is a particle with spin quantum number $s(x)$ and with $n = 2s(x) + 1 = dim(\mathcal{H}_x)$ degrees of freedom. The well-known spin operators S_i^{x}, S_i^{y} and S_i^{z} are elements of local sub-algebras $\mathfrak{A}_\Lambda$, where $i \in \Lambda$. While in mathematical physics the notation x and y is preferred for lattice points, the notion i and j is preferred in condensed matter theory. But this is just a matter of convention and we will use both notations. In every case, the lower index of a spin operator denotes its location (the site) in the lattice, while the upper index denotes the x-,y-, or z-component of the spin operator. i and j are seemingly well-suited for spin chains. If $\Lambda_1 \cap \Lambda_2 = \emptyset$, then

$\mathcal{H}_{\Lambda_1\cup\Lambda_2} = \mathcal{H}_{\Lambda_1} \otimes \mathcal{H}_{\Lambda_2}$ and $\mathfrak{A}_{\Lambda_1}$ is isomorphic to the C^*-subalgebra $\mathfrak{A}_{\Lambda_1} \otimes \hat{1}_{\Lambda_2}$ of $\mathfrak{A}_{\Lambda_1\cup\Lambda_2}$, where $\hat{1}_{\Lambda_2}$ denotes the identity operator on $\mathcal{H}_{\Lambda_2}$. If $\Lambda_1 \subseteq \Lambda_2$ then $\mathfrak{A}_{\Lambda_1} \subseteq \mathfrak{A}_{\Lambda_2}$ and operators with disjoint support commute, i.e., $[\mathfrak{A}_{\Lambda_1}, \mathfrak{A}_{\Lambda_2}] = 0$ whenever $\Lambda_1 \cap \Lambda_2 = \emptyset$. The so called "quasi-local algebra" is obtained by the union of all local algebras,

$$\mathfrak{A}_{\text{loc}} = \bigcup_{\Lambda\subset L} \mathfrak{A}_\Lambda. \tag{18}$$

$\mathfrak{A}_{\text{loc}}$ contains the strictly local operators. However, operators of the form

$$A = \sum_{i=1}^{\infty} e^{-ci} S_i^{\text{z}}, \tag{19}$$

where $c > 0$ and $\| A \| < \infty$ can occur in the thermodynamic limit, but they are not contained in $\mathfrak{A}_{\text{loc}}$. They are contained in the quantum spin algebra, which is obtained by taking the closure of the quasi-local algebra in the uniform operator topology:

$$\mathfrak{A} = \overline{\bigcup_{\Lambda\subset L} \mathfrak{A}_\Lambda}^{\|\cdot\|}. \tag{20}$$

This procedure means that we add limit points of uniformly converging Cauchy sequences to $\mathfrak{A}_{\text{loc}}$. There are interesting physical examples of long-range interactions, which provide such a limit point.

3.2 Magnetic interactions

An interaction Φ is defined to be a function from a finite subset $X \subset \mathbb{Z}^d$ into the hermitian elements of $\mathfrak{A}$ such that $\Phi(X) \in \mathfrak{A}_X$. The set of interactions forms a real vector space when equipped with the linear structure $(\Phi_1 + \Phi_2)(X) = \Phi_1(X) + \Phi_2(X)$ and $(\lambda\Phi)(X) = \lambda\Phi(X)$. This vector space can be equipped with a family of norms $\| \cdot \|_\xi$ and $B_\xi = \{\Phi; \| \Phi \|_\xi < \infty\}$ is a Banach space of interactions.

The interactions between the magnetic atoms is mostly described with the Heisenberg interaction Φ_{H} and the Dzyaloshinskii-Moriya interaction Φ_{DM}. Anisotropy energies Φ_{ani}, which are induced by the substrate, and external magnetic fields Φ_{B} are one-body interactions, i.e., they act on each single spin. The explicit expression for the Heisenberg term is as follows:

$$\Phi_{\text{H}}(\{x, y\}) = J_{xy} \vec{S}_x \cdot \vec{S}_y, \tag{21}$$

where $\vec{S}_x, \vec{S}_y$ denote vectors of spin operators at lattice sites $x, y \in L$ and J_{xy} is a constant which describes the interaction strength. For systems with strong spin-orbit coupling, the Dzyaloshinskii-Moriya interaction Φ_{DM} between two magnetic atoms at different lattice points also needs to be considered:

$$\Phi_{\mathrm{DM}}(\{x, y\}) = \vec{D}_{xy} \cdot \left[\vec{S}_x \times \vec{S}_y\right], \tag{22}$$

where $\vec{D}_{xy} \in \mathbb{R}^3$ is the DM-vector. Metallic and semiconducting substrates typically induce anisotropy energies of the form

$$\Phi_{\mathrm{ani}}(\{x\}) = K(S_x^{\mathrm{z}})^2 + E((S_x^{\mathrm{x}})^2 - (S_x^{\mathrm{y}})^2), \tag{23}$$

where K and E are constants and S_x^{x}, S_x^{y}, and S_x^{z} are the x, y, and z-components of the spin operator at site $x \in L$. In field-dependent SP-STM experiments, there is also an external magnetic field

$$\Phi_{\mathrm{B}}(\{x\}) = g\mu_{\mathrm{B}}\vec{B} \cdot \vec{S}_x, \tag{24}$$

where g is a gyromagnetic constant, μ_{B} the Bohr magneton and $\vec{B}$ the external magnetic field. Magnetic STM tips are experimentally used to investigate the spin structure. The corresponding interaction (action on the investigated magnetic atoms) is distinguished, because it can be switched on and off during a measurement by an experimentalist. We will use the notation H_{tip} instead of Φ_{tip}, because the interaction has a special character. If the spin system is not under study, this interaction is absent and does not enter into the Hamiltonian of the system. If a measurement is started, a tunneling current starts to flow between the tip and the magnetic atoms. The tunneling current perturbs the spin system locally and the corresponding interaction is often described with the modified Tersoff-Hamann model [87, 88]:

$$H_{\mathrm{tip}}(\{x\}) = gI_0\mathbb{P}e^{-2\kappa\sqrt{(x-x_0)^2+h^2}}\vec{m}_{\mathrm{tip}} \cdot \vec{S}_x \tag{25}$$

where g is a coupling constant, I_0 is the spin-polarized current averaged over the surface and $\mathbb{P}$ denotes the polarization of the tunneling current. $\vec{m}_{\mathrm{tip}}$ is a unit vector in the direction of the tip-magnetization. The position of the tip is given by the height h above the sample and the lattice point x_0. Thus we have $g, I_0, \mathbb{P} \in \mathbb{R}$. The notation

$$P = \lim_{\Lambda\to\infty} \sum_{X\subset\Lambda} H_{\mathrm{tip}}(X) \in \mathfrak{A}, \tag{26}$$

emphasizes the connection to the theoretical investigations of perturbations $P \in \mathfrak{A}$ in [44, 60]. Interesting analysis tools for stability properties of QSS

under local perturbations P are stated in Corollary 5.4.7. and Proposition 5.4.10. Of course, for different purposes we can also denote other interactions by the symbol P. The Hamiltonian of a subsystem $\Lambda \subset L$ is given by the sum of all interactions which are contained in Λ:

$$H_\Phi(\Lambda) = \sum_{X \subset \Lambda} \Phi(X). \tag{27}$$

Thus, in our applications to experiments, the interaction H_{tip} is *not* contained in the Hamiltonian $H_\Phi(\Lambda)$ and we can have $H_\Phi(\Lambda)$ or $H_\Phi(\Lambda) + H_{\text{tip}}$ (also $H_\Phi(\Lambda) + P$) to describe the physical situation. The dynamical evolution of an observable $A \in \mathfrak{A}_\Lambda$ for a finite-dimensional system with Hamiltonian $H_\Phi(\Lambda) \in \mathfrak{A}_\Lambda$ can be described by the Heisenberg relations

$$\tau_t^\Lambda : \mathfrak{A}_\Lambda \to \mathfrak{A}_\Lambda, \quad A \mapsto \tau_t^\Lambda(A) = e^{\frac{itH_\Phi(\Lambda)}{\hbar}} A e^{-\frac{itH_\Phi(\Lambda)}{\hbar}}. \tag{28}$$

Thus, the map $t \in \mathbb{R} \mapsto \tau_t^\Lambda$ is a one-parameter group of *-automorphisms of the matrix algebra $\mathfrak{A}_\Lambda$. The generator of the time evolution of an infinite system is in general not an element of $\mathfrak{A}$. Nevertheless, classes of interactions exist for which the dynamics of the infinite system is given by a strongly continuous one-parameter group of *-automorphisms and therefore the system can be described by a C^*-dynamical system $(\mathfrak{A}, \tau)$. A generator of this group is given by a derivation, i.e., a linear operator δ defined on the domain $D(\delta) = \mathfrak{A}_{loc}$. The action of δ is given by

$$\delta(A) = i \sum_{X \cap \Lambda \neq \emptyset} [\Phi(X), A], \qquad A \in \mathfrak{A}_\Lambda. \tag{29}$$

For finite-dimensional systems, there is a connection to the Heisenberg dynamics:

$$A(t) = e^{i\frac{t}{\hbar}H_\Phi(\Lambda)} A e^{-i\frac{t}{\hbar}H_\Phi(\Lambda)} = e^{\frac{t}{\hbar}\delta}(A) = \tau_t^\Lambda(A). \tag{30}$$

The norm-closure $\bar{\delta}$ generates a strongly-continuous one-parameter group of *-automorphisms for a large class of interactions, which are given in Theorem 6.2.4. [44] (see also the appendix). Thus, as a generator the derivation plays the role of the Hamiltonian in the ordinary language of quantum mechanics. It is now import to know that for finite-range interactions, which are commonly used to model realistic magnetic quantum systems, the group τ^Λ converges strongly to a group of *-automorphisms τ, i.e.,

$$\lim_{\Lambda \to \infty} \parallel \tau_t^\Lambda(A) - \tau_t(A) \parallel = 0 \tag{31}$$

for all $A \in \mathfrak{A}$ and $t \in \mathbb{R}$, see for example Theorem 6.2.11. [44]. The group τ generates the time evolution over $\mathfrak{A}$.

If a hermitian bounded operator $P = P^*$, $P \in \mathfrak{A}_\Lambda$, is added to the Hamiltonian $H_\Phi(\Lambda)$, i.e., $H_\Phi(\Lambda) \to H_\Phi(\Lambda) + P$, a perturbed group $\tau_t^{\Lambda P}$ is generated and we have

$$\tau_t^{\Lambda P} : \mathfrak{A}_\Lambda \to \mathfrak{A}_\Lambda, \quad A \mapsto \tau_t^{\Lambda P}(A) = e^{\frac{it(H_\Phi(\Lambda)+P)}{\hbar}} A\, e^{-\frac{it(H_\Phi(\Lambda)+P)}{\hbar}}. \tag{32}$$

A state ω_Λ on the finite-dimensional matrix algebra $\mathfrak{A}_\Lambda$ is given by a density matrix ρ_Λ:

$$\omega_\Lambda : \mathfrak{A}_\Lambda \to \mathbb{C}, \quad A \mapsto \omega_\Lambda(A) = Tr(\rho_\Lambda A), \quad A \in \mathfrak{A}_\Lambda. \tag{33}$$

3.3 Thermodynamic equilibrium and KMS states

A (τ, β)-KMS state ω^β is defined to be a state, which satisfies the *KMS condition*

$$\omega^\beta(A\tau_{i\beta}(B)) = \omega^\beta(BA), \tag{34}$$

for $\beta \in \mathbb{R}$ and $A, B \in \mathfrak{A}$. A mathematical precise definition requires more technical fineness and is given by Definition 5.3.1. in [44] (see appendix). However, the formula (34) is the same. There are several general justifications of KMS states as thermodynamic equilibrium states [44]. It is important to mention that for QSS in the thermodynamic limit several different states can exist satisfying the KMS condition (34), i.e., there are coexisting different thermodynamic equilibrium states for the same system at a fixed temperature. The equilibrium states at each fixed temperature form a convex set with the extremal points corresponding to pure phases and the mixed states to mixtures of phases. This immediately motivates much of the analysis of decomposition theory, invariant states, periodic states, almost periodic states, etc., described in [44]. The *local Gibbs state* ω_Λ^β over $\mathfrak{A}_\Lambda$ at inverse temperature β is defined by the expectation values

$$\omega_\Lambda^\beta(A) = \frac{Tr(e^{-\beta H_\Phi(\Lambda)} A)}{Tr(e^{-\beta H_\Phi(\Lambda)})}. \tag{35}$$

It is also the single and unique (τ^Λ, β)-KMS state, because $\mathfrak{H}_\Lambda$ is finite dimensional. These states are invariant under the action of τ^Λ, i.e., $\omega_\Lambda^\beta(\tau_t(A)) = \omega_\Lambda^\beta(A)$. Perturbed KMS states $\omega_\Lambda^{\beta P}$ are $(\tau^{\Lambda P}, \beta)$-KMS states and the associated expectation values on a finite-dimensional system are given by

$$\omega_\Lambda^{\beta P}(A) = \frac{Tr(e^{-\beta(H_\Phi(\Lambda)+P)} A)}{Tr(e^{-\beta(H_\Phi(\Lambda)+P)})} \quad A \in \mathfrak{A}_\Lambda. \tag{36}$$

If the thermodynamic limit is a suitable approximation for the magnetic particle, as indicated in SP-STM experiments of magnetic nano-islands [43,

75], the local Gibbs state is not always the best and unique description for a QSS in thermodynamic equilibrium. This is our motivation for the introduction of approximated KMS states on finite-dimensional systems in the next section. However, this presupposes an investigation of KMS states on infinite-dimensional systems. In preparation for a theorem for KMS states on infinite-dimensional systems we will briefly discuss the entropy of a system. The next proposition establishes, that the KMS property is preserved in the thermodynamic limit.

Proposition 3.1. *([44], 6.2.17.): Let Φ be an interaction of a quantum spin system, ω_Λ^β the local Gibbs state and τ^Λ the corresponding local automorphism group. Assume that τ^Λ converges strongly to an automorphism group τ, i.e.,*

$$\lim_{\Lambda\to\infty} \parallel \tau_t^\Lambda(A) - \tau_t(A) \parallel = 0 \tag{37}$$

for all $A \in \mathfrak{A}$ and $t \in \mathbb{R}$.

It follows that every thermodynamic limit point ω^β of ω_Λ^β is a (τ, β)-KMS state over $\mathfrak{A}$.

The *maximum entropy principle* describes equilibrium as the state of maximum disorder compatible with a given energy or particle density, etc. Each state ω_Λ on a local subalgebra $\mathfrak{A}_\Lambda$ is determined by a unique density matrix ρ_Λ on $\mathfrak{H}_\Lambda$ and we define the (von Neumann) *entropy* $S_\Lambda(\omega_\Lambda)$ of ω_Λ as

$$S_\Lambda(\omega_\Lambda) \doteq -\operatorname{Tr}_{\mathfrak{H}_\Lambda}(\rho_\Lambda \log \rho_\Lambda). \tag{38}$$

The function

$$\omega_\Lambda \in E_{\mathfrak{A}_\Lambda} \mapsto \omega_\Lambda(H_\Phi(\Lambda)) - \beta^{-1} S_\Lambda(\omega_\Lambda) \tag{39}$$

is called the *free energy* of the spin system at inverse temperature β. The local Gibbs state ω_Λ^β is the unique state which minimizes the free energy. However, the occurrence of multiple magnetic equilibrium states at a fixed temperature indicates that a complete description of equilibrium phenomena requires extensions of this point of view. The algebraic investigation of KMS states of QSS in the thermodynamic limit has provided comprehensive results in this direction, which are of paramount importance for an accurate analysis of the equilibrium phenomena of magnetic quantum systems. In order to extend the maximum entropy principle accordingly, it is necessary to analyze properties of the entropy $S_\Lambda(\omega)$. However, we will just state the final results and refer the reader to the chapter 6.2.3. of the book [44] for the details and proofs.

Definition 3.2. *([44] 6.2.27): Let $S_\Lambda(\omega)$ denote the entropy of the subsystem Λ of the QSS in the state $\omega \in E_{\mathfrak{A}}$ The corresponding conditional entropy $\tilde{S}_\Lambda(\omega)$ is defined by*

$$\tilde{S}_\Lambda(\omega) = \lim_{\Lambda' \to \Lambda^c} (S_{\Lambda \cup \Lambda'}(\omega) - S_{\Lambda'}(\omega)). \tag{40}$$

If $\Lambda \subset \Lambda'$ is a subsystem, then the energy of interaction across the border of Λ and $\Lambda' \setminus \Lambda$ is given by

$$W_\Phi(\Lambda, \Lambda') = \sum_{\substack{X \cap \Lambda \neq \emptyset, X \cap \Lambda^c \neq \emptyset, \\ X \subseteq \Lambda'}} \Phi(X). \tag{41}$$

The *surface energy* $W_\Phi(\Lambda)$ is now defined by

$$W_\Phi(\Lambda) \doteq \lim_{\Lambda' \to \infty} W_\Phi(\Lambda, \Lambda'), \tag{42}$$

if this expression is well-defined, i.e., the limit exists in norm $\| W_\Phi(\Lambda) \| < \infty$. The surface energy enters the next definition and is used in the derivation of approximated KMS states in the next subsection.

Example:
The surface energy $W_\Phi(\{j\})$ of a point j which has two nearest neighboring points $j-1$ and $j+1$ in a (one-dimensional) spin chain with nearest-neighbor Heisenberg interaction and Hamiltonian

$$H = J \sum_i \vec{S}_i \cdot \vec{S}_{i+1} + \sum_i \left(K (S_i^{\mathrm{z}})^2 + E((S_i^{\mathrm{x}})^2 - (S_i^{\mathrm{y}})^2) + \vec{B} \vec{S}_i \right) \tag{43}$$

is given by

$$W_\Phi(\{j\}) = J\big(\vec{S}_j \cdot \vec{S}_{j+1} + \vec{S}_j \cdot \vec{S}_{j-1}\big). \tag{44}$$

Thus, the surface energy consists of the interactions which connect the point $j \in L$ with the outer regions.

Next we give a definition which relates KMS states on an infinite system and the local Gibbs state on a finite system. In the original definition of the "*Gibbs condition with respect to* $\beta\Phi$" there are two conditions which have to be satisfied. However, one of them is slightly too technical and not of direct use for our purpose. Therefore, we state the definition with just the one condition which is of interest for us. For completeness we mention that the other condition states that ω has to be faithful, i.e., Ω_ω is separating for $\pi_\omega(\mathfrak{A})''$. For the mathematical properties of the weak closure $\pi_\omega(\mathfrak{A})''$ of $\mathfrak{A}$ and the definition of a separating vector we refer, one more time, to [44].

Definition 3.3. *([44], 6.2.16.): Let Φ be an interaction of a QSS such that the surface energy $W_\Phi(\Lambda)$ is a well-defined element of $\mathfrak{A}$ for all $\Lambda \subset \mathbb{Z}^d$. A state ω over $\mathfrak{A}$ is defined to satisfy the Gibbs condition with respect to $\beta\Phi$ if the following condition is fulfilled:*

1. *$\omega^{P_\Lambda} = \omega_\Lambda^\beta \otimes \widetilde{\omega}$ for all $\Lambda \subset \mathbb{Z}^d$, where ω_Λ^β is the local Gibbs state, $\widetilde{\omega}$ is a state over $\mathfrak{A}_{\Lambda^c}$, ω^{P_Λ} is the perturbation of ω constructed in Theorem 5.4.4 [44], and $P_\Lambda = \beta W_\Phi(\Lambda)$.*

The foregoing definition enters the next theorem and is of use for the derivation of the approximated KMS states in the next subsection. The next Theorem is valid for a large class of interactions and states the equivalence of the KMS condition and the extended maximum entropy principle, which is also referred to as *local thermodynamic stability.*

Theorem 3.4. *([44] 6.2.37): Let Φ be an interaction of a QSS satisfying*

$$\| \Phi \|_\xi = \sum_{n \geq 0} e^{\xi n} \Big(\sup_{x \in L} \sum_{\substack{x \ni X \\ |X| = n+1}} \| \Phi(X) \| \Big) < \infty \tag{45}$$

for some $\xi > 0$ and let τ be the associated automorphism group (see Theorem 6.2.4. [44])

The following conditions are equivalent for each $\beta \in \mathbb{R}$:

1. *ω satisfies the Gibbs condition with respect to $\beta\Phi$,*
2. *ω is a (τ, β)-KMS state,*
3. *ω satisfies the maximum entropy principle*

$$\tilde{S}_\Lambda(\omega) - \beta\omega(\tilde{H}_\Phi(\Lambda)) = \sup_{\omega' \in C_\Lambda^\omega} \{\tilde{S}_\Lambda(\omega') - \beta\omega'(\tilde{H}_\Phi(\Lambda))\} \tag{46}$$

for all $\Lambda \subset L$, where $\tilde{S}_\Lambda$ is the conditional entropy, $\tilde{H}_\Phi(\Lambda) = H_\Phi(\Lambda) + W_\Phi(\Lambda)$ the conditional energy, and

$$C_\Lambda^\omega = \{\omega'; \omega' \in E_\mathfrak{A}, \omega'|_{\mathfrak{A}_{\Lambda^c}} = \omega|_{\mathfrak{A}_{\Lambda^c}}\}. \tag{47}$$

Thus, if we identify different KMS states for a certain system at fixed temperature, we know that these states are thermodynamic equilibrium states and by the satisfaction of the Gibbs condition with respect to $\beta\Phi$ we can derive approximated KMS states in the next subsection. As an example for the occurrence of multiple KMS states we reflect Theorem 6.2.49. of [44]:

Theorem 3.5. *([44] 6.2.49.): Let Φ denote the ferromagnetic, anisotropic Heisenberg interaction*

$$\Phi(\{x,y\}) = -J_{xy}\big(\gamma(S_x^{\mathrm{x}}S_y^{\mathrm{x}} + S_x^{\mathrm{y}}S_y^{\mathrm{y}}) + S_x^{\mathrm{z}}S_y^{\mathrm{z}}\big) \tag{48}$$

with nearest-neighbor coupling $J_{xy} > 0$, zero external magnetic field and $\gamma \in (-1,1)$. Assume $dim(L) > 2$ and

$$j = \inf_{x,y} J_{xy} > 0. \tag{49}$$

It follows that there is a $\beta_c > 0$ such that there exists at least two extremal (τ,β)-KMS states for all $\beta > \beta_c$.

Note that this result does not establish nonuniqueness of the KMS states for the isotropic model, i.e., for the case $\gamma = 1$. In fact if $dim(L) = 2$ the criterion of nonzero spontaneous magnetization, $\omega^\beta(S_x^{\mathrm{z}}) \neq 0$, fails by symmetry arguments [44].

3.4 Mean-field type approximated KMS-states and $\mathfrak{F}_\Lambda$

A high density data storage device requires very stable magnetization structures, such that the stored information will not be lost after some time. The algebraic reformulation of QSS led to the conclusion that the states which possess a maximum of thermodynamic stability are KMS states. A data storage unit certainly requires at least two different stable magnetization structures, which means that at least two different extremal KMS states should exist. However, the exact analysis of KMS states can only be performed in the thermodynamic limit, where the numerical methods often fail to work. Therefore, we introduce approximated KMS states on finite-dimensional systems such that they can be handled with a numerical method.

The well-known density matrix $\rho = e^{-\beta H}$ describes a system with Hamiltonian H, which is in equilibrium at inverse temperature β. It is the commonly used density matrix for numerical simulations in modern condensed matter theory. Thus, the usage of the density matrix $\rho = e^{-\beta H}$ to model a system in equilibrium sometimes only matches a specific case. The possible other equilibrium states are not correctly described by $\rho = e^{-\beta H}$. Approximated KMS states are represented by density operators of finite-dimensional systems and obtained by adding a further self-adjoint operator R_Λ^ω to the Hamiltonian. Thus, the operator R_Λ^ω is responsible for the generation of the different approximated equilibrium states.

Mean-field type approximated KMS states

We are searching for a map $\mathfrak{R}^{\omega}_{\Lambda}$ which maps a KMS state ω^{β} of the infinite-dimensional system to a state $\omega^{\beta}_{R^{\omega}_{\Lambda}}$, which approximates ω^{β} on a finite-dimensional system $\mathfrak{A}_{\Lambda}$. The index ω on $\mathfrak{R}^{\omega}_{\Lambda}$ means that the map depends on the state to which it is applied. We have

$$\mathfrak{R}^{\omega}_{\Lambda} : E_{\mathfrak{A}} \longrightarrow E_{\mathfrak{A}_{\Lambda}}, \quad \omega^{\beta} \mapsto \mathfrak{R}^{\omega}_{\Lambda}(\omega^{\beta}). \tag{50}$$

Since $\rho_{\Lambda} = e^{-\beta H_{\Phi}(\Lambda)}$ is the density matrix of the unique (τ^{Λ}, β)-KMS state ω^{β}_{Λ}, we also have to modify the automorphism group τ^{Λ}. Hence, we also need a map $\breve{R}^{\omega}_{\Lambda}$ on the space $\mathrm{Aut}(\mathfrak{A})$ of the automorphisms on $\mathfrak{A}$ to $\mathrm{Aut}(\mathfrak{A}_{\Lambda})$. This means

$$\breve{\mathfrak{R}}^{\omega}_{\Lambda} : \mathrm{Aut}(\mathfrak{A}) \longrightarrow \mathrm{Aut}(\mathfrak{A}_{\Lambda}), \quad \tau \mapsto \breve{\mathfrak{R}}^{\omega}_{\Lambda}(\tau). \tag{51}$$

By Theorem 3.4 (6.2.37 [44]) and Definition 3.3 (6.2.37 [44]) we know that for a KMS state ω^{β} on the infinite system, we have $\omega^{\beta P_{\Lambda}} = \omega^{\beta}_{\Lambda} \otimes \widetilde{\omega}$ if $P_{\Lambda} = \beta W_{\Phi}(\Lambda)$. For our purpose we propose a mean-field type operator R^{ω}_{Λ} which is then added to $W_{\Phi}(\Lambda)$, such that we have $\omega^{\beta P^{\omega}_{\Lambda}}$, where $P^{\omega}_{\Lambda} = \beta\big(W_{\Phi}(\Lambda) + R^{\omega}_{\Lambda}\big)$. We suggest that

$$R^{\omega}_{\Lambda} = \sum_{\substack{X, X'; \Phi(X \cup X') \neq \hat{0} \\ X \subseteq \Lambda, X' \cap \Lambda = \emptyset}} \Phi(X) \omega^{\beta}_{i}(\tilde{\Phi}_{X}(X')), \tag{52}$$

where $\hat{0}$ is the zero operator and $\tilde{\Phi}_{X}(X')$ means that the spin operators in $\Phi(X \cup X')$, which are strictly located in X, are replaced by the unit operator. For example, if $\Phi(\{i,j\}) = S^{z}_{i} \otimes S^{z}_{j}$ we have $\tilde{\Phi}_{\{i\}}(\{j\}) = \hat{1}_{i} \otimes S^{z}_{j}$. Thus, the spins outside the region Λ act as a field on the spins which are located in Λ. Our map is now given by

$$\omega^{\beta} \mapsto \mathfrak{R}^{\omega}_{\Lambda}(\omega^{\beta}) = \omega^{\beta P^{\omega}_{\Lambda}} \tag{53}$$

and by the Gibbs condition with respect to $\beta\Phi$, Theorem 3.4 (6.2.37 [44]), and Definition 3.3 (6.2.37 [44]), we obtain

$$\mathfrak{R}^{\omega}_{\Lambda}(\omega^{\beta}) = \omega^{\beta}_{R^{\omega}_{\Lambda}} \otimes \widetilde{\omega}, \tag{54}$$

where

$$\omega^{\beta}_{R^{\omega}_{\Lambda}}(A) = \frac{Tr(e^{-\beta(H_{\Phi}(\Lambda) + R^{\omega}_{\Lambda})} A)}{Tr(e^{-\beta(H_{\Phi}(\Lambda) + R^{\omega}_{\Lambda})})} \tag{55}$$

is the approximated KMS state on $\mathfrak{A}_{\Lambda}$. For the map $\breve{\mathfrak{R}}^{\omega}_{\Lambda}$ on $\mathrm{Aut}(\mathfrak{A})$ we have accordingly

$$\breve{\mathfrak{R}}^{\omega}_{\Lambda}(\tau) = \tau^{R^{\omega}_{\Lambda}} \otimes \tilde{\tau}, \tag{56}$$

where $\tilde{\tau}$ acts on $\mathfrak{A}_{\Lambda^c}$, $\tau_t^{R_\Lambda^\omega} : \mathfrak{A}_\Lambda \longrightarrow \mathfrak{A}_\Lambda$ and

$$\tau_t^{R_\Lambda^\omega}(A) = e^{i\frac{t}{\hbar}(H_\Phi(\Lambda)+R_\Lambda^\omega)} A e^{-i\frac{t}{\hbar}(H_\Phi(\Lambda)+R_\Lambda^\omega)}, \quad A \in \mathfrak{A}_\Lambda, \tag{57}$$

is the automorphism group corresponding to the approximated KMS state $\omega^\beta_{R_\Lambda^\omega}$, i.e., $\omega^\beta_{R_\Lambda^\omega}$ is the unique $(\tau^{R_\Lambda^\omega}, \beta)$-KMS state.

Example I:
If $\Lambda = \{i\}$ contains only the single site i of a spin chain with nearest-neighbor Ising interaction, we have

$$R_\Lambda^\omega = S_i^z(J_{i,i-1}\omega^\beta(S_{i-1}^z) + J_{i,i+1}\omega^\beta(S_{i+1}^z)). \tag{58}$$

Mathematically, the action of the spins outside Λ has the same form like an additional local magnetic field, which acts individually on the spins in Λ.

Example II:
Assume that we have a QSS which is in the KMS state ω^β and the spin-component S_x^z at site $x \in \Lambda$ is forced out of equilibrium by some kind of a local magnetic field acting only on site x, given by $P = B^z S_x^z$. Then we model the relaxation process with the function

$$t \mapsto \omega^{\beta P}_{R_\Lambda^\omega}(\tau_t^{R_\Lambda^\omega}(S_x^z)) = \frac{Tr(e^{-\beta(H_\Phi(\Lambda)+R_\Lambda^\omega+B^z S_x^z)} e^{i\frac{t}{\hbar}(H_\Phi(\Lambda)+R_\Lambda^\omega)} S_x^z e^{-i\frac{t}{\hbar}(H_\Phi(\Lambda)+R_\Lambda^\omega)})}{Tr(e^{-\beta(H_\Phi(\Lambda)+R_\Lambda^\omega+B^z S_x^z)})}. \tag{59}$$

Evidently, the local magnetic field $P = B^z S_x^z$ is only included in the approximated KMS state and not in the automorphism group and can of course also be given by the modified Tersoff-Hamann model.

Example III:
We calculate $\omega^{\beta P}_{R_\Lambda^{\omega_i}}(\tau_t^{R_\Lambda^{\omega_i}}(S_x^z))$ for the two dimensional, nearest-neighbor, anisotropic and ferromagnetic Heisenberg interaction. ω_i^β, $i = 1, 2, 3$, shall denote three different KMS states. From Theorem 3.5 ([44] 6.2.49.), we know that at least two extremal (τ, β)-KMS states exist for a sufficiently low temperature. At least one of our states can be a superposition of the two different extremal KMS states. However, we don't know the absolute temperature and we are therefore just interested in an exemplary behavior of the dynamical evolution. We are not able to estimate $\omega_i^\beta(S_y^z)$ exactly and assume that the values of $\omega_i^\beta(S_y^z)$ for all spins outside Λ take the values 0 for the KMS state $i = 1$, -0.006 for $i = 2$ and $0,006$ for $i = 3$. The cases $i = 2$ and $i = 3$ provide very similar dynamical evolutions and we concentrate on $i = 1$ and $i = 2$ for simplicity. Fig. 1 (a) shows the short-time behavior of the relaxation processes $\omega^{\beta P}_{R_\Lambda^\omega}(\tau_t^{R_\Lambda^\omega}(S_x^z))$ for two different equilibrium states $i = 1, 2$. In both

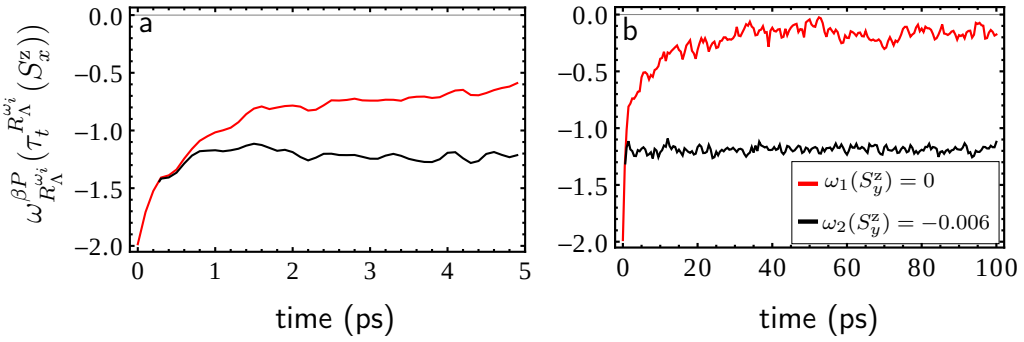

Figure 1: Relaxation processes for two different approximated KMS states $i = 1, 2$. (a) The short-time behavior is similar until ≈ 0.6 ps. (b) It can be seen that the dynamics of the two different equilibrium states stabilizes at two different magnetization directions.

initial states the z-component of the spin is forced into the $|-2\rangle$ state due to the perturbation $P = B^z S_x^z$. In fig. 1 (b) one can see that the dynamics for the two different initial states stabilizes at the two different magnetization directions $\langle S_x^z \rangle_1 \approx -0.2$ and $\langle S_x^z \rangle_1 \approx -1.2$. This result is partially desired. However, the dynamics of the third approximated KMS state $\omega^{\beta}_{R^{\omega_3}_{\Lambda}}$ (which is not shown on this fig.) is very similar to the dynamics of the second state $\omega^{\beta}_{R^{\omega_2}_{\Lambda}}$ and stabilizes at $\langle S_x^z \rangle_1 \approx -1.3$. This seems to be an error, which is caused by finite size effects and the numerical method of exact diagonalization. A stabilization of the third state at $\langle S_x^z \rangle_1 \approx +1.2$ is more desirable. For future work we suggest to use the Lindblad-Master equation for the dynamics of approximated KMS states,

$$\dot{\rho} = -\frac{i}{\hbar}[H, \rho] + \sum_{n,m=1}^{N^2-1} h_{nm}\big(L_n \rho L_m^{\dagger} - \frac{1}{2}(\rho L_m^{\dagger} L_n + L_m^{\dagger} L_n \rho)\big), \tag{60}$$

where ρ is the density matrix of the approximated KMS state, H the Hamiltonian, h_{mn} are constants and L_m are operators.

The bound ϵ for the map $\mathfrak{F}_\Lambda$.

We are now interested in a related question. We want to know in which cases the density matrix $\rho = e^{-\beta H}$ is well-suited to describe the equilibrium cases when several KMS states exist. Thus we are interested in the radius ϵ on state space, which provides the distance between a KMS state ω^{β} of the infinite system and a state which uses $\rho = e^{-\beta H}$ to model equilibrium. We use the sup-norm eq. (8) and define

$$\mathfrak{F}_\Lambda(\omega^{\beta}) \doteq \parallel \omega^{\beta} - \omega^{\beta}_{\Lambda} \otimes \tilde{\omega} \parallel \leqslant \epsilon, \tag{61}$$

where $\tilde{\omega}$ is some state on $\mathfrak{A}_{\Lambda^c}$. Theorem 5.4.4. [44] enables us to estimate [85]

$$\epsilon = \frac{2\beta \parallel W_\Phi(\Lambda) \parallel}{1 - 2\beta \parallel W_\Phi(\Lambda) \parallel}, \tag{62}$$

where $W_\Phi(\Lambda)$ is the surface energy as defined above.

3.5 Lieb-Robinson bounds

The theory of QSS is not based on relativity theory, which has the consequence that the speed of light is not the limit speed in this theory. Indeed, the signal speed in QSS is infinite. However, Lieb and Robinson found a method to show, that outside an effective light-cone the signal propagation is exponentially damped. A Lieb-Robinson bound is a mathematical bound on velocities in the non-relativistic theory of QSS, which is in analogy to the speed of light as maximum velocity in relativity theory. We will first present simplified formulas for the latest, most general bound [89], while the proof of our bound is shifted to the end of this subsection.

Roughly speaking, if the observables S_j^z and $S_i^z(t)$ commute, i.e.,

$$\parallel [S_i^z(t), S_j^z] \parallel = 0, \tag{63}$$

it is implied that no signal can propagate from the lattice site i to the site j within the time t. Certainly one can construct interactions, such that the foregoing sentence is not true. To eliminate such possibilities, one uses Lieb-Robinson bounds which provide an upper bound on this commutator in the more general form

$$C_A(t, X) = \sup_{B \in \mathfrak{A}_X; \|B\|=1} \parallel [B, \tau_t(A)] \parallel, \tag{64}$$

where $A \in \mathfrak{A}_Y$ and $\mathfrak{A}_Y$ is the C^*-algebra associated with $Y \subset L$. $C_A(t, X)$ is a quantitative measure for the amount of information, which is propagated from Y to X at time t. If this number is close to zero and much smaller than the norm of A for all times t, with $0 \leq t \leq t'$, then there can be no significant information transport from Y to X within the time t'.

Now we will present a simplified formula [85, 86] for the latest, most general bound [89]. Eq. (68) and (69), the next steps and the intermediate result eq. (79) are taken from [89], but our iteration [85, 86] provides:

$$C_A(t, X) \leq 2 \parallel A \parallel \sum_{\gamma; X \to Y} \frac{|2t|^{L(\gamma)}}{L(\gamma)!} w(\gamma) \doteq \mathfrak{B}(t), \tag{65}$$

where $L(\gamma)$ is the length of the path γ from X to Y and $w(\gamma)$ is the weight of the path, defined in eq. (81). The proof states, that only interactions on the sets $Z \in \partial X$ of the boundary of X, eq. (70), contribute and the bound is clearly independent of one-body interactions, e.g., external magnetic fields, anisotropy energies and the modified Tersoff-Hamann model-type interaction. In a lattice of dimension d the number of paths with length L is bounded by $(2(2d-1))^L$. For nearest neighbor Heisenberg interaction the bound $\mathfrak{B}$ can be simplified to [85, 86]

$$\| [S_i^z(t), S_j^z(t')] \| \leq s^2 \left(\frac{v|t-t'|}{|i-j|} \right)^{|i-j|}, \tag{66}$$

with $v = 4e(2d-1)Js^2$, where d is the dimension of the lattice and s is the spin quantum number. In contrast to the old bound $\mathfrak{L}$ [44], the new bound $\mathfrak{B}$ is independent of the arbitrary choice of a number $\xi > 0$ and there is no factor $|X|(2s+1)^{2|X|}e^{\xi D(X)}$ (see eq. 110) which provides an unnecessary increase of the corresponding limit speed. The specific bound in [90] for the XY-model is multiplied with the square n^2 of the chain length n, which is certainly a disadvantage for a large chain length. The general bounds are independent of the undesired n^2-dependence. The removal of this n^2 dependency in [91] is a further example, where a better mathematical technique can improve a Lieb-Robinson bound.

Now we will state the proof for our bound $\mathfrak{B}$, in which the starting points eq. (68) and (69), the next steps, and the intermediate result eq. (79) are taken from [89]. We assume that each algebra $\mathfrak{A}_X$ has a time evolution as a strongly continuous one-parameter group of *-automorphisms, which is checked by Theorem 6.2.4. in [44]. There is an integral equation for the full time evolution τ_t of $A \in \mathfrak{A}_\Lambda$:

$$\tau_t(A) = A + i \sum_{X \cap \Lambda \neq \emptyset} \int_0^t dt' \tau_{t'}([\Phi(X), \tau_{t-t'}^{\text{ultra}}(A)]), \tag{67}$$

where $\tau_t^{\text{ultra}}(\mathfrak{A}_\Lambda) \subset \mathfrak{A}_\Lambda$. An iteration provides a solution under rather general conditions for the interaction. We have

$$\begin{aligned} C_A(t,X) &= \sup_{B \in \mathfrak{A}_X; \|B\|=1} \| [B, \tau_t(A)] \| \\ &= \sup_{B \in \mathfrak{A}_X; \|B\|=1} \| [\tau_{-t}\tau_t^X(B), A] \| . \end{aligned} \tag{68}$$

There is a differential equation for $f(t) = [\tau_{-t}\tau_t^X(B), A]$:

$$\frac{1}{i}\frac{d}{dt} f(t) = \sum_{Z \in \partial X} [[\tau_{-t}(\Phi(Z)), \tau_{-t}\tau_t^X(B)], A], \tag{69}$$

where ∂X is the boundary of X, which is given by

$$\partial X = \{Z \subset L; Z \cap X \neq \emptyset, Z \nsubseteq X\}. \tag{70}$$

The Jacobi identity for double commutators states

$$\begin{aligned}[[\tau_{-t}(\Phi(Z)), \tau_{-t}\tau_t^X(B)], A] = &[[\tau_{-t}(\Phi(Z)), A], \tau_{-t}\tau_t^X(B)] \\ &+ [\tau_{-t}(\Phi(Z)), \underbrace{[\tau_{-t}\tau_t^X(B), A]}_{f(t)}],\end{aligned} \tag{71}$$

and we define

$$a(t) \doteq \sum_{Z \in \partial X} [[\tau_{-t}(\Phi(Z)), A], \tau_{-t}\tau_t^X(B)]. \tag{72}$$

The differential equation for f can now be expressed as

$$\frac{1}{i}\frac{d}{dt}f(t) = a(t) + [H(t), f(t)]. \tag{73}$$

We have

$$\frac{1}{i}\frac{d}{dt}U(t) = H(t)U(t), \quad U(0) = 1 \tag{74}$$

and define

$$g(t) \doteq U^{-1}(t)f(t)U(t). \tag{75}$$

A relation between g and a is obtained by

$$\begin{aligned}\frac{1}{i}\frac{d}{dt}g(t) =& U^{-1}(t)\frac{1}{i}\frac{d}{dt}f(t)U(t) \\ &- U^{-1}(t)[H(t), f(t)]U(t) \\ =& U^{-1}(t)a(t)U(t).\end{aligned} \tag{76}$$

It follows that

$$g(t) = g(0) + \int_0^t ds U^{-1}(s)a(s)U(s) \tag{77}$$

and

$$f(t) = f(0) + U(t)\int_0^t ds U^{-1}(s)a(s)U(s)U^{-1}(t). \tag{78}$$

Now we can state an inequality for $C_A(t, X)$, which crucially depends on a:

$$C_A(t, X) \leq C_A(0, X) + 2\sum_{Z \in \partial X}\int_0^{|t|} ds\, C_A(s, Z) \parallel \Phi(Z) \parallel . \tag{79}$$

The iteration involves finite sequences of sets $Z_1, ..., Z_n$ with

$$Z_1 \in \partial X, Z_2 \in \partial Z_1, ..., Z_n \in \partial Z_{n-1}, \quad Z_n \cap Y \neq \emptyset, \tag{80}$$

for $A \in \mathfrak{A}_Y$. Such a sequence is called a path γ of length $L(\gamma) = n$ from X to Y. The weight of a path is defined by

$$w(\gamma) \doteq \prod_{i=1}^{n} \parallel \Phi(Z_i) \parallel, \tag{81}$$

which enables us to estimate the simplified formula for the bound.

4 Real-time dynamics of single magnetic atoms

First, the functionality and measurement process of a spin-polarized scanning tunneling microscope will be described by a Hamiltonian framework. This framework serves then as a starting point for an application of the C^*-approach to QSM for the description of SP-STM. A general principle will be introduced which provides the foundation of the structural application as well as the interface between the algebraic techniques and the experimental investigations. It states that the experimentalist basically decides whether the C^*-dynamical system $(\mathfrak{A}, \tau)$ or $(\mathfrak{A}, \tau^P)$ describes the actual real situation. The perturbation P describes the action of the magnetic tip on the investigated sample or it can also be the interaction between the tip and sample. Examples can be chosen to be the modified Tersoff-Hamann model or a model consisting of creation and annihilation operators. Using the numerical method of "exact diagonalization" we calculate the dynamics of single quantum spins during and after SP-STM measurement/manipulation processes at finite temperatures. A comparison with experimental data obtained from Fe adatoms on InSb and Co adatoms on Pt(111) shows good agreement and verifies the validity of our model. For simplicity in this section we will neglect the notation that the Hamiltonian $H_\Phi(\Lambda)$ depends on Φ and Λ. The same will be done for the local Gibbs states and the automorphism groups. Thus, we will just write H, ω^β, $\omega^{\beta P}$, τ and τ^P instead of $H_\Phi(\Lambda)$, ω^β_Λ, $\omega^{\beta P}_\Lambda$, τ_Λ, and τ^P_Λ.

4.1 Spin-polarized scanning tunneling microscopy

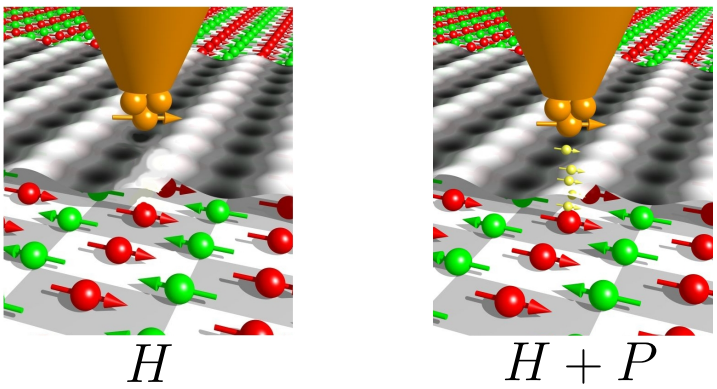

Figure 2: H describes the free system and $H + P$ describes the perturbed system, i.e. the system with interaction between the tip and the sample.

The SP-STM set-up of a finite-dimensional system is approximated by (in

general) two different Hamiltonians in our approach. There is a Hamiltonian H for the free QSS (Fig. 2, left) and, if a measurement is started (at $t = 0$), we get an additional hermitian operator P for the interaction of the tip with the sample (Fig. 2, right), i.e., the Hamiltonian $H + P$. We will use the automorphism group τ with Hamiltonian H

$$\tau_t : \mathfrak{A} \to \mathfrak{A}, \quad A \mapsto \tau_t(A) = e^{\frac{itH}{\hbar}} A\, e^{-\frac{itH}{\hbar}}. \tag{82}$$

to describe the free QSS without any interaction with the magnetic tip. When the spin-polarized current starts to flow through the system under investigation, we will use the perturbed automorphism group τ^P with perturbed Hamiltonian $H + P$:

$$\tau_t^P : \mathfrak{A} \to \mathfrak{A}, \quad A \mapsto \tau_t^P(A) = e^{\frac{it(H+P)}{\hbar}} A\, e^{-\frac{it(H+P)}{\hbar}}. \tag{83}$$

Thermal equilibrium at inverse temperature β is modeled by the Gibbs canonical ensemble state which is also the unique (τ, β)-KMS state, denoted by ω^β and given by

$$\omega^\beta(A) = \frac{Tr(e^{-\beta H} A)}{Tr(e^{-\beta H})}. \tag{84}$$

These states are invariant under the action of τ, i.e., $\omega^\beta(\tau_t(A)) = \omega^\beta(A)$, but in general not invariant under the action of τ^P. If the magnetic tip influenced the QSS for a suitable long time, we will use the corresponding perturbed (τ^P, β)-KMS state

$$\omega^{\beta P}(A) = \frac{Tr(e^{-\beta(H+P)} A)}{Tr(e^{-\beta(H+P)})}. \tag{85}$$

Now we can plug the perturbed dynamics into the unperturbed equilibrium state

$$\omega^\beta(\tau_t^P(A)) \equiv \langle A \rangle_1(t). \tag{86}$$

The brackets $\langle ... \rangle(t)$ shall mean that we calculate the time evolution of an expectation value for the observable A. This corresponds to the situation when the spin-polarized tunneling current is switched on at the time $t = 0$ and the system was in thermal equilibrium for $t < 0$. The function (86) is used to model the process of a measurement of a magnetization curve. We can also plug the unperturbed dynamics into the perturbed equilibrium state

$$\omega^{\beta P}(\tau_t(A)) \equiv \langle A \rangle_2(t). \tag{87}$$

In this case a spin-polarized current is switched off at the time $t = 0$. The state $\omega^{\beta P}$ can be prepared with SP-STM. The function (87) can also be used to model the process of return to equilibrium. If a certain model Hamiltonian

is associated with H and P, the evaluation of expectation values with (86) and (87) can be calculated with different numerical methods. Some other examples for which this approach can be applied can be found in [92]-[88]. To make connection to the more common theoretical models for SP-STM, we notice that P could, for example, be given by a kind of s-d interaction or the modified Tersoff-Hamann model. The choice of P to be a local magnetic field is an approximation of the modified Tersoff-Hamann model and appropriate to save memory, which is needed by the calculation of a relaxation process.

A measurement in SP-STM is a time average over a time period Δt. For example, the time resolution of the measurement in [12] is $\Delta t = 10$ ms. Each point on a measured magnetization curve corresponds then to the value:

$$\langle A \rangle_{\Delta t} = \frac{1}{\Delta t} \int_0^{\Delta t} dt\, \omega^\beta(\tau_t^P(A)), \tag{88}$$

where A is a spin component, i.e., $S^{\mathrm{x}}, S^{\mathrm{y}}$ or S^{z}.

It is worth to mention, that for infinite systems the equations (86) and (87) are widely analyzed in mathematical physics [44], but it seems that they were never applied to real physical spin systems. If the substitution $H \rightleftarrows H + P$ is replaced by $(\mathfrak{A}, \tau) \rightleftarrows (\mathfrak{A}, \tau^P)$, comprehensive mathematical structures [44, 60], can be applied for the analysis of physical systems. The algebraic approach to QSM provides appropriate mathematical tools to verify the dynamical relaxation of a disturbed system (return to equilibrium) analytically [44, 93]. Particularly, it is proven that a mathematically exact return to equilibrium is ensured if the dynamical system satisfies some form of asymptotic abelianness and if the initial state is a perturbed KMS state [44]. If any form of asymptotic abelianness is satisfied one finds

$$\lim_{t\to\infty} \omega^\beta(\tau_t^P(A)) = \omega^{\beta P}(A), \tag{89}$$

which motivates the application of perturbed KMS states as states which can be prepared with an SP-STM. On the other hand

$$\lim_{t\to\infty} \omega^{\beta P}(\tau_t(A)) = \omega^\beta(A), \tag{90}$$

which motivates the application of (87) to calculate a relaxation process after the spin current has been switched off. Special results which are related with these problems are Proposition 5.4.6, Corollary 5.4.7., Proposition 5.4.10. and the following consequences on the next pages in [44]. The *Møller morphisms* $\gamma_\pm$ are central tools in those questions [44]. Furthermore, one finds that ground states, which are zero temperature KMS states, have a tendency to be less stable than KMS states at finite temperature.

The functionality of an SP-STM in the algebraic framework of QSM can now be described with a C^*-dynamical system $(\mathfrak{A}, \tau)$ and a perturbed system $(\mathfrak{A}, \tau^P)$, see Fig. 3. The two general options for an SP-STM are now

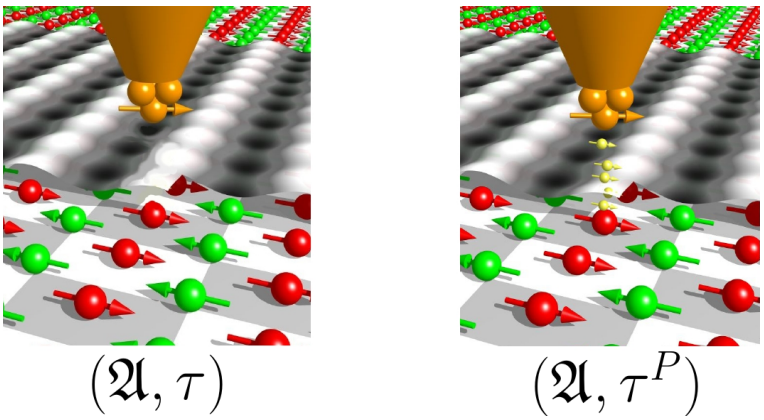

Figure 3: The interaction between the tip and the sample is identified as a local perturbation P of the dynamical group τ. The experimentalist who runs the spin-polarized scanning tunneling microscope decides whether the system $(\mathfrak{A}, \tau)$ or $(\mathfrak{A}, \tau^P)$ is actually realized and she/he determines the place where P is acting.

associated as follows:

1. The tip is moved away from the sample and there is no interaction between the tip and the sample. This corresponds to the free system

$$(\mathfrak{A}, \tau) \tag{91}$$

2. The tip is near the surface of the sample and interacts with it. This corresponds to the perturbed C^*-dynamical system

$$(\mathfrak{A}, \tau^P). \tag{92}$$

If the system was in thermal equilibrium and a measurement is started at the time $t = 0$, the expectation values are given by

$$\omega^\beta(\tau_t^P(A)) \tag{93}$$

for $t \geq 0$ and $A \in \mathfrak{A}$. Otherwise, if an interaction between the tip and the magnetic spin system *was* active for a suitable long time and the interaction is switched off at $t = 0$, the expectation values of the system are determined by

$$\omega^{\beta P}(\tau_t(A)) \tag{94}$$

for $t \geq 0$ and $A \in \mathfrak{A}$.

4.2 Single atom magnetization curves of Co/Pt(111)

Magnetization curves obtained in experiments are typically described using the expectation values of observables using a time independent, i.e., kinematic, Gibbs ensemble average [12, 94]. However, an SP-STM measurement is a time-average of the orientation of a spin component selected by the given spin orientation of the probe tip. Therefore, the dynamics of the magnetization in the sample under the study remains unknown within the experimental time resolution. It would be helpful to compensate this lack of knowledge with theoretical investigations. Therefore, we calculate the real-time non-equilibrium dynamics of quantum spin systems at finite temperatures to investigate the dynamics of a sample for shorter times than the time resolution of the experimental setup. When the STM tip comes towards an atom or a cluster under the study, the Hamilton operator of the system changes due to the interactions with tunneling electrons. The perturbed dynamics drives the state out of equilibrium and the ergodicity is not a priory ensured. Therefore, the ergodicity of a system has to be checked for a reliable interpretation of experimental results. A still unexplained finding is the extremely high switching frequency of Co atoms on Pt(111) at zero magnetic field [12]. In contrast to magnetic atoms on insulating substrates, Co/Pt(111) possesses very strong out-of-plane anisotropy (9 meV) without any transversal contributions. Hence, the Hamiltonian of the free system is diagonal in the $|S^{\mathrm{z}}\rangle$ basis and, therefore, the tunneling rate is zero [12]. The anisotropy barrier is approximately 100 times larger than the temperature used in experiments. Therefore, the Boltzmann probability to pass this barrier by thermal activation is also negligible. The measured time-averaged magnetization, in contrast, is zero at zero field even in the regime of elastic tunneling, where the tunneling current density is minimal. Our calculated time-averaged expectation values agree with the time-averaged experimental data for magnetization curves. A main conclusion is that the description of the single magnetic Co atom by a classical spin-model is unsuitable and quantum effects are important.

Now we will apply Eq. (86) and (88) to model the STM measurement process as a time average. As an example we take cobalt adatoms on platinum (111) [12]. As described in the introduction the reason for zero time-averaged magnetization of a Co adatom on Pt(111) at zero external field was still unclear. The Hamiltonian for the cobalt atom is given by [12]

$$H_{\mathrm{Co}} = -mB^{\mathrm{z}}S^{\mathrm{z}} - K(S^{\mathrm{z}})^2, \tag{95}$$

with $m = 3.7\ \mu_B$ and $K = 9$ meV. If a classical spin model in thermal equilibrium is used one finds that the probability distribution $\rho(z)$ (Boltzmann

distribution) between the up and the down state is nearly zero, see Fig. 4 for the case of a zero magnetic field. In a quantum spin model a nearly vanishing

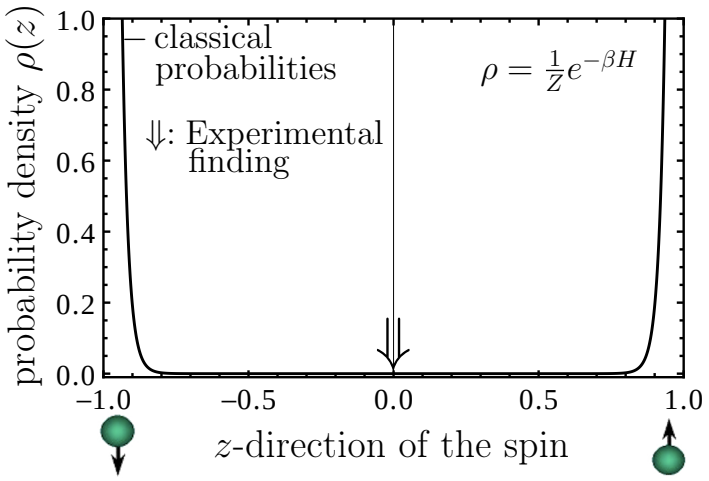

Figure 4: In a classical spin model as used in [12], the high anisotropy energy forces the magnetization direction in thermal equilibrium strongly in the up or down direction. A thermal activated switching between these two states has a vanishing probability.

probability for the states $|-\frac{3}{2}\rangle$, $|-\frac{1}{2}\rangle$, $|\frac{1}{2}\rangle$ and $|\frac{3}{2}\rangle$ can be found in thermal equilibrium at low temperatures from this Hamiltonian, as indicated in Fig. 5.

If the spin has been prepared to be polarized in positive or negative z-direction it is not a priori clear how the spin can switch in the opposite state because of the high anisotropy barrier. The temperature of $T = 0.3$ K and $T = 4.2$ K used in this experiment is much too low to switch the spin over the anisotropy barrier of $K = 9$ meV. The Néel-Brown law predicts a switching time of a few million years, which is in disagreement with the short time resolution of 10 ms of the SP-STM technique used in [12]. The absence of the transverse anisotropy term $E((S^{\mathrm{x}})^2-(S^{\mathrm{y}})^2)$ in the free system prevents direct transitions under the barrier between the $|\frac{5}{2}\rangle$ and $|-\frac{5}{2}\rangle$ states. To explain the zero expectation value of $S^{\mathrm{z}}_{\mathrm{Co}}$ at zero magnetic field (see Fig. 5) a quantum tunneling or a current induced magnetization switching mechanism has been speculatively proposed [12]. Here, we check this proposition by numerical calculations and our quantum mechanical approach.

The perturbation is taken to be $P = J\sum_i \vec{S}\vec{\sigma}_i + \sum_i \vec{m}_{\mathrm{tip}}\vec{\sigma}_i$, with the magnetization $\vec{m}_{\mathrm{tip}}$ of the tip and the Pauli matrices corresponding to the tunneling electrons. When the cobalt atom gets perturbed because of the interaction with the tunneling electrons it gets out of equilibrium and the

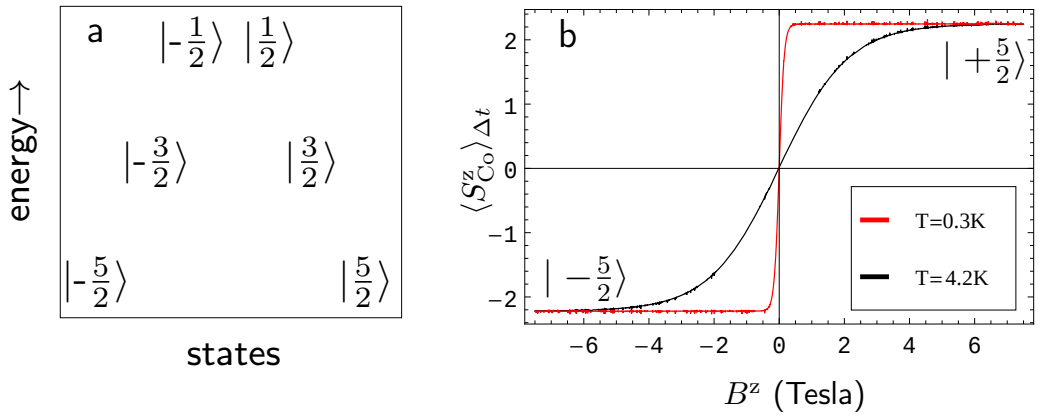

Figure 5: a) The high energy states $|-\frac{3}{2}\rangle$, $|-\frac{1}{2}\rangle$, $|\frac{1}{2}\rangle$ and $|\frac{3}{2}\rangle$ got a vanishing probability in thermal equilibrium. The preferred states are those where the spin points "up" $|\frac{5}{2}\rangle$ or "down" $|-\frac{5}{2}\rangle$. b) The time averaged magnetization curves for two different temperatures show agreement of Eq. (88) with the experimental data in [12]. For high positive magnetic field mostly the $|\frac{5}{2}\rangle$ state is occupied and for high negative field it is the $|-\frac{5}{2}\rangle$ state.

question about the occupation probability of the states $|\frac{5}{2}\rangle$,...,$|-\frac{5}{2}\rangle$ arises. A related question is, in which way the spin gets from the $|\frac{5}{2}\rangle$ to the $|-\frac{5}{2}\rangle$ state. Especially interesting is the case of zero magnetic field where the SP-STM measurement provides a time averaged expectation value $\langle S^z_{\rm Co}\rangle_{\Delta T} = 0$. Fig. 5 b) shows agreement for our quantum mechanical time-average and the time-averaged experimental data in [12]. The classical spin description [12] was only able to show agreement between the *ensemble* average and the experimental data. Fig. 6 a), b) gives the time evolution $\omega^\beta(\tau_t^P(S^z_{\rm Co}))$ for the z-component of the magnetization, for two different values of external magnetic field B^z. In agreement with experimental data $\langle S^z_{\rm Co}\rangle_{\Delta t} = 0$ for $B^z = 0$, while it increases with increasing B^z. As it is seen in Fig. 6 c), d) at $t = 0$ the total signal is composed of the superposition of $|\frac{5}{2}\rangle$ and $|-\frac{5}{2}\rangle$. As the tunneling current is switched on the occupation probabilities of those states start to oscillate. The amplitude of oscillations increases with increasing parameter J and also depends on $\vec{m}_{\rm tip}$. The appearance of fluctuations in the occupation probabilities means that not only $|\pm\frac{5}{2}\rangle$ states become occupied. In other words magnetization switching occurs. The results demonstrate that even a weak perturbation due to tunneling electrons initiates a quantum tunneling in otherwise diagonal systems. The expectation value of magnetization at $B^z = 0$ remains nearly zero.

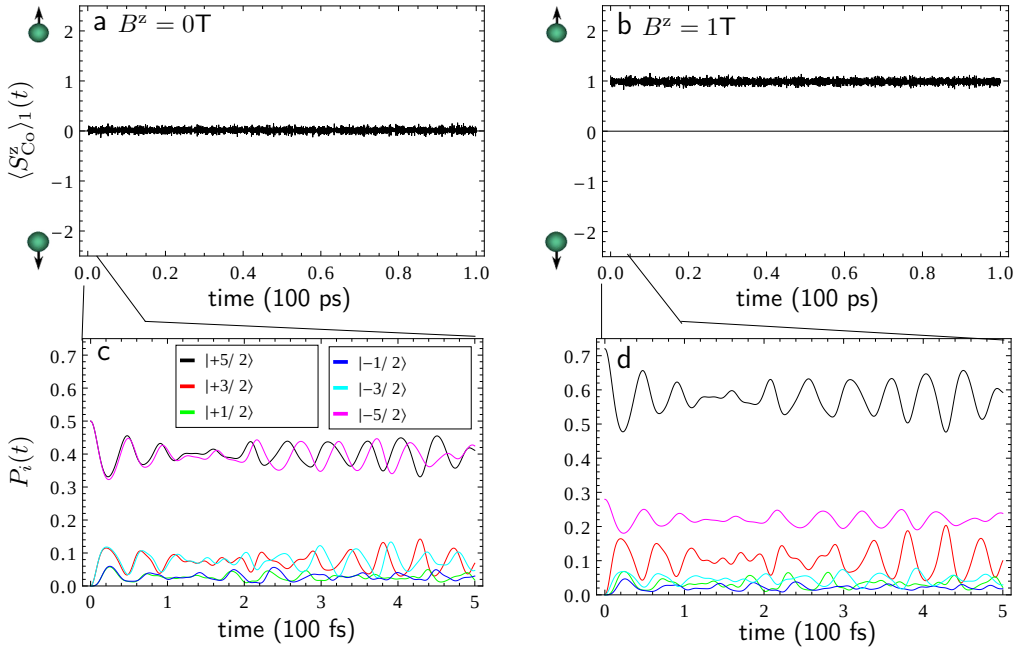

Figure 6: The time evolution of the adatom spin for the z-component as a function of time are shown for a), c) $B^z = 0$ and b), d) $B^z = 1$ Tesla. The expectation value fluctuates around thermal equilibrium at $T = 4.2$ K. The occupation probabilities P_i for the states $i = |\frac{5}{2}\rangle,...,|-\frac{5}{2}\rangle$ as a function of time are shown for c) $B^z = 0$ and d) $B^z = 1$ Tesla.

4.3 Return to equilibrium of Fe/InSb

Predictions for relaxation times of single spins on metallic and semiconductor surfaces are made. The magnetic STM-tip can be used to prepare a system with desired expectation values. For the corresponding state we choose a perturbed KMS state $\omega^{\beta P}$. Quantum fluctuations around thermal equilibrium will be analyzed and calculated. Approximated thermalization is found numerically for the expectation values of the spin operators. It is generally believed, that only large systems show a relaxation process. We demonstrate that also expectation values of relatively small quantum spin systems, containing less than 10 particles, return approximately to equilibrium when a perturbed KMS state is used as an initial state. Especially interesting is the theoretical analysis of the dynamics on time scales which are not accessible for an STM. We demonstrate that the relaxation times of those quantum objects on different substrates lie in the femto-, pico-, or nanosecond regime. To check whether the short time dynamics has a reliable behavior, the calculated relaxation time has been compared with experimentally determined

life times for single spins [94].

Magnetic adatoms on a metallic or a semiconductor surface can often be modeled with a Hamiltonian of the form

$$H = \sum_i \big(- D(S_i^{\mathrm{z}})^2 + E((S_i^{\mathrm{x}})^2 - (S_i^{\mathrm{y}})^2) \big) + \sum_{i,j,\alpha}^{n} J_{ij}^{\alpha} S_j^{\alpha} \sigma_i^{\alpha}. \tag{96}$$

The first term of the Hamiltonian describes the magnetic properties of adatoms. The second summation approximates the interaction of magnetic atoms with substrate electrons and is sometimes called s-d interaction. S^{α} are the components $\alpha = \mathrm{x}, \mathrm{y}, \mathrm{z}$ of the spin operators of the adatoms and σ_i^{α} are Pauli matrices corresponding to the spin components of the substrate electrons at a lattice site i. J_{ij}^{α} is the strength of the Heisenberg interaction between the adatom and the substrate electrons. The strength of $|J_{ij}^{\alpha}|$ in Eq. (96) has been distributed randomly between 0 and 0.8 meV, corresponding to the typical strength of exchange interaction between magnetic adatoms on conducting or semiconducting surfaces. For our model calculations we choose the perturbation

$$P = \sum_{i,\alpha} g \mu_B B^{\alpha} S_i^{\alpha}, \tag{97}$$

where B^{α} is a local magnetic mean field acting on the sample, g a gyromagnetic constant and μ_B is the Bohr magneton. Thus, the choice of P corresponds to the modified Tersoff-Hamann model when it's action is restricted to the magnetic atom directly under the tip.

It is a priori not clear, whether the described finite quantum system is able to approach its equilibrium. It will be demonstrated that already $n = 8$ substrate (or bath) electrons acting as a heat bath are sufficient, for a single adatom at zero magnetic field, to reach thermal equilibrium, when a perturbed KMS state is used. After a characteristic time t_0, the expectation value $\langle S^{\mathrm{z}} \rangle_2(t)$ relaxes and fluctuates around its thermal equilibrium value, i.e.,

$$\omega^{\beta P}(\tau_t(S^{\mathrm{z}})) \longrightarrow\!\!\approx \omega^{\beta}(S^{\mathrm{z}}) = \frac{Tr\big(e^{-\beta H} S^{\mathrm{z}}\big)}{Tr\big(e^{-\beta H}\big)}. \tag{98}$$

The amplitude and the form of fluctuations are temperature dependent. To make sure that we get realistic relaxation times, we compare our calculations with the life-time of an Fe adatom on InSb estimated in recent SP-STM experiments [94, 95]. The corresponding parameters $g_{Fe} = 2$, $D = 1.4$ meV (in our Hamiltonian we use $-D$), $E = 0.22$ meV and $S = 1$ for the iron atom are taken from [94]. To calculate the relaxation time we use the expression $\omega^{\beta P}(\tau_t(S_{\mathrm{Fe}}^{\mathrm{y}}))$, in which the time evolution is generated by the Hamiltonian

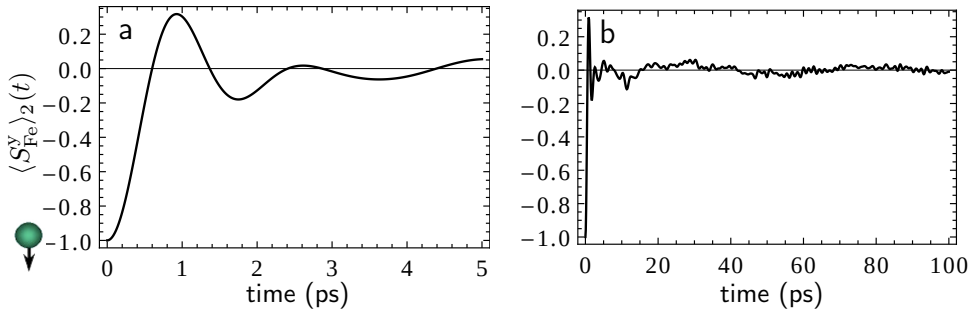

Figure 7: Return to equilibrium for the spin component S^y_{Fe} of an iron atom on an indium antimonide surface for short and long times at $T = 4.2$ K. Fig. 7 a): The experimentally estimated life-time of 800 fs is in good agreement with the calculated relaxation process. Fig. 7 b): After the relaxation is done the expectation value remains near thermal equilibrium $\omega^\beta(S^y_{Fe}) = 0$.

Eq. (96) and S^y_{Fe} denotes the y-component of the spin operator of the iron atom, which was investigated in this experiment [94].

In Fig. 7 the agreement of the interpretation of $\omega^{\beta P}(\tau_t(S^y_{Fe})) = \langle S^y_{Fe}\rangle_2(t)$ as a relaxation process with experimental data [94, 95] is verified. As one can see from Fig. 7, the expectation value of the magnetization increases from -1 to zero and then fluctuates around thermal equilibrium. The experimental estimation of the lifetime $t_{l.t.}$ of the excited state was done by the formula $t_{l.t.} = \frac{\hbar}{2\Delta E}$, where ΔE is the energy difference between the states, obtained from inelastic SP-STM[94, 95].

In Fig. 8 and 9 the calculated functions for a high temperature of $T = 100$ K and a low temperature of $T = 4$ K are shown. The short time and the long time behavior are analyzed for different values of the parameters E and D in Eq. (96). In Fig. 8 a)-d) the function $\omega^{\beta P}(\tau_t(S^z))$ is plotted for different values of E and fixed D, while E is fixed and D is varied in Fig. 9 a)-d). It can be seen that in all cases the fluctuations decrease with increasing temperature. Depending on the time scale, in all cases the evaluated function $\omega^{\beta P}(\tau_t(S^z))$ can be approximated by a function starting from -1 with an exponential decay to zero. Fluctuations induced by the temperature are not able to switch the spin back to $\langle S^z\rangle \approx -1$. A similar behavior has been found experimentally in [96], where a single Fe spin was excited with a high voltage pump, corresponding to a strong perturbation in our model, and the relaxation process of this single spin was investigated. The magnetization showed the exponential decay for first time period, followed by small fluctuations near thermal equilibrium. The temperature was unable to switch the spin to its initial value for $t = 0$. The appearance of larger fluctuations for

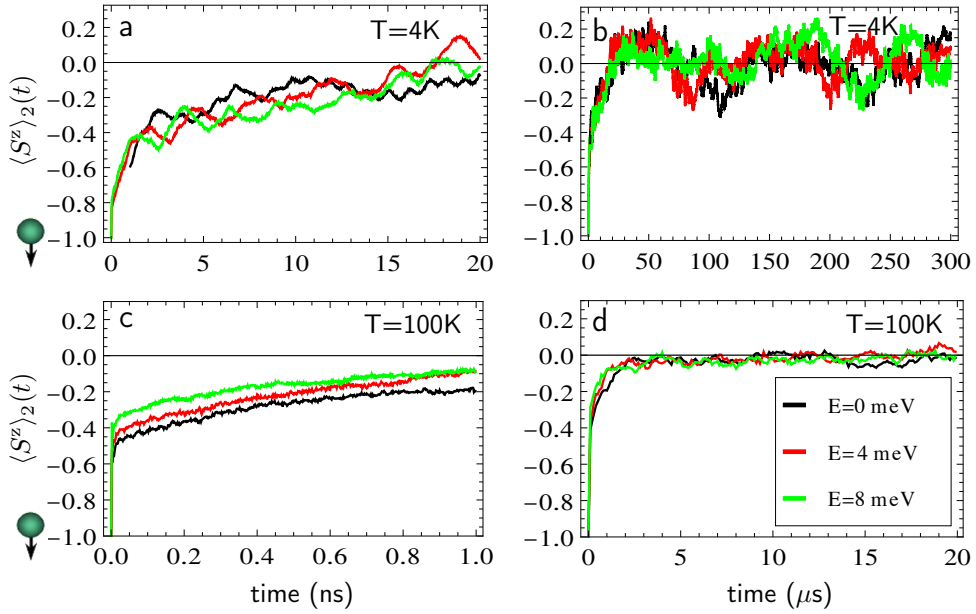

Figure 8: Return to equilibrium for S^z of a single adatom spin coupled to 8 substrate electrons. The relaxation is shown for temperatures of $T = 4$ K, $T = 100$ K, different values of E and fixed $D = 1$ meV. Fig. 8 a) and 8 c): The short time behavior shows a faster relaxation for a higher temperature. Fig. 8 b) and 8 d): The long time behavior shows smaller quantum fluctuations around thermal equilibrium for higher temperatures. The different time scales on the x-axis should be noted.

a lower temperature might be explained by energy considerations. A system at a lower temperature has less energy than a system at a higher temperature. A perturbation P corresponds to an additional amount of energy. Notice that for an infinite system this additional energy is negligible and an exact thermalization might take place [44]. The relative ratio between the energy of perturbation and the energy of the free system is larger at lower temperatures. This might be a reason for the stronger fluctuations at lower temperatures. Another important effect at low temperatures are "quantum fluctuations", which become extinct with increasing temperature. We can also see that for higher temperatures the quantum spin of the adatom returns faster to equilibrium, i.e., the adatom relaxation time becomes shorter. With increasing value of D the relaxation time also increases. This is in agreement with the statement that a spin "up" or "down" state becomes more stable with increasing anisotropy barrier. For increasing E (see Fig. 8 a,c) an inverted behavior has been observed for short times.

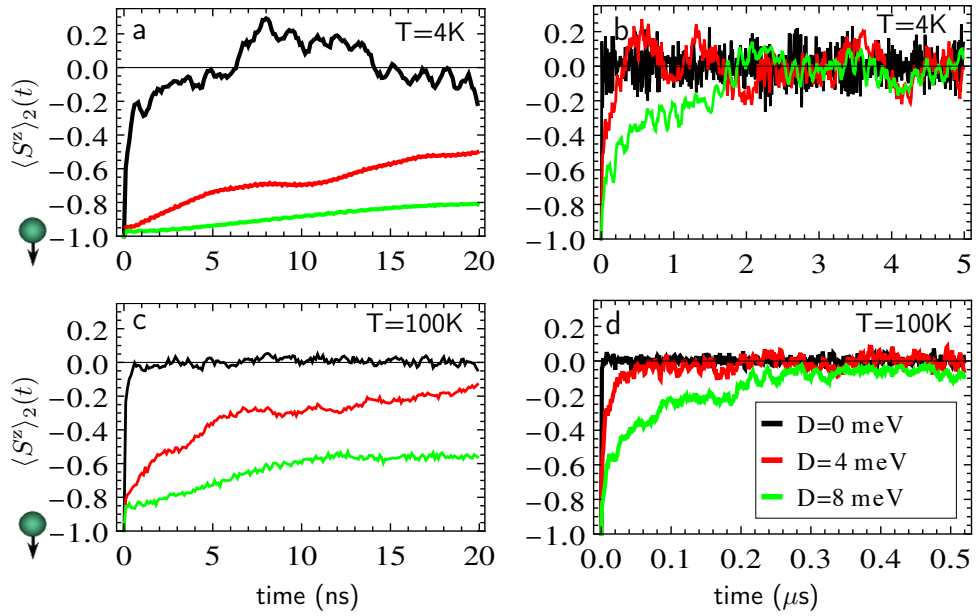

Figure 9: Return to equilibrium for S^z and different values of D of a single adatom spin coupled to 8 substrate electrons. The relaxation time grows with increasing value of the anisotropy barrier D. Fig. 9a) and 9c): The short time behavior shows a faster relaxation for a higher temperature. Fig. 9b) and 9d): The long time behavior shows smaller quantum fluctuations around thermal equilibrium for higher temperatures. The different time scales on the x-axis should be noted.

4.4 Outlook to algebraic Quantum Field Theory

Quantum field theory as well as fermionic lattice systems (FLS) can also be formulated with a quasi-local algebra. They provide a more realistic model system for the action of the magnetic tip on the sample than the Tersoff-Hamann model for a QSS does. The tunneling current between the magnetic tip and the sample can be incorporated in a more realistic fashion by the usage of a QFT or a FLS. The modified Tersoff-Hamann model which is used in a QSS has the mathematical structure of an exponentially declining external magnetic field, when one is moving away from the lattice site which is directly under the tip. While the Tersoff-Hamann model provides a basis for explaining many STM results, it acts physically like a position dependent magnetic field and there are no tunneling particles. There is basically no particle reservoir which models the magnetic tip, such that electrons could tunnel between the tip and the sample. Moreover, it is not a very realistic model, especially if the applied bias voltage is considered. Thus, we will give a brief explanation how a QFT can be applied to remove these weaknesses.

Since the application of a FLS is structurally very close to that, we will just concentrate on QFT.

The application of a QFT is made by an identification of an element of a quasi-local algebra, $P \in \mathfrak{A}$, with the interaction *between* the tip of the scanning tunneling microscope and the investigated sample with substrate. Thus, $P \in \mathfrak{A}$ contains information of the tunneling probabilities. Principally one chooses a C^*-algebra of the form

$$\mathfrak{A} = \mathfrak{A}_1 \otimes \mathfrak{A}_2 \otimes \mathfrak{A}_3, \tag{99}$$

where $\mathfrak{A}_1$ could be associated with electrons of the substrate, $\mathfrak{A}_2$ corresponds to the actually investigated magnetic atom(s) which is/are directly under the magnetic tip, which itself is described by $\mathfrak{A}_3$. Thus, $\mathfrak{A}_3$ can be seen as a particle reservoir of tip-electrons and $\mathfrak{A}_1$ as a particle reservoir of substrate electrons. $\mathfrak{A}_1$ and $\mathfrak{A}_3$ are therefore infinite-dimensional systems, while $\mathfrak{A}_2$ is a finite-dimensional matrix algebra. The free dynamics is then of the form

$$\tau = \tau^{1,2} \otimes \tau^3, \tag{100}$$

where $\tau^{1,2}$ is the dynamics on $\mathfrak{A}_1 \otimes \mathfrak{A}_2$, which is not of tensor product structure because there is a permanent interaction between the substrate electrons and the investigated magnetic atom(s). τ^3 is the free dynamics of the electrons contained in the tip. As the Tersoff-Hamann model indicates, the tunneling current decreases exponentially with the distance Δh between the tip and the sample. Therefore, the tensor product structure between $\tau^{1,2}$ and τ^3 is a good approximation for sufficiently large distances Δh. If the tip is moved towards the sample, the resulting tunneling current is responsible for the occurrence of an interaction $P \in \mathfrak{A}$ which connects $\mathfrak{A}_1 \otimes \mathfrak{A}_2$ with $\mathfrak{A}_3$. Thus, the perturbed dynamics τ^P during a measurement is not of the Tensor product structure as the free dynamics. A natural equilibrium state of the free system $(\mathfrak{A}, \tau)$ is of the form

$$\omega_{1,2}^{\beta\mu_1} \otimes \omega_3^{\beta\mu_3}, \tag{101}$$

where $\beta \in \mathbb{R}$ is the inverse temperature, μ_1 is the chemical potential of the substrate, and μ_3 is the chemical potential of the tip. The applied bias voltage eV, which is an important experimental parameter, is then given by

$$eV = \mu_1 - \mu_3. \tag{102}$$

A simple perturbation that could be chosen for a quantum field theoretic system might be of the form

$$\sum_x \gamma \vec{m}_{\text{tip}} \big(a^*(f_1) \vec{S}_x a(g_1) + a(f_2) \vec{S}_x a^*(g_2) + a^*(g_3) \vec{S}_x a(g_4) + ... \big), \tag{103}$$

where $\vec{S}_x$ is the spin operator of the investigated magnetic adatom at position x, $a^*(f_i) \in \mathfrak{A}_1$ and $a^*(g_i) \in \mathfrak{A}_3$ are creation operators of the tip and the substrate, while $a(f_i) \in \mathfrak{A}_1$ and $a(g_i) \in \mathfrak{A}_3$ are the corresponding annihilation operators. See [44] for a detailed description of algebraic QFT. γ assesses the "strength" of the tunneling current. The interpretation of the perturbation P is as follows: in the first term a conduction electron "with matter distribution g" is annihilated in the tip, then it interacts with the investigated magnetic atom $\vec{S}_x$ and is then created with matter distribution f in the substrate. The interpretation of the other terms is accordingly. This was a brief discussion how AQFT can be applied for a more realistic description of SP-STM experiments.

5 Information transport in atomic spin chains

A fast information transfer via spin chains is crucial for the efficiency of future spintronic devices. Iron chains on the surface of an iridium crystal and copper(111) were experimentally identified as suitable systems for a transport of magnetic information [76] [2, 76]. We perform simulations of an exact signal propagation for the Fe/Ir(001) system and magnetic atoms on metallic surfaces. There are different experimental parameters which can be used to modify the information transport in magnetic quantum systems, e.g., external magnetic fields, differently prepared states, the temperature or the bias voltage of the STM. The enhancement of the signal velocity is of primary interest. This naturally raises the question of a possible maximum velocity in quantum spin systems, in analogy to the speed of light as maximum velocity in relativity theory. In 1972, Lieb and Robinson provided a general limit on signal velocities in the theory of quantum spin systems, which is expressed as a mathematical bound [97]. While the speed of light as maximum velocity is physically realized in nature by photons, it is an interesting question how close real velocities in magnetic quantum systems can come to the mathematical Lieb-Robinson bound. We suggest that SP-STM is a suitable experimental setup for a quantitative investigation of the quality of Lieb-Robinson bounds and provide applications of Lieb-Robinson bounds as upper limits on the enhancement of the real signal speed for information transport in spintronic devices. It is shown, that the signal speed in a spin chain with Heisenberg interaction can't be increased more than a factor of 4 by varying certain experimental parameters. The observed discrepancy between the bounds and the exact signal velocities is investigated.

Fig. 10 shows a visualized SP-STM experiment, where information is transferred via spin chains consisting of iron atoms on the surface of an iridium crystal [76]. Magnetic STM tips are experimentally used to investigate the spin system and if a measurement is started, a tunneling current starts to flow between the tip and the magnetic atoms. The corresponding interaction is described by the modified Tersoff-Hamann model [87, 88],

$$H_{\text{tip}}(\{x\}) = gI_0\mathbb{P}e^{-2\kappa\sqrt{(x-x_0)^2+h^2}}\vec{m}_{\text{tip}} \cdot \vec{S}_x, \tag{104}$$

where the parameters are explained following eq. (25). We will use the theoretical idealization, that the tip acts only on the atom which is directly underneath the tip, i.e., $P = H_{\text{tip}}(\{x_0\})$, where x_0 is the position of the tip at the beginning of the spin chain. In accordance to [13], we will distinguish between a *free* spin system (the tip is moved away from the surface such that there is no interaction between the tip and the sample) and a *perturbed*

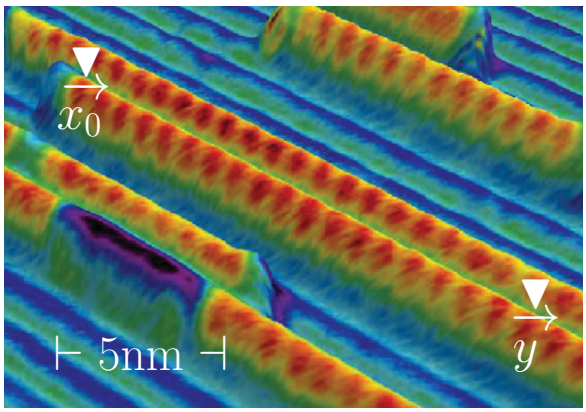

Menzel et al., PRL **108**, 197204 (2012)
Fe chains/Ir(001)

Figure 10: Example of an SP-STM experiment, where information is transported via spin chains consisting of iron atoms on the surface of an iridium crystal [76]. A magnetic tip (upper white triangle) starts to act on lattice site x_0 at time $t = 0$. After some time $t > 0$, the signal can be detected at lattice site y.

spin system, which means that there is an interaction between the magnetic tip and the sample. Thus, the Hamiltonian of the spin system switches from $H_{\text{chain}}(\Lambda)$ to $H_{\text{chain}}(\Lambda) + H_{\text{tip}}(\{x_0\})$ in the moment $(t = 0)$, when the tunneling current starts to interact with the magnetic atoms. The action of the magnetic tip influences the dynamics of the spin system and disturbances start to propagate through the chain. The dynamics of the free spin system without the action of the tip is given by the Heisenberg relations

$$S_y^{\text{z}}(t) = e^{i(t/\hbar)H_{\text{chain}}(\Lambda)} S_y^{\text{z}} e^{-i(t/\hbar)H_{\text{chain}}(\Lambda)} = \tau_t^{\Lambda}(S_y^{\text{z}}). \tag{105}$$

The corresponding dynamics of the perturbed system with interaction between tip and spin chain is given by

$$\tau_t^{\Lambda P}(S_y^{\text{z}}) = e^{i(t/\hbar)(H_{\text{chain}}(\Lambda)+H_{\text{tip}}(\{x_0\}))} S_y^{\text{z}} e^{-i(t/\hbar)(H_{\text{chain}}(\Lambda)+H_{\text{tip}}(\{x_0\}))}. \tag{106}$$

In thermal equilibrium, the state of the free spin chain is given by the Gibbs state ω_Λ^β whose expectation value is given by

$$\omega_\Lambda^\beta(S_y^{\text{z}}) = \frac{Tr(e^{-\beta H_{\text{chain}}(\Lambda)} S_y^{\text{z}})}{Tr(e^{-\beta H_{\text{chain}}(\Lambda)})}, \tag{107}$$

where β is the inverse temperature. The dynamics for the exact velocities is now given by

$$\omega_\Lambda^\beta(\tau_t^{\Lambda P}(S_y^{\text{z}})) \equiv \langle S_y^{\text{z}} \rangle(t), \tag{108}$$

where the perturbation P is located at site x_0 and the observed spin component S_y^z is located at site y, e.g., the z-component of the output atom's magnetization in fig. 10. We use the numerical method of exact diagonalization for the exact signal velocities. There is no phenomenological term for a dissipation process.

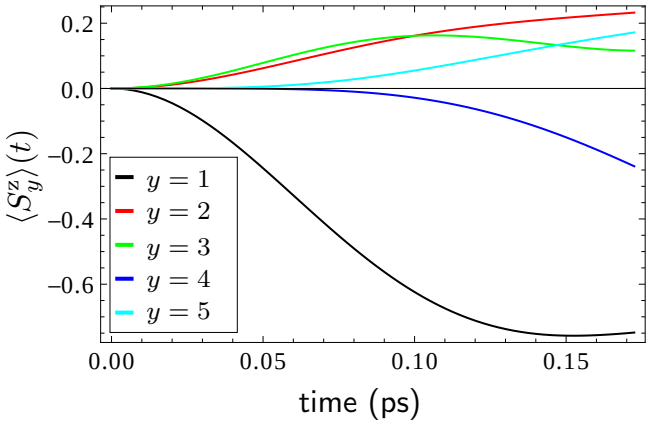

Figure 11: Propagation velocities (arrival times) for an iron chain on iridium at $T = 4$ K. The required propagation time is not a linear function of the chain length y.

5.1 Real-time information transfer in Fe chains on Ir(001)

The Hamiltonian of the Fe/Ir(001) spin chain is given by

$$H_{\text{chain}} = \sum_{ij} \left(J_{ij} \vec{S}_i \vec{S}_j + \vec{D}_{ij} \cdot \left[\vec{S}_i \times \vec{S}_j \right] \right) + \sum_i K (S_i^z)^2. \tag{109}$$

We include nearest and next to nearest neighbor interactions between the Fe atoms, which are modeled by particles of spin quantum number $s = 1$. We use the exchange and anisotropy parameters as in the experiment [76] for a realistic description. Our idealized, modified Tersoff-Hamann model is of the form $P = \alpha \vec{m}_{\text{tip}} \vec{S}_{x_0} = \alpha S_1^z$, where the constant α is chosen to be $\alpha = 10$ meV, corresponding to typical interaction strengths in SP-STM experiments. We perform the simulations for the temperatures of $T = 4$ K and $T = 100$ K. The perturbation P drives the magnetization of the first atom in the chain at $x_0 = y = 1$ out of equilibrium, which then influences the magnetizations of the nearest and the next to nearest neighboring atoms at $y = 2$ and $y = 3$. The magnetization directions of the atoms in the chain start changing after

some time t when the signal, which was caused by the magnetic tip at position x_0, arrives at site y.

Fig. 11 shows the magnetization change $\langle S_y^z \rangle(t)$, eq. (108), of the atom at position y in the Fe/Ir(001) chain. It can be seen that the first atom ($x_0 = y = 1$) in the chain responds earliest. The third atom (at $y = 3$) responds earlier than the second atom (at $y = 2$), because the interaction strength between the next to nearest neighbor atoms is stronger than between nearest neighbor atoms [76]. The other atoms show the same behavior, the fifth atom responds earlier than the fourth atom. Thus, for an odd number of atoms the signal arrives earlier at the end of the chain than for the case with one atom less. The required propagation time is therefore not a linear function of the chain length. However, it is difficult to define the exact speed for this system. If we define, that the signal arrives at site y when the expectation value $\langle S_y^z \rangle(t)$ has changed by the value ≈ 0.05, we obtain the results which are shown in table 1. The signal speed through the iron chain is on average approximately 50 $\frac{\text{sites}}{ps}$. Next we compare the information transport through

y	t
1	0.02 ps
2	0.045 ps
3	0.04 ps
4	0.12 ps
5	0.095 ps

Table 1: Required time t for a significant change (≈ 0.05) of the spin's z-component expectation value $\langle S_y^z \rangle(t)$ at lattice site y. The signal speed is on average approximately 50 $\frac{\text{sites}}{ps}$.

the iron chains on iridium for the two different temperatures of $T = 4$ K and $T = 100$ K and show also the long-time behavior.

Figs. 12, 13, 14, and 15 show the magnetization change of all eight spin 1 particles in the Fe/Ir(001) spin chain as a function of time. For all eight spins it can be seen that the magnetization starts earlier to change and the amplitude is larger for the lower temperature of 4 K. The magnetization of the first atom (fig. 12) which is directly influenced by the magnetic tip changes earliest and remains aligned along the negative z-direction. The lower temperature causes that the $|-1\rangle$ state of the first atom is relatively more occupied after the action of the tip than in the case for the higher temperature. The magnetization of the second atom in the chain (fig. 12) starts changing into the positive z-direction with a reduced amplitude compared

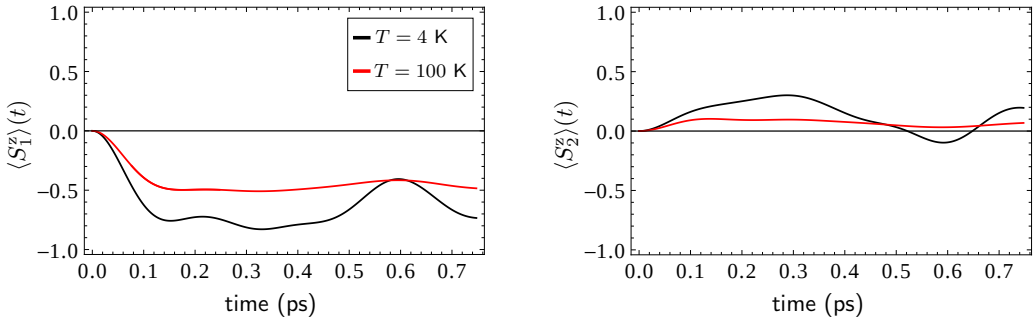

Figure 12: The magnetization change of the first atom (left fig.) and the second atom (right fig.) in the iron spin chain on iridium for the temperatures of $T = 4$ K and $T = 100$ K.

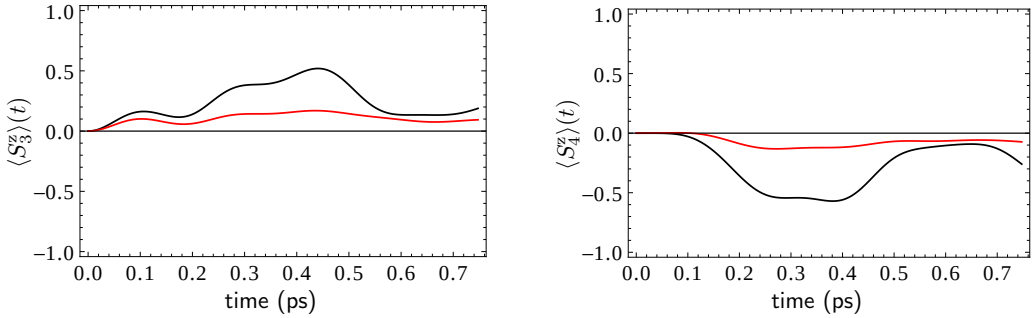

Figure 13: The magnetization change of the third atom (left fig.) and the fourth atom (right fig.) in the iron spin chain on iridium for the temperatures of $T = 4$ K and $T = 100$ K.

to the first atom. For the higher temperature of $T = 100$ K the magnetization remains more stable in that position, while the magnetization shows more quantum fluctuations and is less stable for the lower temperature of $T = 4$ K. There is a similar behavior for the third and fourth atom in fig. 13. The magnetization of the fifth, sixth, seventh, and eighth atom in fig. 14 and 15 approaches to its original equilibrium magnetization after ≈ 0.5 ps. Numerical calculations of information transport in spin chains with a pure Heisenberg interaction show a less stable magnetization change and more periodic oscillations. Thus, the Dzyaloshinskii-Moriya interaction is responsible for thermalization properties.

5.2 Lieb-Robinson bounds on the signal velocity

Since the introduction in 1972, there were several investigations of Lieb-Robinson bounds in the algebraic framework of mathematical physics [89, 98–

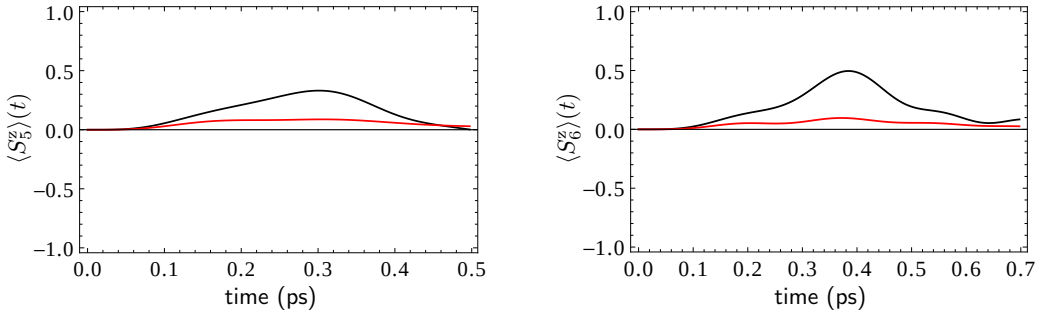

Figure 14: The magnetization change of the fifth atom (left fig.) and the sixth atom (right fig.) in the iron spin chain on iridium for the temperatures of $T = 4$ K and $T = 100$ K.

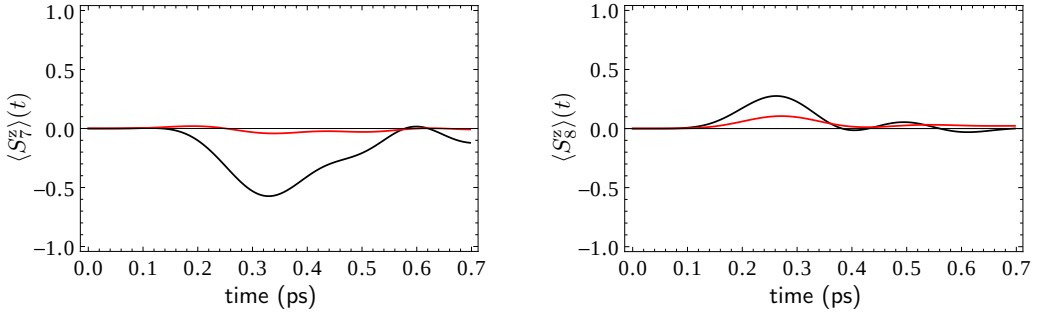

Figure 15: The magnetization change of the seventh atom (left fig.) and the eighth atom (right fig.) in the iron spin chain on iridium for the temperatures of $T = 4$ K and $T = 100$ K.

100]. A central aim of these investigations is the improvement of the bound, which means a reduction of the corresponding upper mathematical limit down to real existing velocities. The new improvements on Lieb-Robinson bounds arose from remarks in [101] and the first two important results in this direction were [102] and [103]. The authors in [104] derived a theoretical speed limit for the Bose-Hubbard model, which was interpreted to be some kind of a Lieb-Robinson bound, and investigated experimentally the propagation of correlations in a one-dimensional quantum gas. However, the general Lieb-Robinson bounds derived in mathematical physics were never applied to real physical systems and the corresponding discrepancy between the bound and exact velocities remained unclear. Hence, the corresponding potential for a further improvement of the bounds as well as the maximum enhancement of the signal speed, by varying certain experimental parameters, remained unknown. The latest, most general bound [89] is presented in

a simplified formula [85, 86] and applied to realistic interactions of magnetic quantum systems as used in spin-based nanotechnology [105]. We derive a bound $\tilde{\mathfrak{B}}$ which provides a strictly mathematical relation between the bound $\mathfrak{B}$ and the exact velocities eq. (108). This allows a quantitative analysis for further improvements of Lieb-Robinson bounds and provide an upper limit on the enhancement of exact velocities, if experimental parameters are changed which leave the bound invariant. It is shown, that the latest, most general bound $\mathfrak{B}$, is better by a factor of 100 than the old bound [44] and approximately 4 times faster than some estimates of exact signal velocities in atomic spin chains. Thus, the latest, most general bound derived in [89] is already in the correct order of magnitude. A specific bound which is only valid for the XY-model [90] is incorporated into the discussion. The interaction between the magnetic STM tip and the sample is identified as an interesting experimental parameter which influences the exact signal propagation as well as $\tilde{\mathfrak{B}}$, but leave $\mathfrak{B}$ invariant. A corresponding SP-STM experiment is simulated with explicit calculations. But first we will investigate the original bound for a comparison and to demonstrate which kinds of improvements were done.

The interaction norm $\| \Phi \|_\xi$ for the old Lieb-Robinson bound in [44] is given by

$$\| \Phi \|_\xi = \sup_{x \in L} \sum_{X \ni x} |X|(2s+1)^{2|X|} e^{\xi D(X)} \| \Phi(X) \| < +\infty, \tag{110}$$

for some $\xi > 0$, where $|X|$ is the number of points in X, $D(X)$ is the diameter of X and s is the spin quantum number. The upper limit on propagation velocities is given by [44, 97] (Theorem 6.2.11.):

$$\| [S_x^z(t), S_y^z] \| \leq 2 \| S_x^z \| \| S_y^z \| \, e^{-|t|(\frac{\xi|x-y|}{|t|} - 2\|\Phi\|_\xi)} \doteq \mathfrak{L}(t), \tag{111}$$

where $\mathfrak{L}$ is the Lieb-Robinson bound. The proof of the related theorem [44] states that this bound is independent of one-body interactions, e.g., external magnetic fields, anisotropy energies, and the Tersoff-Hamann type interaction. Thus, for the Lieb-Robinson velocity we have to concentrate on the Heisenberg- and the Dzyaloshinskii-Moriya interactions, while the exact velocities also depend on the one-body interactions.

If the norm of the commutator in inequality (111) is very small, e.g., compared to the norm of the spin observable, the commutator can be assumed to be zero. For table 2 and 3 the value

$$\| [S_x^z(t), S_y^z] \| \leq 10^{-4} \approx 0 \tag{112}$$

was chosen, but one could also choose a smaller value. For large and complex systems, the commutator in eq. (111) cannot be calculated with a standard numerical procedure, but the bound on the right hand side can be calculated. The quantum mechanical interpretation of two commuting observables is that they can be measured independently. The latest calculated time point for which eq. (112) is valid is denoted by $t_{\min}$. Certainly $t_{\min}$ depends on x and y, and $t_{\min}$ *is interpreted to be the time which is at least needed for a propagating signal to overcome the distance* $|x-y|$. Therefore, the fastest possible information transport from a point x to a point y is given by $t_{\min}$. The upper bound on velocities is then given by $v_{\text{L.R.}} \doteq \frac{|x-y|}{t_{\min}}$.

Fig. 16 shows a visualized situation in a possible, experimental SP-STM setup and the small blue and green cones in fig. 16 correspond to magnetic atoms. The Lieb-Robinson bound states that after some time $t > 0$, all magnetic disturbances which were caused by the event $H_\Phi(\Lambda) \to H_\Phi(\Lambda) + H_{\text{tip}}(\{x_0\})$ are contained in a circle (green cones in fig. 16) whose center is given by the position x_0 of the tip. The radius of the circle is calculated as a function of time, see table 2.

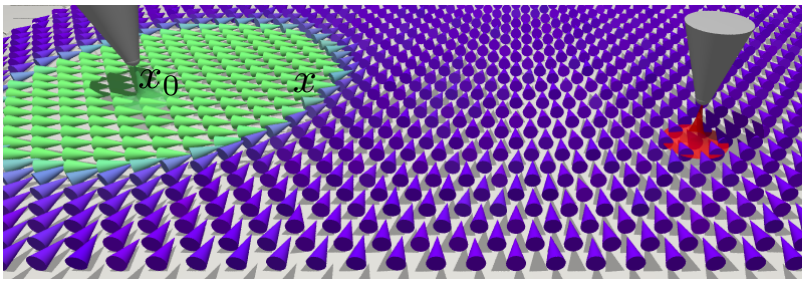

Figure 16: A magnetic tip acts over the lattice site x_0. After some time t, only spins with a distance smaller than $|x_0 - x|$ (green cones) could be influenced by the tip.

Next, we solve the Lieb-Robinson bound Eq. (111) for the spin 1/2 Heisenberg model in one, two, and three dimensions with nearest neighbor interaction and arbitrary one-body interactions. We define

$$J_{\max} = \sup_{x,y \in L} | J_{xy} | \tag{113}$$

and the Lieb-Robinson velocity $v_{\text{L.R.}}$ is then a function of $J_{\max}$.

Table 2 shows the fastest possible information transport for the two-dimensional $s = 1/2$ quantum Heisenberg model with nearest neighbor interaction. $|x_0 - x|$ is the radius of the circle where the center x_0 is the position of the STM tip, as in fig. I. A signal which starts from x_0 at $t = 0$ is after

the time $t_{\min}$ contained in the circular area which is smaller than the radius $|x_0 - x|$ obtained from the Lieb-Robinson bound.

$\lvert x_0 - x\rvert$	$t_{\min}$
100	1.19 ps
1000	11.9 ps
10 000	119 ps
100 000	1.19 ns
1 000 000	1.19 ns
100 000 000	1.19 μs

$\lvert x_0 - x\rvert$	$t_{\min}$
100	0.119 ps
1000	1.19 ps
10 000	11.9 ps
100 000	119 ps
1 000 000	1.19 ns
100 000 000	119 ns

Table 2: Minimum time needed to overcome the distance $|x_0 - x|$ for the two-dimensional Heisenberg model. *Left*: $J_{\max} = 0.1$ meV. *Right*: $J_{\max} = 1$ meV.

$dim(L)$	$v_{\text{L.R.}}$
1	0.04 sites/fs
2	0.08 sites/fs
3	0.12 sites/fs

$dim(L)$	$v_{\text{L.R.}}$
1	0.4 sites/fs
2	0.8 sites/fs
3	1.2 sites/fs

Table 3: Maximum propagation velocities $v_{\max}$ in lattice sites per time for the one-, two- and three-dimensional quantum Heisenberg model. *Left*: $J_{\max} = 0.1$ meV. *Right*: $J_{\max} = 1$ meV.

Table 3 shows the maximum velocities in lattice sites per time for different values of $dim(L)$ and $J_{\max}$. The values for $J_{\max}$ were chosen to be $J_{\max} = 0.1$ meV and $J_{\max} = 1$ meV, corresponding to typical magnetic interaction strengths. For every case there is a $t_{\min} \propto \frac{1}{J_{\max}}$ dependence and $t_{\min}$ depends linearly on the distance $|x - y|$. Hence, $v_{\text{L.R.}} \propto J_{\max}$ and there is a $\frac{1}{J_{\max}}$ dependence of $t_{\min}$, which can also be found for exact velocities, if all $J_{ij}^{\alpha} = J$ are equal. $v_{\max} \propto dim(L)$ for the above cases.

Fig. 17 shows an exact change (a) of the last atom's magnetization (site $y = 8$) and the fastest possible change (b), which is given by the Lieb-Robinson bound $\mathfrak{L}(t)$ (right hand side of eq. (111)). For both cases a comparison was done for the pure Heisenberg-, the pure DM, and both interactions together. In all cases the spin chains consist of 8 particles with spin quantum number $s = 1/2$ and the coupling constants were chosen to be $J = D = 1$ meV. It can be seen that the exact speed is nearly equal for the pure Heisenberg and the pure DM interaction. But the Lieb-Robinson speed is faster for the pure DM interaction than for the pure Heisenberg interaction, because the interaction norm eq. (110) possesses a larger value for the

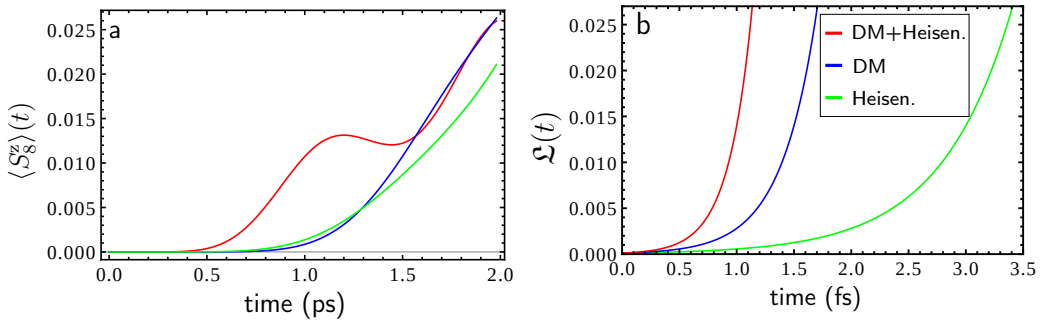

Figure 17: The "arrival time" of some exact (a) and the Lieb-Robinson (b) velocities for a signal propagation through a spin chain of 8 atoms. For both kind of velocities, the pure Heisenberg (green lines), the pure DM interaction (blue lines), and both interactions together (red lines) were calculated. In all cases the coupling constants were chosen to be of strength 1 meV.

DM interaction. For both interactions together the speed is enhanced for the Lieb-Robinson and the exact velocity. The old Lieb-Robinson velocities are approximately 400 times faster than the obtained exact velocities.

5.3 The latest, most general bound

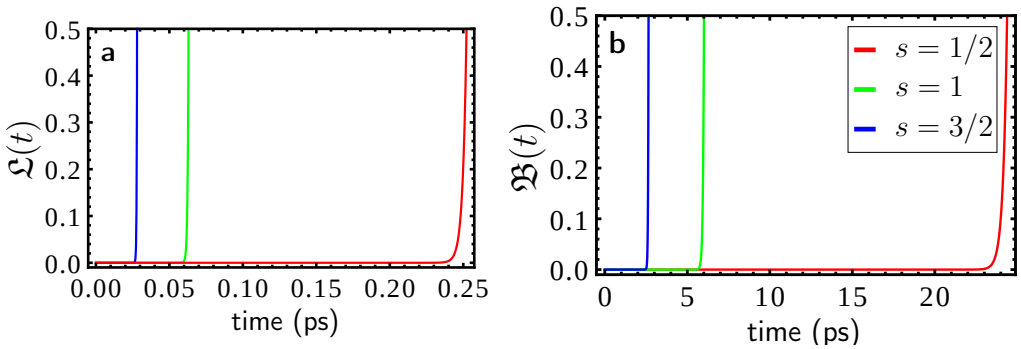

Figure 18: The old a) and the new bound b) are compared for the $s = 1/2, 1$, and $3/2$ nearest neighbor $J = 1$ meV Heisenberg chain consisting of 100 quantum spins. The Lieb-Robinson velocity of the new bound is approximately 100 times slower and therefore 100 times closer to real existing velocities.

First we will solve the old bound $\mathfrak{L}$ and the newer bound $\mathfrak{B}$, eq. (66), for the Heisenberg interaction and compare them as a function of time. After that we discuss the observed discrepancy. We will then solve the bound $\tilde{\mathfrak{B}}$ to compare the latest, most general bound $\mathfrak{B}$ and the exact signal velocities, eq. (108), which are generated in the simulated SP-STM experiment.

Fig. 18 shows the Lieb-Robinson velocities concerning a) the original bound $\mathfrak{L}$ and b) the latest, most general bound $\mathfrak{B}$ for the $s = 1/2, 1$, and $3/2$ nearest neighbor Heisenberg quantum spin chain with interaction strength $J = 1$ meV. The chain length is chosen to be $l = 100$ lattice sites. While the old bound $\mathfrak{L}(t)$ states for $s = 1/2$ (red lines) that it is impossible to transfer information through the chain faster than 0.24 ps, the new and better bound $\mathfrak{B}(t)$ states that it is impossible to do this faster than 23.5 ps. The new bound is therefore approximately 100 times slower, i.e., stays longer close to zero with increasing time, and is 100 times closer to real existing velocities. Note that the improved Lieb-Robinson bound is a *lower* bound on the *velocities* than the original bound, which means that the *arrival time* (which is shown on the figures) of the improved bound is *increased*. In the original bound $\mathfrak{L}$ the time is multiplied with the factor $|X|(2s+1)^{2|X|}e^{\xi D(X)}$, from which the new bound $\mathfrak{B}$ is independent. This factor provides an unnecessary increase of the corresponding speed limit. In our calculations we have $|X|(2s+1)^{2|X|}e^{\xi D(X)} \approx 86,99$ and ξ was chosen nearly to 1, such that $\mathfrak{L}(t)$ has a minimum value. Thus, the disappearance of this factor in the new bound $\mathfrak{B}$ provides the main contribution of the 100 fold improvement for the Lieb-Robinson velocity v_{LR}.

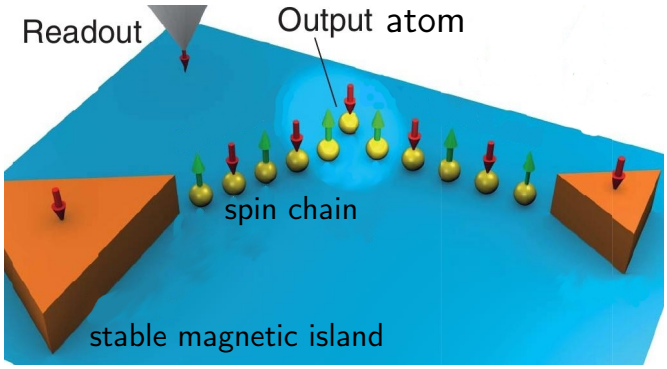

Figure 19: Example of an SP-STM experiment, where information is transported via spin chains in an all-spin-based atomic-scale logic device consisting of iron and cobalt atoms placed on copper(111) [2]. If the magnetization of a triangular island is switched, a signal starts to propagate through the chain towards the output atom.

Next we estimate some exact velocities in spin chains and include the interaction of the magnetic tip. Our model calculations will be performed for systems where the interaction between the atoms can be described by the Heisenberg interaction, which is for example the case for the atomic-scale spin-based logic device in fig. 19. A $s = 1$ nearest neighbor interaction

Heisenberg quantum spin chain consisting of 8 atoms with anisotropy energy will be used for our next example:

$$H_{\text{chain}} = \sum_{i,i+1}^{8} J\vec{S}_i \cdot \vec{S}_{i+1} + \sum_{i=1}^{8} K(S_i^z)^2, \tag{114}$$

where we choose $J = 1$ meV and $K = 2$ meV, corresponding to typical values of magnetic atoms on the surface of a metallic substrate. While the particle number is mostly the limiting factor for numerical methods, Lieb-Robinson bounds can be solved for an arbitrary number of quantum spin particles.

Fig. 20 shows a comparison between three different exact velocities (colored lines) and the upper bound $\mathfrak{B}(t)$ (black line). The parameter of the modified Tersoff-Hamann model are chosen to be

$$\parallel P \parallel = gI_0\mathfrak{P}e^{-2\kappa\sqrt{h^2}} = 1, 2 \text{ and } 4 \text{ meV}. \tag{115}$$

The speed limit, obtained from $\mathfrak{B}(t)$, is approximately 4 times faster than the exact velocities and independent of $\parallel P \parallel$. This means that there is no possibility to enhance the exact velocity above the black line, by changing the experimental parameters temperature, external magnetic fields, anisotropy energies, differently prepared initial states or the variables $gI_0\mathfrak{P}e^{-2\kappa\sqrt{h^2}}$ in $\parallel P \parallel$. The speed of the bound $\mathfrak{B}$ as well as the speed of the exact velocities are scaling with $\frac{1}{J}$.

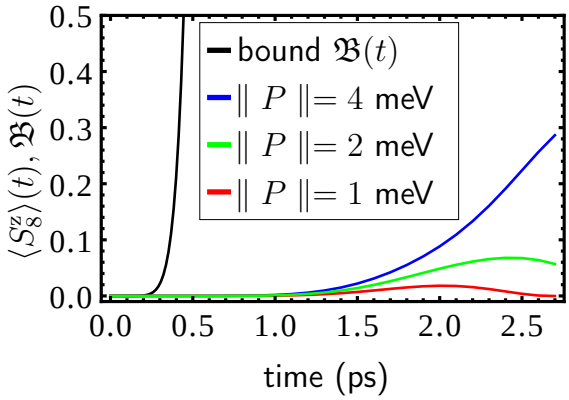

Figure 20: The arrival of a signal with Lieb-Robinson velocity v_{LR} (black line) is approximately 4 times faster than the arrival of the exact velocities (colored lines), for the case of a Heisenberg quantum spin chain with $J = 1$ meV and a length of 8 lattice sites. The energy of the action of the tip is chosen to be $\parallel P \parallel = 4, 2$, and 1 meV.

However, this comparison between the bound $\mathfrak{B}$ and the exact velocities eq. (108) is based on a physical interpretation instead of a mathematical

relation. To prevent possible errors which might arise from a physical interpretation without a mathematical relation, we will also introduce a strictly mathematically related bound $\tilde{\mathfrak{B}}$ on the exact velocities. This is done with the help of Proposition 5.4.1. in [44] and one obtains

$$\begin{aligned} \mid \omega(\tau_t^P(S_i^{\mathrm{z}})) - \omega(S_i^{\mathrm{z}}) \mid \leq & \sum_{n=1}^{\infty} \int_0^t dt_1 \cdots \int_0^{n-1} dt_n \times \\ & \times (2 \parallel P \parallel)^{n-1} \mathfrak{B}(t_n) \parallel S_i^{\mathrm{z}} \parallel \\ = & \parallel S_i^{\mathrm{z}} \parallel \int_0^t dt' \mathfrak{B}(t') \times \\ & \times \sum_{n=1}^{\infty} \frac{(t-t')^{n-1}}{(n-1)!} (2 \parallel P \parallel)^{n-1} \\ = & \parallel S_i^{\mathrm{z}} \parallel \frac{d}{d\lambda} \frac{e^{\lambda t} - 1}{\lambda} \doteq \tilde{\mathfrak{B}}(\parallel P \parallel, t), \end{aligned} \tag{116}$$

for $\lambda = 2 \parallel P \parallel$ after the differentiation in the last line. The bound $\tilde{\mathfrak{B}}$ depends on the norm of the perturbation, $\parallel P \parallel$, which contains the parameters of the modified Tersoff-Hamann model. Thus, we have prevented potential errors which might arise from a physical interpretation by the cost of an additional dependence of the parameters from the modified Tersoff-Hamann model. But still, the bound is independent of the other one-body interactions and valid for all initial states, e.g., all temperatures. Now, we will solve the bound $\tilde{\mathfrak{B}}$, eq. (116),which relates $\mathfrak{B}$ and the exact signal velocities, eq. (108), mathematically. $\tilde{\mathfrak{B}}$ contains a dependence of the perturbation $\parallel P \parallel = gI_0\mathfrak{P}e^{-2\kappa\sqrt{h^2}}$, but is still independent of the other experimental parameters: external magnetic fields, anisotropy energies and differently prepared initial states, e.g., different temperatures.

Fig. 21 shows a comparison of the improved bound $\mathfrak{B}(t)$ (black line) and the bounds $\tilde{\mathfrak{B}}(\parallel P \parallel, t)$ (colored lines), which give a strictly mathematically related bound on the exact velocities, but depend on the Tersoff-Hamann model. We have used the parameters $\parallel P \parallel = 0.5, 1, 2,$ and $4\,\mathrm{meV}$ for the bound $\tilde{\mathfrak{B}}$, as in the case of the exact velocities in fig. 20. It can be seen that the bounds $\tilde{\mathfrak{B}}(\parallel P \parallel, t)$ rise a little bit earlier than $\mathfrak{B}(t)$, but for low energies the increase of $\tilde{\mathfrak{B}}(\parallel P \parallel, t)$ comes more and more slower. However, $\tilde{\mathfrak{B}}$ and $\mathfrak{B}$ are basically of the same order of magnitude.

There are different reasons which are responsible for the discrepancy by a factor of approximately 4. The generality and the way of the mathematical construction of the bounds are two of these reasons. There are two kinds of generalities. The first generality, mentioned by the authors in [90], is the applicability to a large class of model systems. They used this reason as

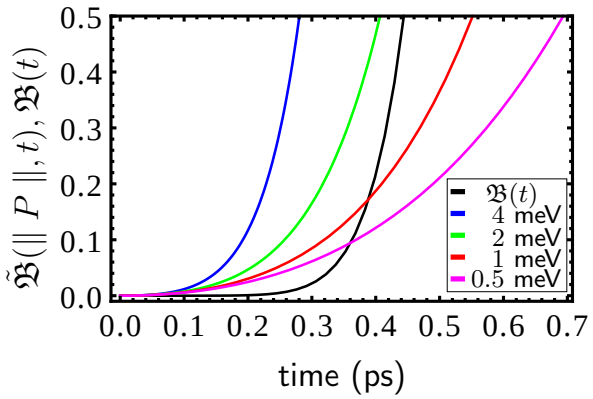

Figure 21: The bound $\mathfrak{B}(t)$ (black line) for the physical interpretation is compared with the bounds $\tilde{\mathfrak{B}}(\| P \|, t)$ (colored lines) which give a strictly mathematically related bound on the exact velocities. As in fig. 20 a Heisenberg quantum spin chain with $J = 1$ meV and a length of 8 lattice sites is used. The energy of the action of the tip is chosen to be $\| P \| = 4, 2, 1$, and 0.5 meV.

motivation for the derivation of the specific bound [90], which is only valid for the XY-model. A reduction of this discrepancy might be obtained, if improved bounds for more specific interactions are constructed, as for the XY-type model in [90]. However, the specific bound for the XY-model is questionable for a realistic description of an experimental setup. The bound [90] is multiplied by the square n^2 of the chain length n which is a disadvantage for large chain lengths. But the results in [91] make the development of specific bounds interesting. The second kind of generality is the independence of one-body interactions and the validity for all states. Since we have chosen the numerical method of exact diagonalization, we are able to treat the problem quite realistically and the values which are obtained from the calculation are exact in the framework of the chosen Hamiltonian. However, we have to choose certain parameters of the Hamiltonian which change the values of the exact speed but leave the bounds invariant. Furthermore, a specific state has to be chosen for the exact numerical calculation while the bound is valid for all states. Therefore, there is some freedom of choice on the side of the numerical calculation, which is not on the side of the bounds. The reflections while the signal propagates through the chain might be described by some kind of a random walk. These reflections depend on the choice of the state. Therefore, one might reduce the reflections in the signal propagation by choosing a different initial state and enhance the exact speed.

Next, we will use the temperature as an example for an experimental parameter which changes the exact signal speed, but leaves the bound $\mathfrak{B}$

as well as $\tilde{\mathfrak{B}}$ invariant. We will also use the Heisenberg interaction without anisotropy:

$$H_{\text{chain}} = \sum_{i,i+1}^{8} J\vec{S}_i \cdot \vec{S}_{i+1}, \tag{117}$$

which changes our exact signal propagation in contrast to the previous example of fig. 20. In fig. 22 we can see the arrival time $\langle S_8^z \rangle(t)$ of a signal

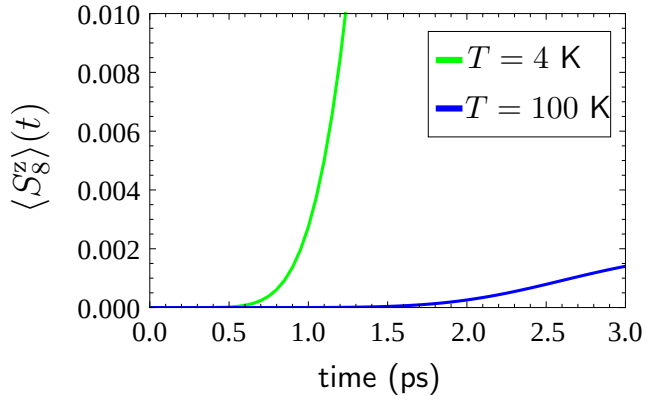

Figure 22: The arrival time of the exact signal speed for the two different temperatures of $T = 4$ K (green line) and $T = 100$ K (blue line). There is an enhancement of the signal speed by a factor of ≈ 2.7, caused by the different temperatures.

propagating through an $s = 1$ Heisenberg spin chain with the same interaction strength of $J = 1$ meV as above, but for the two different temperatures of $T = 4$ K and $T = 100$ K. One finds visible deviations at ≈ 0.7 ps for the 4 K signal and at ≈ 1.9 ps for the 100 K signal. A reduction of the temperature from 100 K to 4 K causes an enhancement of the signal speed by a factor of ≈ 2.7. However, the amplitude of the signal traveling at $T = 100$ K is relatively small, such that the functions $\langle S_8^z \rangle(t)$ are just plotted up to a value of 0.01. In this example, the influence of anisotropy energy has a less strong influence on the signal velocity than the temperature has, i.e., the observed signal speed in fig. 22 is similar to the signal speed in 20 (note that the scale for the expectation value is different).

Information transport in fermionic systems

According to the bounds on velocities and magnetic information transport of fixed magnetic atoms, we want to mention an interesting example (6.2.14A and 6.2.14B [44]) for an information transport which is related with the

transport of electrons in a substrate ("hopping" of the electrons). The Fermi algebra $\mathfrak{A}^F$ is defined as the C^*-algebra generated by elements $\{c_i, c_i^*; i \in \mathbb{Z}\}$ satisfying the anticommutation relations

$$\{c_i, c_j^*\} = \delta_{i,j}, \quad \{c_i, c_j\} = 0 \tag{118}$$

for all $i, j \in \mathbb{Z}$. Now consider the Hamiltonian

$$H_n = H_\Phi([-n, n]) = 2J \sum_{i=-n}^{n-1} (c_i^* c_{i+1} + c_{i+1}^* c_i) + h \sum_{i=-n}^{n} (2c_i^* c_i - \hat{1}), \tag{119}$$

where $J, h \in \mathbb{R}$. The infinitesimal time change is then given by

$$\delta_\Phi(c_j^*) = \lim_{n\to\infty} i[H_n, c_j^*] = 2iJ(c_{j-1}^* + c_{j+1}^*) + 2ihc_j^* \tag{120}$$

which can be integrated by Fourier transformation [44] to give

$$\tau_t(c_j^*) = \sum_{i\in\mathbb{Z}} G_t(j-i)c_i^*, \tag{121}$$

where

$$G_t(x) = \frac{1}{2\pi} \int_0^{2\pi} d\theta e^{ix\theta} e^{it(4J\cos\theta + 2h)}. \tag{122}$$

If $A = c_0^* c_0$ counts the particles at $i = 0$ and τ_j denotes the space translation operator, e.g., $\tau_j(c_0) = c_j$, then $\| [\tau_j \tau_t(A), A] \|$ is proportional to $|G_t(j)|$. One finds that $|G_t(Vt)|$ decreases exponentially with t if $|V| > 4J$ and decreases like $|t|^{-1/2}$ if $|V| < 4J$ [44]. It seems that there is no restriction by the number of particles, when $G_t(x)$ is solved.

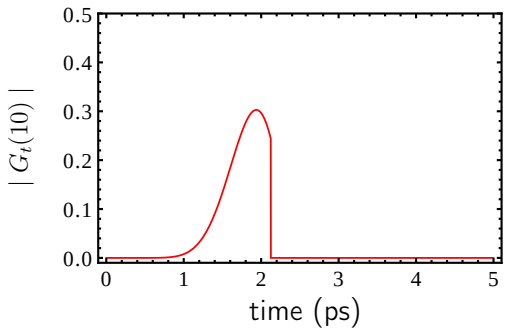

Figure 23: Propagation as a function of time in accordance to commutator norms $|G_t(j)| \propto \| [\tau_j \tau_t(c_0^* c_0), c_0^* c_0] \|$ and electron hopping in metallic substrates for $j = 10$ lattice sites, $h = 0$, and $J = 1$ meV.

6 Application to spin-based nanotechnology

Future spintronic devices should consist of several interacting magnetic atoms [2, 106], which are theoretically described as quantum spin particles. While theoretical calculations often led to a significant progress in the interpretation of experimental data obtained by SP-STM [38], the particle number of these systems is mostly the limiting factor for quantum mechanical calculations. A variety of different numerical methods were developed to estimate the expectation values of large quantum systems [92, 107]. Depending on the considered problem, different physical approximations are used in these methods. The error which is made by these approximations is difficult to estimate and remains unknown in most cases. We examine an upper bound on expectation values of quantum subsystems, which enables the estimation of a limit on the error that can be made by physical approximations outside the subsystem. This is of special interest for perturbation theory, where the bath is commonly approximated with simplified interactions. A recently realized all-spin-based atomic-scale logic device, consisting of iron atoms and cobalt islands placed on a copper substrate, serves as a specific example for an application of the bound. Strength and weakness of these methods will be critically discussed. For certain cases a quantitative answer to the old question when a small quantum system can be used instead of a large one, will be provided.

A common approximation is the decomposition of the Hamiltonian $H = H_{\mathrm{loc}} + H_{\mathrm{int}} + H_{\mathrm{bath}}$ for the full system H into a Hamiltonian for a local subsystem H_{loc}, an environment H_{bath} and a term H_{int} (it can also be H_{hyb}) which describes the interaction between the local subsystem and the environment (bath), e.g., a quantum impurity model [41]. The interactions H_{bath} for the environment are often simplified, while H_{loc} and H_{int} are treated more realistically. The expectation values are then estimated by numerical methods as perturbation theory [108] and quantum Monte Carlo [41]. The exact size of the error which is made by the approximation for the interactions in H_{bath} remains unknown in most cases and the quantitative value of the result is difficult to verify. In general, one does not know whether the expectation values of the local subsystem would change drastically, if more realistic interactions would be used for the environment.

Motivated by the lack of knowledge of this error, we estimate an exact upper bound on expectation values of quantum subsystems, when different environments are coupled to the subsystem. The environment is also treated fully quantum mechanically for the estimation of the bound. Furthermore, the bound provides the maximum difference of the expectation value of a quantum subsystem, when the subsystem is coupled to or decoupled from the

environment. Thus, for certain cases the inequality enables a quantitative answer to the old question when a small quantum system can be used instead of a large one, to save valuable memory capacity for numerical simulations. As in the case of a Lieb-Robinson bound $\mathfrak{B}$ on the signal velocity [77], the bound ϵ can also be solved for an arbitrary number of quantum spin particles.

6.1 The all-spin based atomic-scale logic device

The origin of the research efforts in spintronic devices might be dated to the late 1977, where the Apple I was the invention of the first home computer. It was developed by Steve Wozniak and sold to the public by Steve Jobs, who founded the two-man company Apple Inc. in 1976. The reduction of size and price of computer components made the application as home computer possible. Influenced by the economic success of the Apple II, International Business Machines Corp. (IBM), founded in 1896, entered the market of home computers in 1981. In the same year the scanning tunneling microscope was developed as a bottom up approach in the labs of IBM in Zürich. Since that time there is an ongoing development towards smaller, cheaper and more efficient computer devices. Subsequently, STM lead to a large progress in experimental condensed matter physics and Binnig and Rohrer won the Nobel price for this development in 1986. However, a STM is only able to investigate the topography of surfaces and is unable to investigate or influence the magnetic properties. This problem was solved by the usage of a magnetic tip in 1990 [109].

For the specific physical application we chose an all-spin-based logic device, which was recently realized in SP-STM. The device consists of 11 RKKY-coupled iron atoms and two cobalt islands placed on the surface of a copper substrate, see fig. 24. The Hamiltonian for the output is H_{loc} in our example. H_{int} consists of the interactions between the output and the nearest chain atoms and H_{bath} is the rest of the system, i.e., the spin chains and the cobalt islands. The device is therefore too large for an exact numerical calculation and has to be approximated by an idealized model. We use our inequality to examine the maximum error which is made by such approximations and investigate the functionality of the logic device for different temperatures. We suggest how the device can be modified to keep it functional for higher temperatures.

The atoms in the chain and the output atom in fig. 24 are iron atoms which are described by spin 2 particles [2, 106], placed on points i in a mathematical lattice L, i.e., $i \in L$. There is an interaction between the magnetic atoms on nearest neighboring points, $\{i, j\} = X \subset L$, which is

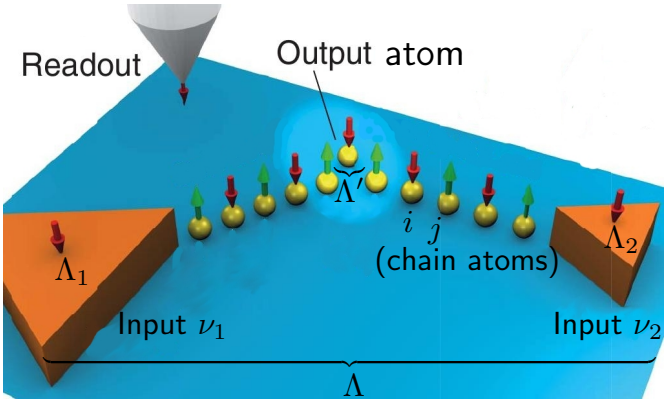

Figure 24: A spin based logic device consisting of 11 RKKY-coupled iron atoms and two cobalt islands placed on the surface of a copper substrate. The magnetization of the output atom depends on the magnetization of the cobalt islands, which serve as the input gates of the device [2]. The full system is too large and complex for purely numerical methods.

described by the Heisenberg interaction

$$\Phi_{\mathrm{H}}(\{i,j\}) = \sum_{\alpha=\mathrm{x,y,z}} J_{ij}^{\alpha} S_i^{\alpha} S_j^{\alpha}. \tag{123}$$

We will also investigate the special case $J_{ij}^{\mathrm{x}} = J_{ij}^{\mathrm{y}} = 0$ and $J_{ij}^{\mathrm{z}} \neq 0$, which is the Ising interaction. The magnetization of the iron atoms agrees with experimental data for the nearest neighbor Heisenberg and Ising interaction J_{ij}^{α}/s^2, where $s = 2$, $J_{ij}^{\alpha} = 0.1$ meV between atoms in the chain and $J_{ij}^{\alpha} = 0.025$ meV between the output atom and the ends of the chain [2]. The copper substrate induces an anisotropy energy on each single site

$$\Phi_{\mathrm{ani}}(\{i\}) = K(S_i^{\mathrm{z}})^2 \tag{124}$$

where $K \approx 1$ meV. There is also an external magnetic field which is described by

$$\Phi_{\mathrm{B}}(\{i\}) = g\mu_{\mathrm{B}} \vec{B} \cdot \vec{S}_i, \tag{125}$$

where g is a gyromagnetic constant, μ_{B} is the Bohr magneton and $\vec{B}$ the magnetic field. The two islands, placed in the subsets $\Lambda_1 \subset L$ and $\Lambda_2 \subset L$ (triangles in fig. 24), consist of approximately 500 and 300 cobalt atoms. The triangle geometry and the large particle number of the islands prevent any kind of an exact numerical calculation. The exact interaction strength between the cobalt atoms is for our purpose not of relevance, because the algebraically estimated value ϵ in eq. (131) is independent of that. The logic

device is placed on the subset $\Lambda \subset L$, see fig. 24., and has the Hamiltonian which contains all interactions in Λ:

$$H_{\text{logic}}(\Lambda) = \sum_{X \subset \Lambda} \big(\Phi_{\text{H}}(X) + \Phi_{\text{ani}}(X) + \Phi_{\text{B}}(X)\big). \tag{126}$$

The connection to the notation mentioned above is given by

$$H_{\text{loc}} = H_{\Phi}(\Lambda') = K(S_i^{\text{z}})^2 + \vec{B}\vec{S}_i, \tag{127}$$

where i is the site of the output atom and $\Lambda' = \{i\}$.

$$H_{\text{int}} = W_{\Phi}(\Lambda', \Lambda) = \sum_{\alpha=\text{x,y,y}} \big(J_{i-1i}^{\alpha} S_{i-1}^{\alpha} S_i^{\alpha} + J_{ii+1}^{\alpha} S_i^{\alpha} S_{i+1}^{\alpha}\big), \tag{128}$$

$\Lambda' = \{i\}$ and $H_{\text{bath}} = H(\Lambda \setminus \Lambda')$ contains all other interactions without the ones contained in eq. (127) and eq. (128). The magnetization direction of the islands, which is "up" or "down", is stable and can be switched with the help of an external magnetic field pulse [2]. The corresponding Hamiltonian which is responsible for the magnetization direction of the islands is therefore given by

$$H_{\nu_2}^{\nu_1} = \sum_{i \in \Lambda_1} g\mu_{\text{B}} \vec{B}_{\nu_1} \cdot \vec{S}_i + \sum_{i \in \Lambda_2} g\mu_{\text{B}} \vec{B}_{\nu_2} \cdot \vec{S}_i, \tag{129}$$

where $\nu_1 = \pm 1$ describes the direction of the magnetic field which switches the island placed in Λ_1; $+1$ means "up" and -1 means "down" magnetization. The same for ν_2 and the second island in Λ_2.

The magnetization direction of the output atom serves as the output of the logic device and is readout with a magnetic STM tip. The output atom's magnetization direction depends on the magnetization directions of the cobalt islands, which are described by the numbers ν_1 and ν_2. If both islands possess an "up" magnetization, i.e., $\nu_1 = +1$ and $\nu_2 = +1$, the output atom possesses also an "up" magnetization [2]. If both islands possess a "down" magnetization, i.e., $\nu_1 = -1$ and $\nu_2 = -1$, then the output atom possesses also a "down" magnetization. For the other cases, the output atom possesses an "up" magnetization [2]. Hence, the magnetization of the output atom is *controlled* via the magnetization of the cobalt islands, which are switched with external magnetic field pulses. Experimental data [12] as well as theoretical results [13] indicate that the readout of a single atom magnetization state is sufficiently described by a KMS state, which is identical to the thermal equilibrium Gibbs state for finite dimensional systems [44].

Thus, the output of the device, i.e., the magnetization of the output atom, is given by

$$\omega_{\Lambda\nu_2}^{\beta\nu_1}(S_{\text{g}}^{\text{z}}) = \frac{Tr\big(e^{-\beta(H_{\text{logic}}(\Lambda)+H_{\nu_2}^{\nu_1})} S_{\text{g}}^{\text{z}}\big)}{Tr\big(e^{-\beta(H_{\text{logic}}(\Lambda)+H_{\nu_2}^{\nu_1})}\big)}, \tag{130}$$

where $S_{\mathrm{g}}^{\mathrm{z}}$ is the z-component of the output atom's spin operator, β is the inverse temperature and ν_1, ν_2 describe the magnetization directions of the cobalt islands as above. For applications of the device, we are interested in the estimation of the output $\omega_{\Lambda\nu_2}^{\beta\nu_1}(S_{\mathrm{g}}^{\mathrm{z}})$ for higher temperatures than in the experiment [2], which was done at $T = 0.3$ K. Unfortunately, eq. (130) can't be calculated exactly for the logic device because of the system size. We will use analytical techniques of operator algebras [44] as an alternative method.

6.2 Bounds on approximations and modification of the logic device

We use the bound ϵ from eq. (61) of subsection 3.4 in this application. One obtains an inequality which restricts expectation values of large quantum systems to a finite interval, $a \leq \omega_{\Lambda\nu_2}^{\beta\nu_1}(S_{\mathrm{g}}^{\mathrm{z}}) \leq b$. The bound ϵ now enables us to estimate

$$\| \omega_{\Lambda\setminus\Lambda'\nu_2}^{\beta\nu_1} \otimes \omega_{\Lambda'}^{\beta} - \omega_{\Lambda\nu_2}^{\beta\nu_1} \| \leq \frac{2\beta||W_\Phi(\Lambda',\Lambda)||}{1-2\beta||W_\Phi(\Lambda',\Lambda)||} = \epsilon \tag{131}$$

for $2\beta||W_\Phi(\Lambda',\Lambda)|| < 1$.

The state $\omega_{\Lambda\setminus\Lambda'\nu_2}^{\beta\nu_1} \otimes \omega_{\Lambda'}^{\beta}$ means that the small subsystem in Λ', which is the output atom in our case, is isolated from the rest of the system. Thus, $\omega_{\Lambda\setminus\Lambda'\nu_2}^{\beta\nu_1} \otimes \omega_{\Lambda'}^{\beta}$ has the property, that the magnetization of the output atom is independent of the magnetization states of the cobalt islands. Hence, the state describes a device which does not work. In this case, the expression $(\omega_{\Lambda\setminus\Lambda'\nu_2}^{\beta\nu_1} \otimes \omega_{\Lambda'}^{\beta})(S_{\mathrm{g}}^{\mathrm{z}}) = \omega_{\Lambda'}^{\beta}(S_{\mathrm{g}}^{\mathrm{z}})$ can be calculated with the numerical method of "exact diagonalization", because the large system in Λ reduces to the small subsystem in Λ' when an observable located in Λ' is used. For our logic device we obtain

$$\underbrace{\omega_{\Lambda'}^{\beta}(S_{\mathrm{g}}^{\mathrm{z}}) - 2\epsilon}_{\text{lower bound } a} \leqslant \underbrace{\omega_{\Lambda\nu_2}^{\beta\nu_1}(S_{\mathrm{g}}^{\mathrm{z}})}_{\text{full system}} \leqslant \underbrace{\omega_{\Lambda'}^{\beta}(S_{\mathrm{g}}^{\mathrm{z}}) + 2\epsilon}_{\text{upper bound } b}, \tag{132}$$

where the factor 2 arises from the operator norm $\| S_{\mathrm{g}}^{\mathrm{z}} \|$, ϵ depends on the temperature T and the interaction strength $|J_{ij}|$ between the output atom and the end of the spin chains. The lower and the upper bound, a and b, can be solved without problems and provide the borders of the interval which restricts the expectation value of the full system. If ϵ is very small, the magnetization $\omega_{\Lambda\nu_2}^{\beta\nu_1}(S_{\mathrm{g}}^{\mathrm{z}})$ of the output atom is for all magnetizations ν_1, ν_2 of the cobalt islands very close to the magnetization $\omega_{\Lambda'}^{\beta}(S_{\mathrm{g}}^{\mathrm{z}})$ of the idealized isolated output atom. This means that we have only very little control on the output via the input gates of the device.

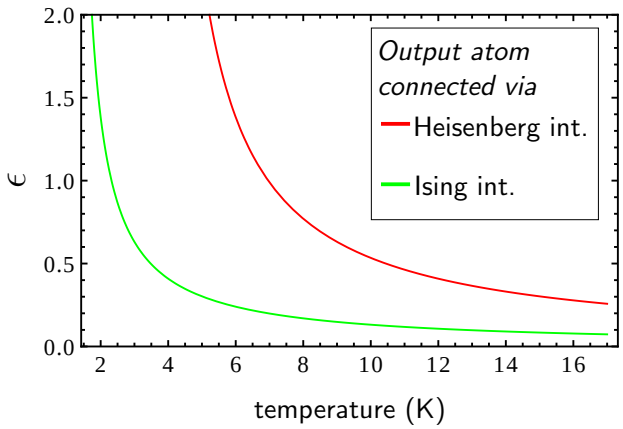

Figure 25: The controllability of the magnetization of the output atom decreases with increasing temperature. The two cases when the output atom is coupled via Heisenberg (red line) or Ising (green line) interaction to the chain ends are considered. A magnetization reversal of the cobalt islands can change the output atom's magnetization maximally by the value 4ϵ.

Fig. 25 shows the bound ϵ on the control of the magnetization of the output atom, when the magnetization states ν_1, ν_2 of the cobalt islands are switched, as a function of temperature. The expectation value $\omega_{\Lambda\nu_2}^{\beta\nu_1}(S_{\mathrm{g}}^{\mathrm{z}})$ of the output atom ranges ideally from -2 ("down state") to $+2$ ("up state"), because it is described as a spin 2 particle. If one or both islands are switched, the magnetization can maximally change by 4ϵ, because of eq. (132). The control on the output atom's magnetization decreases for an increasing temperature. For decreasing ϵ the logic device converges to the device $\omega_{\Lambda\setminus\Lambda'\nu_2}^{\beta\nu_1} \otimes \omega_{\Lambda'}^{\beta}$ in eq. (132), which does not work and the question is how to avoid this problem. The extreme case $\epsilon = 0$ would mean that we have no control on the output atom's magnetization, but this appears only in the infinite temperature limit, which is not of experimental relevance. The value ϵ only gives us the total amount for the magnetization change, but not the specific values, from which value to which value the magnetization maximally changes. This information is given by the values a and b in eq. (132). The bound ϵ is independent of external magnetic fields, which are also applied to the output atom during the reading process [2]. However, the bounds a and b depend on the external magnetic field.

Fig. 26 shows the bounds a and b on the output atom's magnetization change as a function of the external magnetic field for a temperature of $T = 15$ K. The bounds a and b are calculated for the Heisenberg interaction. If the Ising interaction would be chosen, the black lines would be closer to the red line, corresponding to fig. 25. The red curve is the magnetization curve

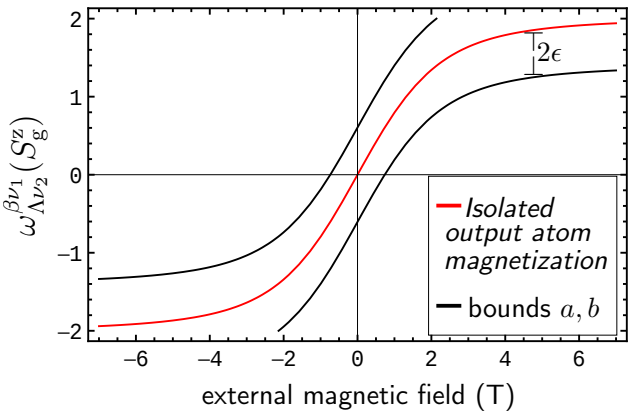

Figure 26: The magnetization of the output atom as isolated subsystem (red line) and the maximum change $\pm 2\epsilon$ (black lines), when this atom is connected via Heisenberg interaction to the spin chains and the magnetization directions of the cobalt islands are switched at $T = 15$ K. All possible magnetization values of the output atom, eq. (130), are between the black lines for all values ν_1, ν_2.

of the output atom as isolated subsystem. The black curves are the bounds a and b on the change of the magnetization for the real device in the experiment, when the magnetization states of the cobalt islands are switched. All possible expectation values for the output atom's magnetization, eq. (130), which is the output of the device, are between the black lines for all values ν_1, ν_2. From fig. 25 we know, that the black lines come closer to the red line when the temperature is increased. It remains to examine, how the logic device should be modified, if it should work at higher temperatures.

Fig. 27 shows the bound ϵ as a function of the interaction strength J_{ij}/s^2 between the output atom and the end of the spin chains for the temperatures $T = 50$ K (red line), $T = 150$ K (green line), and $T = 300$ K (blue line). The bound on the change of the output increases with increasing interaction strength. For lower temperatures the bound increases faster than for higher temperatures. Thus, if the logic device shall work at higher temperatures, ultimately up to room temperature, i.e., $T = 300$ K, it is evident that the interaction strength between the output atom and the atoms in the spin chains should be increased. However, nontrivial is certainly an exact quantitative statement. Fig. 27 states that the interaction strength should at least be increased above approximately $J/s^2 \approx 1$ meV, for $s = 2$ this means $J > 4$ meV. This result is exact in the sense, that it is free of errors from physical approximations which would be made by the usage of macrospins, for

example.

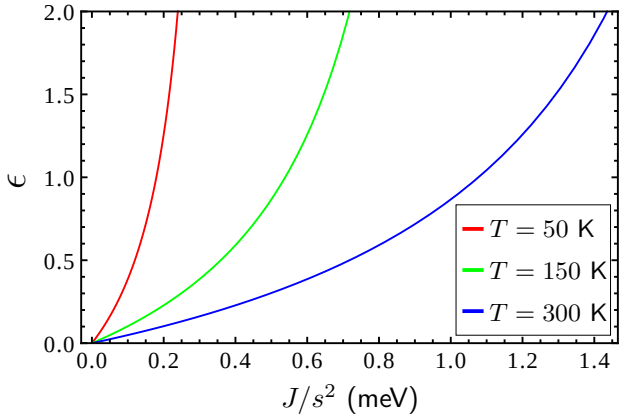

Figure 27: The upper bound ϵ on the maximum possible change of the output atom's magnetization, when the cobalt islands are manipulated. If the logic device shall work at higher temperatures, the interaction strength J_{ij} between the iron atoms should at least be increased above 4 meV.

In [106] it is indicated that this large value for the interaction strength is not achievable by a change of the distance between the RKKY-coupled iron atoms. It seems advisable to use superexchange coupled magnetic molecules. A spin chain consisting of planar geometric, magnetic Co-$(5, 5' - \mathrm{Br}_2 -$ Salophene) molecules was recently realized [110]. The single molecules form a spin chain, when the bromium atoms are removed to achieve a bond between two carbon atoms of different molecules. A further superexchange coupled molecular spin chain was constructed with the help of cobalt phthalocyanine thin films [111]. The phthalocyanine molecule, with empirical formula $C_{32}H_{18}N_8$, has also a planar geometry. The cobalt atom is placed in the center and a spin chain is formed when several cobalt phthalocyanine molecules are placed on top of each other.

7 Conclusion

Exact, perturbative, and mean-field type numerical and algebraic methods were applied to the description of quantum spin systems, which are influenced by a spin-polarized scanning tunneling microscope. All of these methods were included in the general mathematical framework of the C^*-algebraic reformulation of Quantum Statistical Mechanics, which enables the application of comprehensive analytical methods. A general principle $(\mathfrak{A}, \tau) \rightleftarrows (\mathfrak{A}, \tau^P)$ was suggested to describe the functionality of SP-STM in terms of C^*-dynamical systems, which provided the foundation for the application of the algebraic methods. The connection of the abstract theory to the experiments was partially achieved by the numerical method of "exact diagonalization", which was used for the real-time dynamics of the magnetic quantum systems at finite temperatures. Lieb-Robinson bounds and a bound on expectation values of quantum subsystems supplemented this method.

The non-equilibrium dynamics of adatoms on different substrates under the action of a magnetic STM tip has been studied. The equations (86) and (87) are describing the time-evolution of a magnetic atom's spin-components during and after an interaction with the magnetic tip. A satisfactory agreement of these equations with experimental data has been found, where the perturbation has been identified as the interaction between the STM-tip and the investigated sample. It has been shown that the application of a perturbed KMS state in (87) is well suited to model the relaxation dynamics of magnetic atoms at finite temperatures. The theoretical investigation of the spin dynamics of the sample within the experimental time resolution of the SP-STM setup, can be achieved by an application of the perturbed dynamics in eq. (86). We were able to reproduce the experimentally obtained time-averages of expectation values for Co atoms on Pt(111), which clarified the unexplained zero magnetization at zero external magnetic field in [12]. Our quantum mechanical time-average is therefore successful, where the classical dynamics failed to work. Fig. 7, 8, and 9 demonstrate that thermalization can be achieved for relatively small systems, which can be calculated using exact diagonalization. The relaxation can be approximated with an exponential function, which is in agreement with experimental results. It is demonstrated that the lifetime of single adatoms increases with increasing anisotropy barrier D and decreasing temperature. It was demonstrated that quantum fluctuations are reduced with increasing temperatures.

The exact signal transport in spin chains was investigated. For Fe/Ir(001) spin chains an averaged signal speed of about 50 $\frac{\text{sites}}{ps}$ was found. The next to nearest neighboring atom reacted earlier than the nearest neighboring atom. SP-STM was identified as a suitable experimental setup for a quantitative

investigation of Lieb-Robinson bounds. On fig. 18 it was shown that a simplified version of the latest, most general bound, $\mathfrak{B}$, is improved by a factor 100 than compared to the old bound $\mathfrak{L}$. This is mainly caused by the disappearance of the factor $|X|(2s+1)^{2|X|}e^{\xi D(X)}$ in $\mathfrak{B}$. $\tilde{\mathfrak{B}}$ was derived to provide a strictly mathematical relation between Lieb-Robinson bounds and the exact signal velocities in the simulated experiment. In fig. 20 and 21 it is shown that the exact signal velocities in spin chains with Heisenberg interaction are approximately 4 times slower than the Lieb-Robinson velocity v_{LR} (speed limit) provided by $\mathfrak{B}$. This analysis showed that the Lieb-Robinson velocity of the bound $\mathfrak{B}$ is already on the correct order of magnitude in view of exact velocities occurring in realistic magnetic quantum systems. The modification and enhancement of the signal velocity by a change of experimental parameters was investigated, in view of the efficiency of future spintronic devices. It was shown that external magnetic fields, the temperature, anisotropy energies, and differently prepared initial states cannot increase the exact realistic signal velocity by more than a factor of 4, because the speed limit is independent of these parameters. The parameters of the modified Tersoff-Hamann model change the output signal of the last chain atom and the bound $\tilde{\mathfrak{B}}$, but leave $\mathfrak{B}$ invariant. The derivation of improved, eventually specific, bounds and the use of several different experimental parameters for the exact velocities would provide a further reduction of the discrepancy.

The inequality (131) gives an upper bound on the error that is made by using simplified interactions for the environment H_{bath} for a numerical simulation. The bound is applicable to quantum subsystems and perturbative techniques at finite temperature, as Quantum Monte Carlo. A logic device investigated in SP-STM served as a specific example where this inequality provides useful values and the functionality of the device for higher temperatures was examined quantitatively. Fig. 25 shows the control on the output, which is the magnetization of the central atom, when the input is changed as a function of temperature. Fig. 27 shows quantitatively and exactly how much the interaction strength should at least be increased, such that the device can work at higher temperatures, e.g., room temperature. It is advised to use superexchange coupled molecular spin chains to achieve this. A numerical calculation with a simplified environment of the output atom provides an expectation value, where the quality is less assured. The value ϵ can be used to examine exactly and quantitatively the question, whether a small subsystem can be used instead of the full quantum system to save memory of a computer system for numerical simulations. While our proposed method works well for weakly interacting systems (depending on the temperature), it remains an open question as to how far these methods can be extended to investigate also strongly interacting systems.

Mean-field type approximated KMS states were introduced for a numerical handling of the multiplicity of equilibrium states of magnetic quantum systems. In view of spintronic devices, this was motivated by the requirement of the conversion of one thermodynamically stable spin structure into a different thermodynamically stable spin structure. Certainly, these states are useful if one can numerically handle a large enough spin system. However, the numerical method of "exact diagonalization" yielded only a few of the desired results. Moreover, this numerical method has also a striking unsuitability to handle these states, because of the limited system size. The Lindblad master equation or continuous-time quantum Monte Carlo method seem to be more suitable numerical methods for these investigations. The relation between the perturbed and unperturbed KMS states by the truncated functions in Theorem 5.4.4. [44] seems to have a suitable intersection to Quantum Monte Carlo methods for the mean-field type approximated KMS states.

Further potential future work in this area entails an estimation of a bound for the mean-field type approximated KMS states, applications of bounds for ground state approximations [74], and the usage of AQFT for a more realistic modeling of the influence of the substrate and tip electrons.

Bibliography

[1] Roland Wiesendanger. Spin mapping at the nanoscale and atomic scale. *Rev. Mod. Phys.*, 81:1495–1550, Nov 2009.

[2] Alexander Ako Khajetoorians, Jens Wiebe, Bruno Chilian, and Roland Wiesendanger. Realizing all-spin–based logic operations atom by atom. *Science*, 332(6033):1062–1064, 2011.

[3] Andrea Candini, Svetlana Klyatskaya, Mario Ruben, Wolfgang Wernsdorfer, and Marco Affronte. Graphene spintronic devices with molecular nanomagnets. *Nano Letters*, 11(7):2634–2639, 2011.

[4] Péter Földi, Orsolya Kálmán, Mihály G. Benedict, and F. M. Peeters. Networks of quantum nanorings: Programmable spintronic devices. *Nano Letters*, 8(8):2556–2558, 2008.

[5] S. L. Kawahara, J. Lagoute, V. Repain, C. Chacon, Y. Girard, S. Rousset, A. Smogunov, and C. Barreteau. Large magnetoresistance through a single molecule due to a spin-split hybridized orbital. *Nano Letters*, 12(9):4558–4563, 2012.

[6] Régis Decker, Jens Brede, Nicolae Atodiresei, Vasile Caciuc, Stefan Blügel, and Roland Wiesendanger. Atomic-scale magnetism of cobalt-intercalated graphene. *Phys. Rev. B*, 87:041403, Jan 2013.

[7] L. V. Dzemiantsova, M. Hortamani, C. Hanneken, A. Kubetzka, K. von Bergmann, and R. Wiesendanger. Magnetic coupling of single co adatoms to a co underlayer through a pd spacer of variable thickness. *Phys. Rev. B*, 86:094427, Sep 2012.

[8] J. Brede and R. Wiesendanger. Spin-resolved characterization of single cobalt phthalocyanine molecules on a ferromagnetic support. *Phys. Rev. B*, 86:184423, Nov 2012.

[9] Lihui Zhou, Focko Meier, Jens Wiebe, and Roland Wiesendanger. Inversion of spin polarization above individual magnetic adatoms. *Phys. Rev. B*, 82:012409, Jul 2010.

[10] P. Ferriani, K. von Bergmann, E. Y. Vedmedenko, S. Heinze, M. Bode, M. Heide, G. Bihlmayer, S. Blügel, and R. Wiesendanger. Atomic-scale spin spiral with a unique rotational sense: Mn monolayer on W(001). *Phys. Rev. Lett.*, 101:027201, Jul 2008.

[11] A. Kubetzka, M. Bode, and R. Wiesendanger. Spin-polarized scanning tunneling microscopy in field emission mode. *Applied Physics Letters*, 91(1), 2007.

[12] Focko Meier, Lihui Zhou, Jens Wiebe, and Roland Wiesendanger. Revealing magnetic interactions from single-atom magnetization curves. *Science*, 320(5872):82–86, 2008.

[13] K Them, T Stapelfeldt, E Y Vedmedenko, and R Wiesendanger. Non-equilibrium finite temperature dynamics of magnetic quantum systems: applications to spin-polarized scanning tunneling microscopy. *New Journal of Physics*, 15(1):013009, 2013.

[14] Maylis Orio, Dimitrios Pantazis, and Frank Neese. Density functional theory. *Photosynthesis Research*, 102(2-3):443–453, 2009.

[15] Erich Runge and E. K. U. Gross. Density-functional theory for time-dependent systems. *Phys. Rev. Lett.*, 52:997–1000, Mar 1984.

[16] W. M. C. Foulkes, L. Mitas, R. J. Needs, and G. Rajagopal. Quantum monte carlo simulations of solids. *Rev. Mod. Phys.*, 73:33–83, Jan 2001.

[17] Anders W. Sandvik and Juhani Kurkijärvi. Quantum monte carlo simulation method for spin systems. *Phys. Rev. B*, 43:5950–5961, Mar 1991.

[18] P.J. Reynolds, R.N. Barnett, B.L. Hammond, and Jr. Lester, W.A. Molecular physics and chemistry applications of quantum monte carlo. *Journal of Statistical Physics*, 43(5-6):1017–1026, 1986.

[19] Antoine Georges, Gabriel Kotliar, Werner Krauth, and Marcelo J. Rozenberg. Dynamical mean-field theory of strongly correlated fermion systems and the limit of infinite dimensions. *Rev. Mod. Phys.*, 68:13–125, Jan 1996.

[20] K. Yabana and G. F. Bertsch. Time-dependent local-density approximation in real time. *Phys. Rev. B*, 54:4484–4487, Aug 1996.

[21] G. Vignale, C. A. Ullrich, and S. Conti. Time-dependent density functional theory beyond the adiabatic local density approximation. *Phys. Rev. Lett.*, 79:4878–4881, Dec 1997.

[22] C. Jung, A. Lieder, S. Brener, H. Hafermann, B. Baxevanis, A. Chudnovskiy, A.N. Rubtsov, M.I. Katsnelson, and A.I. Lichtenstein. Dual-fermion approach to non-equilibrium strongly correlated problems. *Annalen der Physik*, 524(1):49–61, 2012.

[23] H. Allmaier, L. Chioncel, E. Arrigoni, M. I. Katsnelson, and A. I. Lichtenstein. Half-metallicity in nimnsb: A variational cluster approach with ab initio parameters. *Phys. Rev. B*, 81:054422, Feb 2010.

[24] Two-particle correlations in a functional renormalization group scheme using a dynamical mean-field theory approach. *Physical Review B*, 88(19), 2013.

[25] Universal out-of-equilibrium transport in kondo-correlated quantum dots: Renormalized dual fermions on the keldysh contour. *Physical Review Letters*, 110(1), 2013.

[26] Density matrix embedding: A simple alternative to dynamical mean-field theory. *Physical Review Letters*, 109(18), 2012.

[27] Role of rotational symmetry in the magnetism of a multiorbital model. *Physical Review B*, 86(15), 2012.

[28] Distributional exact diagonalization formalism for quantum impurity models. *Physical Review B*, 86(11), 2012.

[29] Local electronic correlation at the two-particle level. *Physical Review B*, 86(12), 2012.

[30] Efficient treatment of the high-frequency tail of the self-energy function and its relevance for multiorbital models. *Physical Review B*, 85(11):115103, 2012.

[31] Dual boson approach to collective excitations in correlated fermionic systems. *Annals of Physics*, 2012.

[32] Superperturbation theory on the real axis. *Annalen der Physik*, 523(8-9):706, 2011.

[33] Exact diagonalization study of 2d hubbard model on honeycomb lattice: Semi-metal to insulator transition. *Physics Letters A*, 2011.

[34] Dual-fermion approach to non-equilibrium strongly correlated problems. *Annalen der Physik*, page n/a, 2011.

[35] Analytical approximation for single-impurity anderson model. *JETP Letters*, 91(6):319, 2010.

[36] Dynamical mean-field theory within the full-potential methods: Electronic structure of $CeIrIn_5$, $CeCoIn_5$, and $CeRhIn_5$. *Physical Review B*, 81(19):195107, 2010.

[37] M I Katsnelson and A I Lichtenstein. Theory of optically forbidden d–d transitions in strongly correlated crystals. *Journal of Physics: Condensed Matter*, 22(38):382201, 2010.

[38] Stefan Heinze, Kirsten von Bergmann, Matthias Menzel, Jens Brede, Andre Kubetzka, Roland Wiesendanger, Gustav Bihlmayer, and Stefan Blugel. Spontaneous atomic-scale magnetic skyrmion lattice in two dimensions. *Nat Phys*, 7(1):713–718, 2011.

[39] Emil Prodan. Raising the temperature on density-functional theory. *Physics*, 3:99, Nov 2010.

[40] Alternative functional renormalization group approach to the single impurity anderson model. *Physical Review B*, 87(3), 2013.

[41] Emanuel Gull, Andrew J. Millis, Alexander I. Lichtenstein, Alexey N. Rubtsov, Matthias Troyer, and Philipp Werner. Continuous-time monte carlo methods for quantum impurity models. *Rev. Mod. Phys.*, 83:349–404, May 2011.

[42] M. Høgh Jensen and Per Bak. Mean-field theory of the three-dimensional anisotropic ising model as a four-dimensional mapping. *Phys. Rev. B*, 27:6853–6868, Jun 1983.

[43] S. Krause, L. Berbil-Bautista, G. Herzog, M. Bode, and R. Wiesendanger. Current-induced magnetization switching with a spin-polarized scanning tunneling microscope. *Science*, 317(5844):1537–1540, 2007.

[44] Ola. Bratteli and Derek W. Robinson. *Operator algebras and quantum statistical mechanics II.* Springer-Verlag Berlin Heidelberg, 1981.

[45] Fa Yueh Wu. *Exactly Solved Models: A Journey in Statistical Mechanics Selected Papers with Commentaries (1963?2008).* World Scientific, Singapore, 2009.

[46] Ola Bratteli and George A. Elliott. Small eigenvalue variation and real rank zero. *Pacific Journal of Mathematics*, 175(1):47–59, 1996.

[47] Ola Bratteli and Akitaka Kishimoto. Noncommutative spheres. iii. irrational rotations. *Communications in Mathematical Physics*, 147(3):605–624, 1992.

[48] Ola Bratteli, George A. Elliott, David E. Evans, and Akitaka Kishimoto. Quasi-product actions of a compact abelian group on a c^*-algebra. *Tohoku Mathematical Journal*, 41(1):133–161, 1989.

[49] Ola Bratteli. Review: Jerome a. goldstein, semigroups of linear operators and applications. *Bulletin (New Series) of the American Mathematical Society*, 18(1):100–103, 01 1988.

[50] Ola BRATTELI, George A. ELLIOTT, and Derek W. ROBINSON. Strong topological transitivity and c^* -dynamical systems. *Journal of the Mathematical Society of Japan*, 37(1):115–133, 01 1985.

[51] Ola Bratteli and Palle E. T. Jørgensen. Derivations commuting with abelian gauge actions on lattice systems. *Communications in Mathematical Physics*, 87(3):353–364, 1982.

[52] Ola Bratteli, George A. Elliott, and Richard H. Herman. On the possible temperatures of a dynamical system. *Communications in Mathematical Physics*, 74(3):281–295, 1980.

[53] Ola Bratteli, Akitaka Kishimoto, and Derek W. Robinson. Positivity and monotonicity properties of c_0-semigroups. i. *Communications in Mathematical Physics*, 75(1):67–84, 1980.

[54] Ola Bratteli. Crossed products of uhf algebras by product type actions. *Duke Mathematical Journal*, 46(1):1–23, 03 1979.

[55] Ola Bratteli and Uffe Haagerup. Unbounded derivations and invariant states. *Communications in Mathematical Physics*, 59(1):79–95, 1978.

[56] Ola Bratteli, Richard H. Herman, and Derek W. Robinson. Perturbations of flows on banach spaces and operator algebras. *Communications in Mathematical Physics*, 59(2):167–196, 1978.

[57] Ola Bratteli, Akitaka Kishimoto, and Derek W. Robinson. Ground states of quantum spin systems. *Communications in Mathematical Physics*, 64(1):41–48, 1978.

[58] Kolja Them and Marcos Brum. States of low energy in homogeneous and inhomogeneous expanding spacetimes. *Classical and Quantum Gravity*, 30(23):235035, 2013.

[59] Huzihiro Araki and Hajime Moriya. Equilibrium statistical mechanics of fermion lattice systems. *Reviews in Mathematical Physics*, 15(02):93–198, 2003.

[60] Ola. Bratteli and Derek W. Robinson. *Operator algebras and quantum statistical mechanics I / Ola Bratteli, Derek W. Robinson ; [editors, Wolf Beiglbock ... et al.]*. Springer-Verlag, New York :, 1979.

[61] Ola Bratteli, George A. Elliott, and Akitaka Kishimoto. The temperature state space of a c*-dynamical system, ii. *Annals of Mathematics*, 123(2):pp. 205–263, 1986.

[62] Derek W. Robinson. Statistical mechanics of quantum spin systems. *Communications in Mathematical Physics*, 6(2):151–160, 1967.

[63] Derek W. Robinson. Statistical mechanics of quantum spin systems. ii. *Communications in Mathematical Physics*, 7(4):337–348, 1968.

[64] III Lanford, OscarE. and Derek W. Robinson. Statistical mechanics of quantum spin systems. iii. *Communications in Mathematical Physics*, 9(4):327–338, 1968.

[65] Bruno Nachtergaele, VolkherB. Scholz, and ReinhardF. Werner. Local approximation of observables and commutator bounds. In Jan Janas, Pavel Kurasov, Ari Laptev, and Sergei Naboko, editors, *Operator Methods in Mathematical Physics*, volume 227 of *Operator Theory: Advances and Applications*, pages 143–149. Springer Basel, 2013.

[66] Bruno Nachtergaele, Stephen Ng, and Shannon Starr. Ferromagnetic ordering of energy levels for $u_q(\mathfrak{sl}_2)$ symmetric spin chains. *Letters in Mathematical Physics*, 100(3):327–356, 2012.

[67] Sven Bachmann, Spyridon Michalakis, Bruno Nachtergaele, and Robert Sims. Automorphic equivalence within gapped phases of quantum lattice systems. *Communications in Mathematical Physics*, 309(3):835–871, 2012.

[68] Bruno Nachtergaele and Robert Sims. Locality estimates for quantum spin systems. In Vladas Sidoravičius, editor, *New Trends in Mathematical Physics*, pages 591–614. Springer Netherlands, 2009.

[69] Bruno Nachtergaele, Wolfgang Spitzer, and Shannon Starr. Droplet excitations for the spin-1/2 xxz chain with kink boundary conditions. *Annales Henri Poincaré*, 8(1):165–201, 2007.

[70] Bruno Nachtergaele and Shannon Starr. Ordering of energy levels in heisenberg models and applications. In Joachim Asch and Alain Joye, editors, *Mathematical Physics of Quantum Mechanics*, volume 690 of *Lecture Notes in Physics*, pages 149–170. Springer Berlin Heidelberg, 2006.

[71] Bruno Nachtergaele, Wolfgang Spitzer, and Shannon Starr. Ferromagnetic ordering of energy levels. *Journal of Statistical Physics*, 116(1-4):719–738, 2004.

[72] Bruno Nachtergaele and Shannon Starr. Droplet states in the xxz heisenberg chain. *Communications in Mathematical Physics*, 218(3):569–607, 2001.

[73] Bruno Nachtergaele. The spectral gap for some spin chains with discrete symmetry breaking. *Communications in Mathematical Physics*, 175(3):565–606, 1996.

[74] Bruno Nachtergaele and Robert Sims. Lieb-Robinson Bounds in Quantum Many-Body Physics. 2010.

[75] S. Krause, G. Herzog, T. Stapelfeldt, L. Berbil-Bautista, M. Bode, E. Y. Vedmedenko, and R. Wiesendanger. Magnetization reversal of nanoscale islands: How size and shape affect the arrhenius prefactor. *Phys. Rev. Lett.*, 103:127202, Sep 2009.

[76] Matthias Menzel, Yuriy Mokrousov, Robert Wieser, Jessica E. Bickel, Elena Vedmedenko, Stefan Blügel, Stefan Heinze, Kirsten von Bergmann, Andre Kubetzka, and Roland Wiesendanger. Information transfer by vector spin chirality in finite magnetic chains. *Phys. Rev. Lett.*, 108:197204, May 2012.

[77] K. Them. Towards experimental tests and applications of lieb-robinson bounds. *Phys. Rev. A*, 89:022126, Feb 2014.

[78] Niklas Romming, Christian Hanneken, Matthias Menzel, Jessica E. Bickel, Boris Wolter, Kirsten von Bergmann, Andre Kubetzka, and Roland Wiesendanger. Writing and deleting single magnetic skyrmions. *Science*, 341(6146):636–639, 2013.

[79] Rudolf Haag and Daniel Kastler. An algebraic approach to quantum field theory. *Journal of Mathematical Physics*, 5(7):848–861, 1964.

[80] Ola Bratteli and Derek W. Robinson. Unbounded derivations of c^*-algebras. ii. *Communications in Mathematical Physics*, 46(1):11–30, 1976.

[81] Ola Bratteli and Derek W. Robinson. Unbounded derivations and invariant trace states. *Communications in Mathematical Physics*, 46(1):31–35, 1976.

[82] Ola Bratteli and Daniel Kastler. Relaxing the clustering condition in the derivation of the kms property. *Communications in Mathematical Physics*, 46(1):37–42, 1976.

[83] Ola Bratteli and Derek W. Robinson. Green's functions, hamiltonians and modular automorphisms. *Communications in Mathematical Physics*, 50(2):133–156, 1976.

[84] Ola Bratteli and Derek W. Robinson. Unbounded derivations of c^*-algebras. *Communications in Mathematical Physics*, 42(3):253–268, 1975.

[85] Klaus Fredenhagen. *Private communication*, 2012.

[86] Kolja Them, Klaus Fredenhagen, and Roland Wiesendanger. Improvement for lieb-robinson bounds and information transfer in spin chains. *arXiv:1308.2882v1*, 2013.

[87] J. Tersoff and D. R. Hamann. Theory of the scanning tunneling microscope. *Phys. Rev. B*, 31:805–813, Jan 1985.

[88] T. Stapelfeldt, R. Wieser, E. Y. Vedmedenko, and R. Wiesendanger. Domain wall manipulation with a magnetic tip. *Phys. Rev. Lett.*, 107:027203, Jul 2011.

[89] Bruno Nachtergaele, Hillel Raz, Benjamin Schlein, and Robert Sims. Lieb-robinson bounds for harmonic and anharmonic lattice systems. *Communications in Mathematical Physics*, 286:1073–1098, 2009.

[90] Christian K. Burrell and Tobias J. Osborne. Bounds on the speed of information propagation in disordered quantum spin chains. *Phys. Rev. Lett.*, 99:167201, Oct 2007.

[91] Eman Hamza, Robert Sims, and Günter Stolz. Dynamical localization in disordered quantum spin systems. *Commun. Math. Phys*, 315:215–239, 2012.

[92] Matthias Balzer, Nadine Gdaniec, and Michael Potthoff. Krylov-space approach to the equilibrium and nonequilibrium single-particle green's function. *Journal of Physics: Condensed Matter*, 24(3):035603, 2012.

[93] Huzihiro Araki and Eytan Barouch. On the dynamics and ergodic properties of the xy model. *Journal of Statistical Physics*, 31(2):327–345, 1983.

[94] Alexander Ako Khajetoorians, Bruno Chilian, Jens Wiebe, Sergej Schuwalow, Frank Lechermann, and Roland Wiesendanger. Detecting excitation and magnetization of individual dopants in a semiconductor. *Nature*, 467(7319):1084–1087, 2010.

[95] A. A. Khajetoorians, S. Lounis, B. Chilian, A. T. Costa, L. Zhou, D. L. Mills, J. Wiebe, and R. Wiesendanger. Itinerant nature of atom-magnetization excitation by tunneling electrons. *Phys. Rev. Lett.*, 106:037205, Jan 2011.

[96] Sebastian Loth, Markus Etzkorn, Christopher P. Lutz, D. M. Eigler, and Andreas J. Heinrich. Measurement of fast electron spin relaxation times with atomic resolution. *Science*, 329(5999):1628–1630, 2010.

[97] ElliottH. Lieb and Derek W. Robinson. The finite group velocity of quantum spin systems. *Communications in Mathematical Physics*, 28:251–257, 1972.

[98] Bruno Nachtergaele, Yoshiko Ogata, and Robert Sims. Propagation of correlations in quantum lattice systems. *Journal of Statistical Physics*, 124:1–13, 2006.

[99] Hillel Raz and Robert Sims. Estimating the lieb-robinson velocity for classical anharmonic lattice systems. *Journal of Statistical Physics*, 137:79–108, 2009.

[100] Tuscon. Lieb-robinson bounds in quantum many-body physics. entropy and the quantum. *Contemp math*, 529:141–176, 2009.

[101] M. B. Hastings. Lieb-schultz-mattis in higher dimensions. *Phys. Rev. B*, 69:104431, Mar 2004.

[102] Bruno Nachtergaele and Robert Sims. Lieb-robinson bounds and the exponential clustering theorem. *Commun. Math. Phys*, 265:119–130, 2006.

[103] Matthew B. Hastings and Tohru Koma. Spectral gap and exponential decay of correlations. *Commun. Math. Phys*, 265:781–804, 2006.

[104] Marc Cheneau and et. al. Light-cone-like spreading of correlations in a quantum many-body system. *Nature*, 481(7382):484–487, 2012.

[105] Niklas Romming, Christian Hanneken, Matthias Menzel, Jessica E. Bickel, Boris Wolter, Kirsten von Bergmann, Andre Kubetzka, and Roland Wiesendanger. Writing and deleting single magnetic skyrmions. *Science*, 341(6146):636–639, 2013.

[106] Alexander Ako Khajetoorians, Jens Wiebe, Bruno Chilian, Samir Lounis, Stefan Blugel, and Roland Wiesendanger. Atom-by-atom engineering and magnetometry of tailored nanomagnets. *Nat Phys*, 8(1):497–503, 2012.

[107] Irakli Titvinidze, Andrej Schwabe, Niklas Rother, and Michael Potthoff. Dynamical mean-field theory of indirect magnetic exchange. *Phys. Rev. B*, 86:075141, Aug 2012.

[108] A.S. Ovchinnikov, I.G. Bostrem, and Vl.E. Sinitsyn. Cluster perturbation theory for spin hamiltonians. *Theoretical and Mathematical Physics*, 162(2):179–187, 2010.

[109] R. Wiesendanger, H.-J. Güntherodt, G. Güntherodt, R. J. Gambino, and R. Ruf. Observation of vacuum tunneling of spin-polarized electrons with the scanning tunneling microscope. *Phys. Rev. Lett.*, 65:247–250, Jul 1990.

[110] Andrew DiLullo, Shih-Hsin Chang, Nadjib Baadji, Kendal Clark, Jan-Peter Kloeckner, Marc-Heinrich Prosenc, Stefano Sanvito, Roland Wiesendanger, Germar Hoffmann, and Saw-Wai Hla. Molecular kondo chain. *Nano Letters*, 12(6):3174–3179, 2012.

[111] Xi Chen, Ying-Shuang Fu, Shuai-Hua Ji, Tong Zhang, Peng Cheng, Xu-Cun Ma, Xiao-Long Zou, Wen-Hui Duan, Jin-Feng Jia, and Qi-Kun Xue. Probing superexchange interaction in molecular magnets by spin-flip spectroscopy and microscopy. *Phys. Rev. Lett.*, 101:197208, Nov 2008.

8 Publications

- K. Them, T. Stapelfeldt, E. Y. Vedmedenko, and R. Wiesendanger: "Non-equilibrium finite temperature dynamics of magnetic quantum systems: Applications to spin-polarized scanning tunneling microscopy", New Journ. Phys. **15** 013009 (2013)

- K. Them, M. Brum: "States of low energy in homogeneous and inhomogeneous, expanding spacetimes", Class. Quantum Grav. **30** 235035 (2013)

- K. Them: "Towards experimental tests and applications of Lieb-Robinson bounds" Phys. Rev. A 89 022126 (2014)

  In preparation:

- K. Them, E. Y. Vedmedenko, K. Fredenhagen, and R. Wiesendanger: "Bounds on expectation values of quantum subsystems and perturbation theory"

9 Acknowledgements

First of all I want to thank Prof. Wiesendanger for the opportunity to work out my PhD thesis within the "group R". Thanks for the financial support as well as the perfect working conditions, i.e., I was allowed to work absolutely on my own initiative and with a free mind to follow my own ideas. I want to thank Elena Y. Vedmedenko for helping me to work out my ideas in a publishable form and in a better understandable language. Thanks for several discussions in which I acquired a broad understanding of surface physics and for the support as well as the perfect working conditions.

Thanks to Prof. Fredenhagen and Thomas Hack for the helpful, fruitful and enjoyable discussions taking up to 5 hours at once. Thanks to Prof. Fredenhagen for providing eq. (65), (66) and the bound $\mathfrak{F}_\Lambda$ in (61) as well as for referee this thesis. Thanks to Prof. Lichtenstein for being the second evaluator of the Disputation. Thanks to Dr. Thim Stapelfeldt for the collaboration and the development of our computer program QuantumCore, whose motivation originated from Corollary 5.4.7. Thanks to Roberto Mozara for several discussions and our common project which was financed by R. Wiesendanger and supported by E.Y. Vedmedenko. I want to thank Jens Wiebe, Focko Meier and Alex Khajetoorians for several discussions. Especially, the discussions with the experimentalists Focko Meier and Jens Wiebe initiated the first publication of this thesis. Thanks to David Vincent Altwein, Boris Wolter, Julian Hagemeister and Mario Krizanac for funny discussions. Thanks to Ruwn Frassek for discussions on the spectrum of spin chains and the nice times in Berlin. Thanks to Prof. Potthoff and Prof. Lichtenstein for repeated discussions. Thanks to the former aQFT group members Andreas Degner, Katarzyna Rejzner, Falk Lindner and Marcos Brum for inspiring questions on the STM day together with Bruno Chilian.

I want to thank canim, my mother, my father and my sisters as well as my friends Jan, Manfred and Regina Grzybowski, Najim Jawadi, Yassin Muhammed, Jakub Gollasch, Florian Mathe, Timo Allen, Sergej Wolf, Kolja Veihyle and the others... for the wonderful years.

Special thanks to Ola Bratteli and Derek W. Robinson. The fascination with their books "Operator Algebras and Quantum Statistical Mechanics I + II [44, 60]" formed the foundation of this doctoral thesis.

A Operator Algebras in Quantum Statistical Mechanics

We summarize some mathematical structures of [44, 60] which are of relevance for potential future work as well if one is interested in the mathematical details, e.g., continuity properties, a relation between free and perturbed systems which is in close relation to Quantum Monte Carlo Methods, etc.. Thus, this section does not contains own developments of the author of this thesis, but just a little notes to experimentally investigated spin systems.

A.1 Representations

The thermodynamic limit of a QSS seems to be already a suitable approximation for magnetic nano-islands consisting of less than 100 magnetic adatoms, because of the experimentally observed magnetization behavior in [43, 75] and the results of KMS states in [44]. The occurrence of unitarily inequivalent representations for QSS in the thermodynamic limit motivates a more detailed analysis of representations. We summarize basic results from [60].

If $(\mathfrak{H}, \pi)$ is a representation of the C^*-algebra $\mathfrak{A}$ and $\mathfrak{H}_1$ is a subspace of $\mathfrak{H}$, then $\mathfrak{H}_1$ is said to be invariant under π if $\pi(A)\mathfrak{H}_1 \subseteq \mathfrak{H}_1$ for all $A \in \mathfrak{A}$. Note that if $\mathfrak{H}_1^\perp$ is the orthogonal complement of $\mathfrak{H}_1$, i.e.,

$$\mathfrak{H}_1^\perp \doteq \{\xi \in \mathfrak{H}; \langle \xi, \psi \rangle = 0 \quad \forall \psi \in \mathfrak{H}_1\}, \tag{133}$$

then we have

$$\langle \xi, \pi(A)\psi \rangle = 0, \tag{134}$$

for all $A \in \mathfrak{A}$ and all $\xi \in \mathfrak{H}_1^\perp$, $\psi \in \mathfrak{H}_1$. If $\mathfrak{H}_1$ is a closed subspace of $\mathfrak{H}$ and $P_{\mathfrak{H}_1}$ the orthogonal projector with range $\mathfrak{H}_1$, then the invariance of $\mathfrak{H}_1$ under π implies that

$$[P_{\mathfrak{H}_1}, \pi(A)] = 0 \tag{135}$$

for all $A \in \mathfrak{A}$, i.e., the projector $P_{\mathfrak{H}_1}$ commutes with each of the representatives $\pi(A)$. One deduces that $\mathfrak{H}_1$ is invariant under π if, and only if, $P_{\mathfrak{H}_1}\pi(A) = \pi(A)P_{\mathfrak{H}_1}$ for all $A \in \mathfrak{A}$. Furthermore, if $\mathfrak{H}_1$ is invariant under π and

$$\pi_1(A) \doteq P_{\mathfrak{H}_1}\pi(A)P_{\mathfrak{H}_1} \tag{136}$$

then $(\mathfrak{H}_1, \pi_1)$ is a representation of $\mathfrak{A}$. If $\mathfrak{H}_1$ is invariant under π then $\mathfrak{H}_1^\perp$ is also invariant under π. A second representation $(\mathfrak{H}_2, \pi_2)$ is defined by setting $\mathfrak{H}_2 = \mathfrak{H}_1^\perp$ and $\pi_2(A) = P_{\mathfrak{H}_2}\pi(A)P_{\mathfrak{H}_2}$. Clearly $\mathfrak{H}$ has a decomposition as a direct sum, $\mathfrak{H} = \mathfrak{H}_1 \oplus \mathfrak{H}_2$, and each operator $\pi(A)$ then decomposes as a direct sum $\pi(A) = \pi_1(A) \oplus \pi_2(A)$. We write $\pi = \pi_1 \oplus \pi_2$ and $(\mathfrak{H}, \pi) = (\mathfrak{H}_1, \pi_1) \oplus (\mathfrak{H}_2, \pi_2)$.

A representation $(\mathfrak{H}, \pi)$ is said to be nondegenerate if

$$\{\psi; \psi \in \mathfrak{H}, \pi(A)\psi = 0 \quad \forall A \in \mathfrak{A}\} = \{0\}. \tag{137}$$

An important class of nondegenerate representations is the class of cyclic representations. A vector Ω in a Hilbert space $\mathfrak{H}$ is defined to be cyclic for a set of bounded operators $\mathfrak{M}$ if the set $\{A\Omega; A \in \mathfrak{M}\}$ is dense in $\mathfrak{H}$. This establishes

Definition A.1. *([60], 2.3.5.): A cyclic representation of a C^*-algebra $\mathfrak{A}$ is defined to be a triple $(\mathfrak{H}, \pi, \Omega)$, where $(\mathfrak{H}, \pi)$ is a representation of $\mathfrak{A}$ and Ω is a vector in $\mathfrak{H}$ which is cyclic for, in $\mathfrak{H}$.*

The generalization of a direct sum of representations of a C^*-algebra $\mathfrak{A}$ is given by a family $(\mathfrak{H}_\alpha, \pi_\alpha)_{\alpha \in I}$ of representations, where the index set I can be countable or noncountable. The direct sum

$$\mathfrak{H} \doteq \bigoplus_{\alpha \in I} \mathfrak{H}_\alpha \tag{138}$$

of the representation spaces $\mathfrak{H}_\alpha$ is defined in the usual manner [60] and the direct sum representatives are defined by

$$\pi \doteq \bigoplus_{\alpha \in I} \pi_\alpha \tag{139}$$

and setting $\pi(A)$ equal to the operator $\pi_\alpha(A)$ on the component subspace $\mathfrak{H}_\alpha$. By proposition 2.3.1. in [60], the operators $\pi(A)$ on $\mathfrak{H}$ are bounded because $\| \pi_\alpha(A) \| \leq \| \pi(A) \|$. Every state is a vector state for some nondegenerate representation. The next proposition reduces the discussion of general representations to that of cyclic representations.

Proposition A.2. *([60], 2.3.6.): Let $(\mathfrak{H}, \pi)$ be a nondegenerate representation of the C^*-algebra $\mathfrak{A}$. It follows that π is the direct sum of a family of cyclic subrepresentations.*

The foregoing type of decomposition depends upon the existence of nontrivial invariant subspaces. No further reduction is possible in the absence of such subspaces. Thus we are motivated to introduce definition 2.3.7. and proposition 2.3.8.:

Definition A.3. *([60], 2.3.7.): A set $\mathfrak{M}$ of bounded operators on the Hilbert space $\mathfrak{H}$ is defined to be irreducible if the only closed subspaces of $\mathfrak{H}$ which are invariant under the action of $\mathfrak{M}$ are the trivial subspaces $\mathfrak{H}$ and $\{0\}$. A representation $(\mathfrak{H}, \pi)$ of a C^*-algebra $\mathfrak{A}$ is defined to be irreducible if the set $\pi(\mathfrak{A})$ is irreducible on $\mathfrak{H}$.*

There are two standard criteria for irreducibility:

Proposition A.4. *([60], 2.3.8.): Let $\mathfrak{M}$ be a selfadjoint set of bounded operators on the Hilbert space $\mathfrak{H}$. The following conditions are equivalent:*

1. *$\mathfrak{M}$ is irreducible;*
2. *the commutant $\mathfrak{M}'$ of $\mathfrak{M}$, i.e., the set of all bounded operators on $\mathfrak{H}$ which commute with each $A \in \mathfrak{M}$, consists of multiples of the identity operator;*
3. *every nonzero vector $\psi \in \mathfrak{H}$ is cyclic for $\mathfrak{M}$ in $\mathfrak{H}$, or $\mathfrak{M} = 0$ and $\mathfrak{H} = \mathbb{C}$.*

We define two representations $(\mathfrak{H}_1, \pi_1)$ and $(\mathfrak{H}_2, \pi_2)$ to be unitarily equivalent if there exists a unitary operator U from $\mathfrak{H}_1$ to $\mathfrak{H}_2$ such that

$$\pi_1(A) = U\pi_2(A)U^* \tag{140}$$

for all $A \in \mathfrak{A}$ and denote this equivalence with $\pi_1 \simeq \pi_2$.

Purity of a state ω and irreducibility of the representation associated with ω are intimately related which is demonstrated with the next Theorem.

Theorem A.5. *([60], 2.3.19): Let ω be a state over the C^*-algebra $\mathfrak{A}$ and $(\mathfrak{H}_\omega, \pi_\omega, \Omega_\omega)$ the associated cyclic representation. The following conditions are equivalent:*

1. *$(\mathfrak{H}_\omega, \pi_\omega)$ is irreducible;*
2. *ω is pure;*
3. *ω is an extremal point of the set $E_\mathfrak{A}$ of states over $\mathfrak{A}$*

Furthermore, there is a one-to-one correspondence

$$\omega_T(A) = (T\Omega_\omega, \pi_\omega(A)\Omega_\omega) \tag{141}$$

between positive functionals ω_T, over $\mathfrak{A}$, majorized by ω and positive operators T in the commutant π' of π, with $\| T \| \leq 1$.

It follows from Theorem 2.3.16 [60] that $(\mathfrak{H}_1, \pi_1)$ and $(\mathfrak{H}_2, \pi_2)$ are unitarily equivalent if, and only if, the unit vectors of $\mathfrak{H}_1$ and $\mathfrak{H}_2$ define the same set of states of the C^*-algebra $\mathfrak{A}$. Concerning physical applications, there is a slightly weaker but more natural concept of equivalence, which is called quasi-equivalence of two representations.

The double commutant $(\pi(\mathfrak{A})')' = \pi(\mathfrak{A})''$ of a C^*-algebra $\mathfrak{A}$ is a von Neumann algebra.

Definition A.6. *([60], 2.4.25): If π is a representation of a C^*-algebra $\mathfrak{A}$, then a state ω of $\mathfrak{A}$ is said to be π-normal if there exists a normal state ρ of $\pi(\mathfrak{A})''$ such that*

$$\omega(A) = \rho(\pi(A)) \tag{142}$$

for all $A \in \mathfrak{A}$. If there are two representations π_1 and π_2 of a C^*-algebra $\mathfrak{A}$ and each π_1-normal state is π_2-normal and conversely, then π_1 and π_2 are said to be quasi-equivalent, written $\pi_1 \approx \pi_2$.

As a complement, π_1 and π_2 are said to be *disjoint*, written $\pi_1 \divideontimes \pi_2$, if no π_1-normal state is π_2-normal and conversely. Correspondingly, two positive linear functionals ω_1 and ω_2 are said to be *disjoint*, written $\omega_1 \divideontimes \omega_2$, if π_1 and π_2 are disjoint. The property $\pi_1 \divideontimes \pi_2$ is true if, and only if, π_1 and π_2 have no quasi-equivalent subrepresentations, which is equivalent to π_1 and π_2 having no unitarily subrepresentations. This follows immediately from the definition and the next Theorem, which shows that quasi-equivalence is the same as unitary equivalence up to multiplicity.

Theorem A.7. *([60], 2.4.26): Let $\mathfrak{A}$ be a C^*-algebra and let $(\mathfrak{H}_1, \pi_1)$ and $(\mathfrak{H}_2, \pi_2)$ be nondegenerate representations of $\mathfrak{A}$. The following conditions are equivalent:*

1. *there exists an isomorphism $\tau : \pi_1(\mathfrak{A})'' \mapsto \pi_2(\mathfrak{A})''$ such that $\tau(\pi_1(A)) = \pi_2(A)$ for all $A \in \mathfrak{A}$;*

2. *$\pi_1 \approx \pi_2$, i.e., the π_1-normal and the π_2-normal states are the same;*

3. *there exist cardinals n, m projections $E_1' \in n\pi_1(\mathfrak{A})'$, $E_2' \in m\pi_2(\mathfrak{A})'$ and unitary elements $U_1 : \mathfrak{H}_1 \mapsto E_2'(m\mathfrak{H}_2)$, $U_2 : \mathfrak{H}_2 \mapsto E_1'(m\mathfrak{H}_1)$ such that*

$$U_1\pi_1(A)U_1^* = m\pi_2(A)E_2', \tag{143}$$
$$U_2\pi_2(A)U_2^* = n\pi_1(A)E_1' \tag{144}$$

   for all $A \in \mathfrak{A}$;

4. *There exists a cardinal n such that $n\pi_1 \simeq n\pi_2$, i.e., π_1 and π_2 are unitarily equivalent up to multiplicity.*

There are several important results from decomposition theory, which has the aim to express a complex structure as a superposition of simpler components. The simplification procedure depends heavily on the physical application. Concerning numerical calculations the ergodic decomposition might be of interest, because a complicated time dependent system might be

decomposed into some structures which are time invariant and some structures for which the calculation of the time evolution is simpler. We are interested in basic results from orthogonal measures, central and subcentral decomposition and mention a few results from decomposition theory:

Definition A.8. *([60], 4.1.20): If ω_1, ω_2 are positive linear functionals over $\mathfrak{A}$ which satisfy any of the three equivalent conditions of Lemma 4.1.19 [60] then they are said to be orthogonal and we write $\omega_1 \perp \omega_2$.*

The properties of this Lemma are given by

Lemma A.9. *([60], 4.1.19): Let ω_1, ω_2 be positive linear functionals over the C^*-algebra $\mathfrak{A}$ and let $\omega = \omega_1 + \omega_2$. The following conditions are equivalent:*

1. *if ω' is a positive linear functional over $\mathfrak{A}$ satisfying $\omega' \leq \omega_1$ and $\omega' \leq \omega_2$ then $\omega' = 0$;*
2. *there is a projection $P \in \pi_\omega(\mathfrak{A})'$ such that*

$$\omega_1(A) = (P\Omega_\omega, \pi_\omega(A)\Omega_\omega), \quad \omega_2(A) = ((1-P)\Omega_\omega, \pi_\omega(A)\Omega_\omega) \tag{145}$$

3. *the representation associated with ω is a direct sum of the representations associated with ω_1 and ω_2,*

$$\mathfrak{H}_\omega = \mathfrak{H}_{\omega_1} \oplus \mathfrak{H}_{\omega_2}, \quad \pi_\omega = \pi_{\omega_1} \oplus \pi_{\omega_2}, \quad \Omega_\omega = \Omega_{\omega_1} \oplus \Omega_{\omega_2}. \tag{146}$$

2.3.8.) and in section X about equilibrium states, we are again remembered to Proposition X 4.1.19). The next Lemma demonstrates that disjointness of two positive linear functionals implies orthogonality.

Lemma A.10. *([60], 4.2.8): Let ω_1, ω_2 be positive linear functionals over the C^*-algebra $\mathfrak{A}$, and let $\omega = \omega_1 + \omega_2$. The following conditions are equivalent:*

1. *$\omega_1 \divideontimes \omega_2$, i.e.,$\omega_1$ and ω_2 are disjoint;*
2. *there is a projection $P \in \pi_\omega(\mathfrak{A})'' \cap \pi_\omega(\mathfrak{A})'$ such that*

$$\omega_1(A) = (\Omega_\omega, P\pi_\omega(A)\Omega_\omega), \tag{147}$$
$$\omega_2(A) = (\Omega_\omega, (1-P)\pi_\omega(A)\Omega_\omega). \tag{148}$$

In particular, disjointness of ω_1 and ω_2 implies orthogonality.

A.2 von Neumann algebras and Tomita-Takesaki Theorem

Beside the uniform topology several other local convex topologies exist. Thus one is motivated to close the operator algebra in a weaker topology. There are various different topologies on $\mathfrak{L}(\mathfrak{H})$ which are induced by sets of seminorms $\{p\}$. There are seminorms of interest that can be constructed from vectors in a Hilbert space $\xi \in \mathfrak{H}$, which are interpreted as physical states of a quantum mechanical system. Clearly

$$A \mapsto \| A\xi \| \geq 0 \qquad \xi \in \mathfrak{H} \tag{149}$$

is a seminorm on $\mathfrak{L}(\mathfrak{H})$. The locally convex topology on $\mathfrak{L}(\mathfrak{H})$ which is induced by these seminorms is called the strong operator topology. There is a related σ-strong operator topology which is obtained by considering all sequences $\{\xi_n\}$ in $\mathfrak{H}$ such that $\sum_n \| \xi_n \|^2 < \infty$. Then the set of seminorms defined by $A \mapsto \left[\sum_n \| \xi_n \|^2 \right]^{1/2}$ induces the σ-strong topology. The locally convex topology induced by the seminorms $A \mapsto |(\xi, A\eta)|$ for all choices of $\xi, \eta \in \mathfrak{H}$ is called the weak operator topology. The related σ-weak operator topology is obtained by the sequences $\{\xi_n\}$, $\{\eta_n\}$ in $\mathfrak{H}$ for which $\sum_n \| \xi_n \|^2 < \infty$, $\sum_n \| \eta_n \|^2 < \infty$ is valid. The corresponding seminorm is $A \mapsto |\sum_n (\xi_n, A\eta_n)|$. The topologies which are defined by the seminorms $A \mapsto \| A\xi \| + \| A^*\xi \|$ and $A \mapsto \left[\sum_n \| A\xi_n \|^2 + \sum_n \| A^*\xi_n \|^2 \right]^{1/2}$, where $\sum_n \| \xi_n \|^2 < \infty$, are called the strong* and the σ-strong* topologies. Remember that the commutant of any subset $\mathfrak{M} \subset \mathfrak{L}(\mathfrak{H})$ of bounded operators on a Hilbert space $\mathfrak{H}$ is denoted by $\mathfrak{M}'$. If $\mathfrak{M}$ is selfadjoint, then $\mathfrak{M}'$ is a C^*-algebra of operators on $\mathfrak{H}$.

Definition A.11. *([60], 2.4.8.) A von Neumann algebra on $\mathfrak{H}$ is a *-subalgebra $\mathfrak{M}$ of $\mathfrak{L}(\mathfrak{H})$ such that*

$$\mathfrak{M} = \mathfrak{M}''. \tag{150}$$

A von Neumann algebra is called a factor if it has a trivial center.

We introduce a few basic results of the Modular Theory, because of the relation to the KMS condition and the occurrence in the stability analysis under local perturbations (for example the action of a magnetic STM tip on a monolayer of magnetic atoms on the surface of a metallic or semiconducting substrate).

Let $\mathfrak{M}$ be a von Neumann algebra acting on a Hilbert space $\mathfrak{H}$. Define the conjugation operator J, on $\mathfrak{H}$, by

$$JA\Omega = A^*\Omega, \tag{151}$$

where $A \in \mathfrak{M}$ and $\Omega \in \mathfrak{H}$.

Definition A.12. *([60], 2.5.2): Let $\mathfrak{M}$ be a von Neumann algebra on a Hilbert space $\mathfrak{H}$. A subset $\mathfrak{K} \subseteq \mathfrak{H}$ is separating for $\mathfrak{M}$ if for any $A \in \mathfrak{M}$, $A\xi = 0$ for all $\xi \in \mathfrak{K}$ implies $A = 0$.*

Proposition 2.5.3. in [60] establishes that, if Ω is cyclic and separating for $\mathfrak{M}$ then it is also cyclic and separating for $\mathfrak{M}'$. Hence the two antilinear operators S_0 and F_0, given by

$$S_0 A\Omega = A^*\Omega \tag{152}$$

and

$$F_0 A'\Omega = A'^*\Omega \tag{153}$$

for $A \in \mathfrak{M}$ and $A' \in \mathfrak{M}'$ are both well defined on the dense domains $D(S_0) = \mathfrak{M}\Omega$ and $D(F_0) = \mathfrak{M}'\Omega$. It follows that S_0 and F_0 are closable (see Proposition 2.5.9. [60]). The closures of S_0 and F_0 are denoted by S and F. A closed operator has a unique polar decomposition:

$$S = J\Delta^{1/2}. \tag{154}$$

Δ is called the *modular operator associated with the pair* $\{\mathfrak{M}, \Omega\}$ and J is called the *modular conjugation.*

Proposition A.13. *([60], 2.5.11): The following relations are valid:*

$$\Delta = FS, \qquad \Delta = SF, \tag{155}$$

$$S = J\Delta^{1/2}, \qquad F = J\Delta^{-1/2}, \tag{156}$$

$$J = J^*, \qquad J^2 = 1, \tag{157}$$

$$\Delta^{-1/2} = J\Delta^{1/2}J. \tag{158}$$

A fundamental theorem is given by

Theorem A.14. ***Tomita-Takesaki Theorem.*** *([60]) Let $\mathfrak{M}$ be a von Neumann algebra with cyclic and separating vector Ω, and let Δ be the associated modular operator and J the associated modular conjugation. It follows that*

$$J\mathfrak{M}J = \mathfrak{M}' \tag{159}$$

and, moreover,

$$\Delta^{it}\mathfrak{M}\Delta^{-it} = \mathfrak{M}, \tag{160}$$

$$\Delta^{it}\mathfrak{M}'\Delta^{-it} = \mathfrak{M}', \tag{161}$$

for all $t \in \mathbb{R}$.

The modular automorphism group σ_t, defined by $\sigma_t(A) = \Delta^{it} A \Delta^{-it}$, satisfies a condition which had already been used in mathematical physics to characterize equilibrium states in Quantum Statistical Mechanics and Quantum Field Theory - *the Kubo-Martin-Schwinger (KMS) condition.*

Continuity and analytic elements.

Let F denote a norm-closed subspace of the dual X^* of a Banach space X such that either $F = X^*$ or $X = F^*$. We denote with $\sigma(X, F)$ the locally convex topology on X induced by the functionals in F.

Definition A.15. *([60], 2.5.17.): A one-parameter family $t \in \mathbb{R} \mapsto \tau_t$ of bounded, linear maps of X into itself is called a $\sigma(X, F)$-continuous group of isometries of X if*

1. $\tau_{t_1+t_2} = \tau_{t_1}\tau_{t_2}, t_1, t_2 \in \mathbb{R}$, *and* $\tau_0 = \iota$;
2. $\| \tau_t \| = 1$, $t \in \mathbb{R}$;
3. $t \mapsto \tau_t(A)$ *is $\sigma(X, F)$-continuous for all $A \in X$, i.e., $t \mapsto \eta(\tau_t(A))$ is continuous for all $A \in X$ and $\eta \in F$;*
4. $A \mapsto \tau_t(A)$ *is $\sigma(X, F)$-$\sigma(X, F)$-continuous for all $t \in \mathbb{R}$, i.e., $\eta \circ \tau_t \in F$, for $\eta \in F$.*

Definition A.16. *([60], 2.5.20.): Let $t \mapsto \tau_t$ be a $\sigma(X, F)$-continuous group of isometries. An element $Y \in X$ is called analytic for τ_t if there exists a strip*

$$I_\lambda = \{z, |Imz| < \lambda\} \tag{162}$$

in $\mathbb{C}$, a function $f : I_\lambda \mapsto X$ such that

1. $f(t) = \tau_t(A)$ *for $t \in \mathbb{R}$,*
2. $z \mapsto \eta(f(z))$ *is analytic for all $\eta \in F$.*

Under these conditions, we write

$$f(z) = \sigma_z(A), \qquad z \in I_\lambda. \tag{163}$$

Definition A.17. *([60], 3.1.17.): Let S be an operator on the Banach space X. An element $A \in X$ is defined to be an analytic element (entire analytic element) for S if $A \in D(S^n)$, for all $n = 1, 2, ...$, and if*

$$\sum_{n \geq 0} \frac{t^n}{n!} \| S^n A \| < +\infty \tag{164}$$

for some $t > 0$ (all $t > 0$).

Remark Theorem 6.2.4. [44] states that for a large class of QSS $\mathfrak{A}_{\text{loc}}$ is a norm-dense *-subalgebra of analytic elements of the closure $\bar{\delta}$ of the derivation δ. Manganese atoms in a galliumarsenid semiconductor possess theoretically infinite-range interactions, such that the associated elements are not contained in the algebra $\mathfrak{A}_{\text{loc}}$.

Let $j : \mathfrak{M} \to \mathfrak{M}'$ be the antilinear *-morphism defined by $j(A) = JAJ$ and let $\mathfrak{M}$, Ω, Δ and J be as in the Tomita-Takesaki theorem. A mathematical key object $\mathfrak{P}$ is defined by

Definition A.18. *([60], 2.5.25): The natural positive cone $\mathfrak{P}$ associated with the pair $(\mathfrak{M}, \Omega)$ is defined as the closure of the set*

$$\{Aj(A)\Omega; A \in \mathfrak{M}\}. \tag{165}$$

This cone has several interesting properties which are of relevance for a stability analysis. The vector of a perturbed KMS state is contained in the natural positive cone of the corresponding KMS state, see Corollary 5.3.9 [44] and page 157 in [44]. Therefore, we mention some of the properties:

Proposition A.19. *([60], 2.5.26): The closed subset $\mathfrak{P} \subseteq \mathfrak{H}$ has the following properties:*

1. *$\mathfrak{P}$ is a convex cone;*
2. *$\Delta^{it}\mathfrak{P} = \mathfrak{P}$ for all $t \in \mathbb{R}$;*
3. *if f is a positive-definite function then $f(\log \Delta)\mathfrak{P} \subseteq \mathfrak{P}$;*
4. *if $\xi \in \mathfrak{P}$, then $J\xi = \xi$;*
5. *if $A \in \mathfrak{M}$, then $Aj(A)\mathfrak{P} \subseteq \mathfrak{P}$.*

Proposition A.20. *([60], 2.5.30, Universality of the cone $\mathfrak{P}$):*

1. *If $\xi \in \mathfrak{P}$ then ξ is cyclic for $\mathfrak{M}$ if, and only if, ξ is separating for $\mathfrak{M}$.*
2. *If $\xi \in \mathfrak{P}$ is cyclic, and hence separating, then the modular conjugation J_ξ and the natural positive cone $\mathfrak{P}_\xi$ associated with the pair $(\mathfrak{M}, \xi)$ satisfy*

$$J_\xi = J \qquad \mathfrak{P}_\xi = \mathfrak{P}. \tag{166}$$

A.3 Quasi-local algebras

Operator algebras of QSS as well as in QFT possess so-called quasi-local structures. We give a precise definition and mention two interesting and special algebras.

Definition A.21. *([60], 2.6.3.): A quasi-local algebra is a C^*-algebra $\mathfrak{A}$ and a net $\{\mathfrak{A}_\alpha\}_{\alpha\in I}$ of C^*-subalgebras such that the index set I has orthogonality relation and the following properties are valid:*

1. *if $\alpha \geq \beta$ then $\mathfrak{A}_\alpha \supseteq \mathfrak{A}_\beta$;*
2. *$\mathfrak{A} = \overline{\bigcup_\alpha \mathfrak{A}_\alpha}^{\|\cdot\|}$, where the bar denotes the uniform closure;*
3. *the algebras $\mathfrak{A}_\alpha$ have common identity 1;*
4. *there exists an automorphism σ such that $\sigma^2 = \iota$, $\iota(\mathfrak{A}_\alpha) = \mathfrak{A}_\alpha$, and $[\mathfrak{A}^e_\alpha, \mathfrak{A}^e_\beta] = \{0\}$, $[\mathfrak{A}^e_\alpha, \mathfrak{A}^o_\beta] = \{0\}$, $\{\mathfrak{A}^e_\alpha, \mathfrak{A}^o_\beta\} = \{0\}$ whenever $\alpha \perp \beta$, where $\mathfrak{A}^o_\alpha \subseteq \mathfrak{A}_\alpha$ and $\mathfrak{A}^o_\alpha \subseteq \mathfrak{A}_\alpha$ and $\mathfrak{A}^e_\alpha \subseteq \mathfrak{A}_\alpha$ are the odd and even elements with respect to σ.*

The brackets $\{A, B\} = AB + BA$ denote the anti-commutation relation. If $\sigma = \iota$, then $\mathfrak{A}^e_\alpha = \mathfrak{A}_\alpha$ and condition (4) simplifies to the condition

$$[\mathfrak{A}_\alpha, \mathfrak{A}_\beta] = \{0\} \tag{167}$$

whenever $\alpha \perp \beta$. In applications to quantum physics $\sigma = \iota$ corresponds to Bose statistics but for Fermi statistics $\sigma \neq \iota$. $\mathfrak{A}_\alpha$ is interpreted as the algebra of physical observables for a subsystem localized in the region α. In applications to SP-STM these are usually spin observables of magnetic adatoms placed on the substrate at location α. If also algebraic quantum field theory is used, a so called Haag-Araki counter could be introduced to count the tunneling electrons from the tip. This is related with the measured dI/dU signal, where I is the electronic current and U is the applied voltage.

In [44] it is supposed that the commutant algebra $\mathfrak{E}^c_\omega$ and the algebra at infinity $\mathfrak{E}^\perp_\omega$ might have a particular physical significance. The corresponding subcentral decomposition would be of interest. Especially in high density data storage invariant and stable properties of condensed matter systems are of interest.

Definition A.22. *([60], 2.6.4.): If ω is a state over the quasi-local algebra $\mathfrak{A}$ then we define the commutant algebra $\mathfrak{E}^c_\omega$, of the associated representation*

$$(\mathfrak{H}_\omega, \pi_\omega, \Omega_\omega), \tag{168}$$

by

$$\mathfrak{E}_\omega^c = \bigcap_{\alpha\in I}(\pi_\omega(\mathfrak{A}_\alpha)' \cap \pi_\omega(\mathfrak{A}))'' \tag{169}$$

and the algebra at infinity $\mathfrak{E}_\omega^\perp$ *by*

$$\mathfrak{E}_\omega^\perp = \bigcap_{\alpha\in I}\left(\bigcup_{\alpha\perp\beta}\pi_\omega(\mathfrak{A}_\beta)\right)''. \tag{170}$$

A.4 Equilibrium states, perturbations, and asymptotic abelianness

We state the mathematical exact definition of KMS states and mention some of the important and general properties related to KMS states [44].

Definition A.23. *([44] 5.3.1): Let* $(\mathfrak{A},\tau)$ *be a* C^**-dynamical system. The state* ω *over* $\mathfrak{A}$ *is defined to be a* (τ,β)*-KMS state, if*

$$\omega(A\tau_{i\beta}(B)) = \omega(BA) \tag{171}$$

for all A, B *in a norm dense,* τ*-invariant* **-subalgebra* $\mathfrak{A}_\tau$.

If $\mathfrak{A} = M_n$ is the algebra of $n\times n$ matrices acting on the n-dimensional Hilbert space $\mathfrak{H}_n$ and for $H = H^* \in M_n$ the τ is given by

$$\tau_t(A) = e^{itH}Ae^{-itH}, \tag{172}$$

then the Gibbs state

$$\omega^\beta(A) = \frac{Tr(e^{-\beta H}A)}{Tr(e^{-\beta H})} \tag{173}$$

is the unique (τ,β)-KMS state (see [44], 5.3.31.).

The next proposition establishes that the center of a von Neumann algebra $\mathfrak{M}$ is contained in the set of all observables which are invariant under the dynamics of the system,i.e., $\tau_t(A) = A$. A von Neumann algebra $\pi_\omega(\mathfrak{A})''$ of a pure thermodynamic phase ω is a factor, i.e., the only invariant observable is the trivial observable which is proportional to the identity.

Proposition A.24. *([44] 5.3.28.): Let* $(\mathfrak{M})$ *be a von Neumann algebra with a cyclic unit vector* Ω, ω *the corresponding state, and* τ *a* σ*-weakly continuous one-parameter group of* **-automorphisms of* $\mathfrak{M}$. *Let*

$$\mathfrak{M}^\tau = \{A\in\mathfrak{M} : \tau_t(A) = A \quad \forall t\in\mathbb{R}\} \tag{174}$$

be the fixed-point algebra of τ and let

$$\mathfrak{Z}_\omega = \{A \in \mathfrak{M} : \omega(AB) = \omega(BA) \quad \forall t \in \mathbb{R}\} \tag{175}$$

be the centralizer of ω.

If ω is a τ-KMS state then it follows that

$$\mathfrak{Z}_\omega = \mathfrak{M}^\tau. \tag{176}$$

In particular

$$\mathfrak{M} \cap \mathfrak{M}' \subseteq \mathfrak{M}^\tau \tag{177}$$

anf if $\mathfrak{M}$ is abelian, one has $\tau_t = \iota$, for all $t \in \mathbb{R}$

Theorem A.25. *([44] 5.3.9): Let $(\mathfrak{A}, \tau)$ be a C^*-dynamical system, ω a (τ, β)-KMS state on $\mathfrak{A}$, $\beta \in \mathbb{R}$, and $(\mathfrak{H}_\omega, \pi_\omega, \Omega_\omega)$ the corresponding cyclic representation. It follows that Ω_ω is separating for $\pi_\omega(\mathfrak{A})''$.*

Theorem A.26. *([44], 5.3.30.): Let $(\mathfrak{A}, \tau)$ be a C^*-dynamical system and assume that $\mathfrak{A}$ has an identity. For $\beta \in \mathbb{R}$ let K_β be the set of (τ, β)-KMS states.*

It follows that:

1. *K_β is convex and weak*-compact.*
2. *K_β is a simplex.*
3. *$\omega \in K_\beta$ is an extremal point of K_β if, and only if, ω is a factor state.*
4. *Let ω_1 and ω_2 be extremal points of K_β, then ω_1 and ω_2 are either equal or disjoint.*
5. *If $\omega \in K_\beta$, the unique maximal measure on K_β corresponding to ω is identical to the central measure corresponding to ω.*

For the investigation of perturbations we have to introduce perturbed groups of *-automorphisms. The perturbed group is introduced with

Proposition A.27. *([44], 5.4.1): Let $(\mathfrak{A}, \tau)$ be a C^*-dynamical system and let δ denote the infinitesimal generator of τ. Furthermore, for each $P = P^* \in \mathfrak{A}$ define the bounded derivation δ_P by $D(\delta_P) = \mathfrak{A}$ and $\delta_P(A) = i[P, A]$ for $A \in \mathfrak{A}$. It follows that $\delta + \delta_P$ generates a one-parameter group of *-automorphisms τ^P of $\mathfrak{A}$ given by*

$$\tau_t^P(A) = \tau_t(A) + \sum_{n \geq 1} i^n \int_0^t dt_1 \int_0^{t_1} dt_2 \cdots \int_0^{t_{n-1}} dt_n [\tau_{t_n}(P), [\cdots [\tau_{t_1}(P), \tau_t(A)]]]. \tag{178}$$

Moreover, one has

$$\tau_t^P(A) = \Gamma_t^P \tau_t(A) \Gamma_t^{P*}, \tag{179}$$

where $\Gamma_t^P \in \mathfrak{A}$ *is a one-parameter family of unitary elements, determined by*

$$\Gamma_t^P = \hat{1} + \sum_{n\geq 1} i^n \int_0^t dt_1 \int_0^{t_1} dt_2 \cdots \int_0^{t_{n-1}} dt_n \tau_{t_n}(P) \cdots \tau_{t_1}(P) \tag{180}$$

$$\Gamma_t^P = \hat{1} + \sum_{n\geq 1} i^n \int_0^t dt_1 \int_0^{t_1} dt_2 \cdots \int_0^{t_{n-1}} dt_n \tau_{t_1}^P(P) \cdots \tau_{t_n}^P(P). \tag{181}$$

which satisfies the co-cycle relation

$$\Gamma_{t+s}^P = \Gamma_t^P \tau_t(\Gamma_s^P). \tag{182}$$

All integrals converge in the strong topology for the C^**-system. The integrals define norm-convergent series of bounded operators and*

$$\| \tau_t^P(A) - \tau_t(A) \| \leq (e^{|t|\|P\|} - 1) \| A \|, \qquad \| \Gamma_t^P - 1 \| \leq (e^{|t|\|P\|} - 1). \tag{183}$$

The next corollary states properties of the group for a system acting on a Hilbert space.

Corollary A.28. *([44], 5.4.2.): Adopt the assumptions of Proposition X ([44], 5.4.1.) but also assume that* $\mathfrak{A}$ *acts on a Hilbert space* $\mathfrak{H}$ *and*

$$\tau_t(A) = U_t A U_t^*, \tag{184}$$

where $U_t = e^{itH}$ *is a strongly continuous one-parameter group of unitary operators.*

It follows that

$$\tau_t^P(A) = U_t^P A U_t^*, \qquad \Gamma_t^P = U_t^P U_{-t}, \tag{185}$$

where

$$U_t^P = e^{it(H+P)}. \tag{186}$$

If, finally, P_n *is a sequence of selfadjoint elements of* $\mathfrak{A}$ *which converges strongly, then*

$$\lim_{n\to\infty} \| (\Gamma_t^{P_n} - \Gamma_t)\psi \| = 0, \qquad \lim_{n\to\infty} \| (\tau_t^{P_n}(A) - \tau_t(A))\psi \| = 0, \tag{187}$$

for all $\psi \in \mathfrak{H}$ *and* $A \in \mathfrak{A}$*, uniformly for* t *in finite intervals of* $\mathbb{R}$*.*

Perturbed and unperturbed KMS states are related by

Theorem A.29. *([44], 5.4.4.): Let $(\mathfrak{A},\tau)$ be a C^*-dynamical system acting on a Hilbert space $\mathfrak{H}$ such that*

$$\tau_t(A) = U_t A U_t^*, \tag{188}$$

where $U_t = exp\{itH\}$ is a strongly continuous one-parameter unitary group, and Ω a normalized U-invariant cyclic vector such that the associated vector state, $\omega(A) = \big(\Omega, A\Omega\big)$, is a (τ,β)-KMS state. The following statements are valid:

1. *If $P = P^* \in \mathfrak{A}$, then $\Omega \in D(\mathfrak{P}(z))$, where $\mathfrak{P}(z) = \tau_{z_n}(P)\cdots\tau_{z_1}(P) = e^{iz_nH}Pe^{i(z_{n-1}-z_n)H}P\cdots Pe^{-iz_1H}$ for all $z = (z_1,...,z_n)$ in the tube $\mathfrak{D}^{(n)}_{-1/2}$ defined by $\mathfrak{D}^{(n)}_{\alpha} = \{z;\alpha < Imz_1 < \cdots < Imz_n < 0\}$. The vector-valued function $\mathfrak{P}(z)\Omega$ is holomorphic in the tube $\mathfrak{D}^{(n)}_{-1/2}$, strongly continuous and uniformly bounded on its closure $\overline{\mathfrak{D}^{(n)}_{-1/2}}$, and*

$$\sup_{z\in\mathfrak{D}^{(n)}_{-1/2}} \| \mathfrak{P}(z)\Omega \| \leq \| P \|^n . \tag{189}$$

2. *If $P = P^* \in \mathfrak{A}$, then $\Omega \in D\big(e^{(H+P)/2}\big)$ and the vector $\Omega^P = e^{(H+P)/2}\Omega$ has the strongly convergent perturbation expansion*

$$\Omega^P = \Omega + \sum_{n\geq 1}\int_{-1/2\leq s_1\leq\cdots\leq s_n\leq 0} ds_1\cdots ds_n \tau_{is_n}(P)\cdots\tau_{is_1}(P)\Omega. \tag{190}$$

Moreover, the state ω^P defined by

$$\omega^P(A) \doteq \frac{(\Omega^P, A\Omega^P)}{(\Omega^P,\Omega^P)} \tag{191}$$

is a τ^P-KMS state and it is the unique τ^P-KMS normal state if, and only if, $\mathfrak{A}''$ is a factor.

3. *For each $A \in \mathfrak{A}$ and $P = P^* \in \mathfrak{A}$, the truncated function*

$$F_A(t_1,...,t_n) = \omega_T(A, \tau_{t_n}(P),...,\tau_{t_1}(P)) \tag{192}$$

is the boundary value of a function $F_A(z) = \omega_T(A,\tau_{z_n}(P),...,\tau_{z_1}(P))$ which is holomorphic in the tube $\mathfrak{D}^{(n)}_{-1}$, continuous and uniformly bounded on its closure $\overline{\mathfrak{D}^{(n)}_{-1}}$, and

$$\sup_{z\in\mathfrak{D}^{(n)}_{-1}} |F_A(z)| \leq 2^n n! \| P \|^n \| A \| . \tag{193}$$

Moreover, if $2 \parallel P \parallel < 1$ *the perturbed state* ω^P *is determined by the uniformly convergent series*

$$\omega^P(A) = \omega(A) + \sum_{n\geq 1} \int_{-1\leq s_1\leq\cdots\leq s_n\leq 0} ds_1 \cdots ds_n \omega_T(A, \tau_{is_n}(P), ..., \tau_{is_1}(P)) \tag{194}$$

and hence

$$\lim_{\alpha} \parallel \omega^{P_\alpha} - \omega \parallel = 0 \tag{195}$$

for each net $P_\alpha = P_\alpha^* \in \mathfrak{A}$ *such that* $\parallel P_\alpha \parallel \to 0$

The conclusions of Theorem 5.4.4. extend for any $\beta \in \mathbb{R}$ to (τ, β)-KMS states by rescaling. Hence, for each (τ, β)-KMS state ω there is a unique (τ^P, β)-KMS vector state ω^P, which can be constructed with the foregoing procedures. The properties of the map $\omega \mapsto \omega^P$ is summarized with

Corollary A.30. *([44], 5.4.5): Let* $(\mathfrak{A}, \tau)$ *be a* C^**- or a* W^**-dynamical system and for* $P = P^* \in \mathfrak{A}$, $\beta \in \mathbb{R}$, *associate with each* (τ, β)*-KMS state* ω *a* (τ^P, β)*-KMS state* ω^P *by*

$$\omega^P(A) = \frac{(\Omega^P, \pi_\omega(A)\Omega^P)}{(\Omega^P, \Omega^P)} \tag{196}$$

and

$$\Omega^P = \Omega_\omega + \sum_{n\geq 1} (-1)^n \int_0^{\beta/2} ds_1 \int_0^{s_1} ds_2 \cdots \int_0^{s_{n-1}} ds_n \pi_\omega(\tau_{is_n}(P) \cdots \tau_{is_1}(P))\Omega_\omega. \tag{197}$$

It follows that the map $\gamma_\tau^P; \omega \mapsto \omega^P$ *is an isomorphism of the set of* (τ, β)*-KMS states onto the set of* (τ^P, β)*-KMS states which maps extremal points into extremal points. The inverse map is given by* $(\gamma_\tau^P)^{-1} = \gamma_\tau^{-P}$.

Return to equilibrium properties are investigated by asymptotic abelianes.

Proposition A.31. *([44], 5.4.6): If* $(\mathfrak{A}, \tau)$ *is asymptotically abelian in the norm sense, i.e., if* $\lim_{t\to\infty} \parallel [A, \tau_t(B)] \parallel = 0$ *for all* $A, B \in \mathfrak{A}$ *and if* ω^P *is a* (τ^P, β)*-KMS state for* $\beta \in \mathbb{R} \cup \{\pm\infty\}$ *and if* ω *is a weak***-limit point of* $\tau_t^* \omega^P$ *as* t *tends to infinity, then* ω *is a* (τ, β)*-KMS state.*

Note that this proposition does not establish the existence of the limit point of $\tau_i^* \omega^P$, but if there is a unique (τ, β)-KMS state, this follows because all limit points must be equal [44].

Corollary A.32. *([44], 5.4.7): Let ω^P be an extremal (τ^P, β)-KMS state for $\beta \in \mathbb{R} \setminus \{0\}$ and assume that $(\mathfrak{A}, \tau)$ is asymptotically abelian in the norm sense.*

It follows that the limit

$$\omega(A) = \lim_{t\to\infty} \omega^P(\tau_t(A)) \tag{198}$$

exists for all $A \in \mathfrak{A}$, and ω is the unique (τ, β)-KMS vector state of ω^P.

The last result on asymptotic abelianness we mention requires

Definition A.33. *([44], 5.4.8.) A C^*-dynamical system $(\mathfrak{A}, \tau)$ is defined to be $L^1(\mathfrak{A}_0)$-asymptotically abelian if*

$$\int_{-\infty}^{\infty} dt \parallel [A, \tau_t(B)] \parallel < \infty \tag{199}$$

for all A, B in the norm-dense *-subalgebra $\mathfrak{A}_0$.

Consequences of an $L^1(\mathfrak{A}_0)$-asymptotically abelian system are stated in

Proposition A.34. *([44], 5.4.10): Let $(\mathfrak{A}, \tau)$ be an $L^1(\mathfrak{A}_0)$-asymptotically abelian C^*-dynamical system. It follows that the limits*

$$\gamma_\pm(A) = \lim_{t\to\pm\infty} \tau^P_{-t}\tau_t(A) \tag{200}$$

exist in norm for all $A \in \mathfrak{A}$ and $P = P^* \in \mathfrak{A}_0$. The $\gamma_\pm$ are norm-preserving *-morphisms of $\mathfrak{A}$ which satisfy the intertwining relations

$$\gamma_\pm \tau = \tau^P \gamma_\pm. \tag{201}$$

If $\mathfrak{A}$ has an identity, then the adjoints $\gamma_\pm^*$ are affine transformations of the states $E_\mathfrak{A}$ into $E_\mathfrak{A}$ with the following properties:

1. *The $\gamma_\pm^*$ map τ^P-invariant states into τ-invariant states and extremal τ^P-invariant states into extremal τ-invariant states.*

2. *The $\gamma_\pm^*$ map (τ^P, β)-KMS states into (τ, β)-KMS states and extremal (τ^P, β)-KMS states into extremal (τ, β)-KMS states for all $\beta \in (\mathbb{R} \cup \{\pm\infty\}) \setminus \{0\}$.*

3. *If $\beta \in \mathbb{R} \setminus \{0\}$ then the maps $\gamma_\pm^*$ coincide in restriction to the (τ^P, β)-KMS states.*

A.5 Quantum spin systems II

The original definition of the local Gibbs condition is

Definition A.35. *([44], 6.2.16.): Let Φ be an interaction of a quantum spin system such that the surface energy $W_\Phi(\Lambda)$ is a well-defined element of $\mathfrak{A}$ for all $\Lambda \subset \mathbb{Z}^d$. A state ω over $\mathfrak{A}$ is defined to satisfy the Gibbs condition with respect to $\beta\Phi$ if the following conditions are fulfilled:*

1. *ω is faithful, i.e. Ω_ω is separating for $\pi_\omega(\mathfrak{A})''$*
2. *$\omega^{P_\Lambda} = \omega_\Lambda \otimes \widetilde{\omega}$ for all $\Lambda \subset \mathbb{Z}^d$, where ω_Λ is the local Gibbs state, $\widetilde{\omega}$ is a state over $\mathfrak{A}_{\Lambda^c}$, ω^{P_Λ} is the perturbation of ω constructed in Theorem 5.4.4 [44], and $P_\Lambda = \beta W_\Phi(\Lambda)$.*

For an application of algebraic QFT to the description of substrate electrons we mention

Lemma A.36. *([60], 6.2.55.): Let $\mathfrak{A}$ be a C^*-algebra of the form*

$$\mathfrak{A} = M_n \otimes \mathfrak{A}_0, \tag{202}$$

where M_n is the full complex $n \times n$ matrix algebra and $\mathfrak{A}_0$ is an arbitrary C^*-algebra. Let ω_1 and ω_2 be states on $\mathfrak{A}$ such that

$$\omega_1 \mid_{\mathfrak{A}_0} = \omega_2 \mid_{\mathfrak{A}_0} . \tag{203}$$

It follows that ω_1 and ω_2 are quasi-equivalent.

An interesting example for derivations on UHF algebras is:

Example A.37. *([60], 3.2.25.): Let $\mathfrak{A}$ denote a UHF algebra (see Example 2.6.12. [60]). Thus $\mathfrak{A}$ is the norm closure of a family $\{\mathfrak{A}_\Lambda\}_{\Lambda \in I_f}$, of full-matrix subalgebras $\mathfrak{A}_\Lambda$, where I_f denotes the finite subsets of an index set I. If $\Lambda_1 \cap \Lambda_2 = \emptyset$ then $\mathfrak{A}_{\Lambda_1}$ and $\mathfrak{A}_{\Lambda_2}$ commute. Now let $\{\Lambda_n\}_{n \geq 1}$ be any increasing family of subsets of I_f such that $\bigcup_n \Lambda_n = I$ and choose elements $H_n = H_n^* \in \mathfrak{A}_{\Lambda_n}$ such that $H_n - H_{n-1}$ commutes with $\mathfrak{A}_{n-1}$. One can define a symmetric derivation δ of $\mathfrak{A}$ by*

$$D(\delta) = \bigcup_{\Lambda \in I_f} \mathfrak{A}_\Lambda \tag{204}$$

and

$$\delta(A) = i \lim_{n \to \infty} [H_n, A], \qquad A \in D(\delta), \tag{205}$$

because the commutativity condition for $H_n - H_{n-1}$ ensures that the limit exists. But $D(\delta)$ is invariant under the square root operation because each $\mathfrak{A}_\Lambda$ has this invariance.

Last but not least we state one of our favorite theorems to check strong continuity of our time-evolution groups in SP-STM experiments and check analyticity properties of the spin operators. This is of importance for our general principle of the functionality of a SP-STM, because the next theorem states that our considered systems are C^*-dynamical systems. This provides the foundation for an application of a lot of the contents in [44] to our SP-STM experiments.

Theorem A.38. *([44], 6.2.4): Let Φ be an interaction of a quantum spin system satisfying the requirement*

$$\| \Phi \|_\xi = \sum_{n \geq 0} e^{\xi n} \left(\sup_{x \in \mathbb{Z}^d} \sum_{\substack{X \ni x, \\ |X| = n+1}} \| \Phi(X) \| \right) < +\infty \tag{206}$$

for some $\xi > 0$, and define a derivation δ by

$$D(\delta) = \bigcup_{\Lambda \subset \mathbb{Z}^d} \mathfrak{A}_\Lambda \tag{207}$$

and

$$\delta(A) = i \sum_{X \cap \Lambda \neq \emptyset} [\Phi(X), A], \qquad A \in \mathfrak{A}_\Lambda. \tag{208}$$

It follows that $D(\delta)$ is a norm-dense *-subalgebra of analytic elements of the closure $\overline{\delta}$ of δ. Therefore, $\overline{\delta}$ generates a strongly continuous one-parameter group of *-automorphisms τ of $\mathfrak{A}$ and

$$\lim_{\Lambda \to \infty} \| \tau_t(A) - \tau_t^\Lambda(A) \| = 0 \tag{209}$$

for all $A \in \mathfrak{A}$, uniformly for t in compacts, where

$$\tau_t^\Lambda(A) = e^{itH_\Phi(\Lambda)/\hbar} A e^{-itH_\Phi(\Lambda)/\hbar}. \tag{210}$$